Cooperative Urban Driving Strategies at Signalized Intersections

Liu, M.

DOI
10.4233/uuid:c2d123b9-7cf9-4ffd-b495-06a53fe727c2

Publication date
2022

Document Version
Final published version

Citation (APA)
Liu, M. (2022). *Cooperative Urban Driving Strategies at Signalized Intersections*. [Dissertation (TU Delft), Delft University of Technology]. https://doi.org/10.4233/uuid:c2d123b9-7cf9-4ffd-b495-06a53fe727c2

Cooperative Urban Driving Strategies at Signalized Intersections

Meiqi Liu

This thesis is the result of PhD research funded by Delft University of Technology and China Scholarship Council (CSC) under Grant no. 201706320313.

Cooperative Urban Driving Strategies at Signalized Intersections

Dissertation

for the purpose of obtaining the degree of doctor
at Delft University of Technology
by the authority of the Rector Magnificus, Prof.dr.ir. T.H.J.J. van der Hagen
chair of the Board for Doctorates
to be defended publicly on
Wednesday, 26 January 2022 at 15:00 o'clock

by

Meiqi LIU
Master of Engineering in Transportation Planning and Management,
Zhejiang University, China
born in Liaoning, China

This dissertation has been approved by the promotors.

Composition of the doctoral committee:

Rector Magnificus	Chairperson
Prof.dr.ir. S.P. Hoogendoorn	Delft University of Technology, promotor
Dr.ir. M. Wang	Delft University of Technology, copromotor
Independent members:	
Prof.dr.ir. H. van Lint	Delft University of Technology
Prof.dr. R.M.P. Goverde	Delft University of Technology
Prof.dr.ir. I.J.B.F. Adan	Eindhoven University of Technology
Prof.dr.ir. S. Ahn	University of Wisconsin-Madison
Prof.dr.ir. M. Menendez	New York University Abu Dhabi

TRAIL Thesis Series no. T2022/3, the Netherlands Research School TRAIL

TRAIL
P.O. BOX 5017
2600 GA Delft
The Netherlands
E-mail: info@rsTRAIL.nl

ISBN: 978-90-5584-307-7

Printed in the Netherlands

Work like you don't need the money.

Live like it's heaven on Earth.

Acknowledgement

I was like a frightened rabbit when I first met my "interviewers", Serge and Meng, at the poster session in Washington D.C. I still remember it as if it were yesterday. They told a joke at that time, probably in an attempt to comfort me. *I will show you a picture. Look, this house is wonderful! You can live there. Where is it? It's on a lake. So how can I get there? By boat, of course. Will the lake freeze in winter? Ummm, you can break up the ice. And row at the same time? Haha, that's a challenge.* Well, this joke is similar to the Ph.D. research. I have to keep moving on and breaking all the ices that impede me. This challenging journey would be unexpectedly strenuous without support from many people. Herein, I would like to express my sincere gratitude for their help.

I would like to thank my promotor, Serge Paul Hoogendoorn, for offering me the opportunity to conduct my Ph.D. at TU Delft. I am fully supported by you in the field of transportation and control theory during my research. You are glad to put effort into guiding Ph.D. candidates and always motivate me one or several steps forward. It is a pleasant journey to work with you.

I am sincerely grateful to Meng Wang. It is lucky to have a copromotor like you, for all the time we'd discussed together, for all the kindness and patience you had shown me during my Ph.D. Your precise and rigorous attitude shows me how to be an independent researcher; your professional knowledge and academic experience illuminate my research plan in our biweekly progress meetings; your encouragement and enthusiasm inspire me when I wrestle with self-doubt and hesitancy. What I have learned from you is a long story, and this is absolutely not the end of the story. Best of luck to you in Dresden!

My appreciation to Jing Zhao. Congratulations on your smart career move! I am impressed by your timely feedback and practical suggestions. The invaluable discussions with you play an irreplaceable role in formulating my research problem. I cherish every moment we spend together, talking about life, research, presentation skills, sensibility, and emotional control.

Hans, Ivo, Monica, Rob, and Sue, it is a great honor for me to invite all of you to attend my defence, despite our hundreds of email exchanges when determining the defence time. I genuinely thank all of you for your efforts and time on my work. Many thanks to Rob for your constructive feedback on my dissertation.

Special thanks to Conchita, Dehlaila, Edwin, Marije, Moreen, Nicole, Simon, and Tonny, for supporting and assisting me in the administrations. I sincerely thank all my colleagues of the *Transport & Planning* department for all the iridescent moments we shared. In particular, I appreciate Maria's help for the translation of the Dutch summary and for the discussions and recommendations on my work when I was responding to reviewers' comments. I also thank Haneen and Andreas for your elaborate comments on my report before the Go/No Go meeting, and for the warm and cheering emails during the Chinese New Year 2021!

I would like to thank my roommates of offices 4.21 and 4.14 for the companion and cozy chats at the coffee machine. Special thanks to our research team for the bi-weekly group meetings, which have become the most exciting and memorable "routine" during the coronavirus lockdown and working-from-home. I wholeheartedly thank my friends in the Netherlands and in China, for your solicitude and encouragement when I was in depression. I look forward to seeing you again, and please do not hesitate to contact me if you are looking for your name in the acknowledgement!

Finally, I am deeply grateful to my parents and families. Thanks for your understanding, unconditional love, and appreciation of my work. You always listen to me, protect me, and cheer me up without reservation. Wish you good health and happiness always! Although it may not be admirable to commend the author's efforts, I appreciate myself for the weakness that I have overcome and the strength that I have called up. Cheers!

Meiqi
July, 2021
at home

Contents

Chapter 1

Introduction

In this chapter, we introduce the research topic and summarize the main contributions of this thesis. We first present the research background of cooperative vehicle driving strategies at urban signalized intersections. Then, the current knowledge and the main challenges in this line of research are reviewed, followed by discussions on the research gaps. The research objectives and contributions of this thesis are clarified thereafter. Finally, the thesis structure is outlined.

1.1 Background

Vehicle automation has become a domain of substantial development for the recent three decades owing to its potential in enhancing safety, efficiency (energy and fuel), and comfort. Parallel to vehicle automation is the connectivity between vehicles and infrastructures that enables the ability to acquire and anticipate both the motions of surrounding vehicles and information from roadside infrastructures (e.g., traffic lights, road signs, and lane markings). The advances in vehicle autonomy and communication systems pave the way towards vehicle cooperation, which can promote traffic efficiency, safety, and sustainability owing to the completeness of environmental awareness and the possibilities of coordinated control. Although it will take years, even generations, and monumental amounts of investment to realize vehicle cooperation and the requisite infrastructure facilities, the big shift that we are witnessing from legacy vehicles to connected and automated vehicles is expected to revolutionize transportation of people and goods.

According to the Society of Automotive Engineers (SAE) (SAE., 2018), driving automation levels are classified from no automation (Level 0 of full human driver control) to high and full automation (Level 4 and 5 of no required human driver control). Lower level (1 to 2) automation systems, such as Adaptive Cruise Control (ACC) (Xiao & Gao, 2010), are able to control vehicles but require drivers to keep an eye on the driving tasks and even intervene when necessary. Level 3 automation can disengage drivers from driving but still require human override. Level 4 and 5 automation means the system can operate the vehicle in all circumstances, and the human occupants need never be involved in the operational design domain for Level 4 and in all conditions for Level 5 (Shladover, 2018). This thesis focuses on the control strategies of cooperative vehicles under the assumption of Level 4 and 5 vehicle automation.

Providing vehicle-to-vehicle (V2V) and vehicle-to-infrastructure (V2I) communications, automated vehicles can be upgraded to *cooperative vehicles*, which can forecast and utilize information from the downstream/upstream traffic controllers and infrastructures (Sciarretta & Vahidi, 2020). With such information, platooning enables cooperative vehicles to coordinate individual vehicle behaviors for a common goal, e.g., smaller gaps, faster responses, less disturbances and delay (Lu, 2016). Although vehicle technology and legislation challenge the realistic full automation and cooperation, the adop-

tion and deployment of cooperative and automated vehicles is likely to be the trend in the future.

Connected and automated vehicle (CAV) technology will be initiated by the synergy between the advances in communication technologies and revolution in automotive industry over the next several decades (Gutesa et al., 2021). Therefore, the emerging needs arise to utilize the CAV data for better traffic operations and control strategies. Vehicular platoons have been proposed and piloted on highways, but the concept remains challenging researchers in urban environments. Although vehicle speeds are generally lower in the vicinity of signalized intersections than on highways or expressways, the road safety of the vulnerable road users (e.g., pedestrians and cyclists) and the public transport services bring complication to the traffic planning and operations in urban environments. Amongst a multitude of factors contributing to the complexity of traffic operations on urban roads, signal controllers at intersections remarkably complicate the platoon coordination.

Signalized intersections play an important role in separating traffic flows, pedestrians and cyclists from different movements spatiotemporally. Although signal controllers are capable of alleviating traffic congestion, accidents, fuel consumption and emission, and travel delay in the vicinity of intersections, they also cause the interrupted traffic flow and thereby increase the complexity of urban traffic operations. In the CAV environment, real-time data of signals and trajectories can be obtained and adjusted by taking advantage of CAVs as sensors and control actuators. Therefore, we should not lose the opportunities provided by the cooperative urban driving environment, i.e., to improve traffic efficiencies by integrating multiple signal control approaches with CAV trajectory optimization based on utilizing and actuating traffic signals.

To this end, traditional signal control approaches (fixed or pre-timing, actuated, and adaptive signals) should be taken into account in the hierarchical architecture where traffic control is placed on top of vehicle control. Besides, the joint integration between signal optimization with vehicle control by determining traffic signals and vehicle trajectories in a unified and single-layer framework is also promising to be realized in the CAV environment. This thesis focuses on these two topics to improve multiple measures of efficiencies at signalized intersections (comfort, safety, fuel economy, and travel delay).

1.2 CAV trajectory planning and traffic signal optimization

This section provides an overview of cooperative driving strategies and signal control in the urban environments, including CAV trajectory planning under exogenous traffic signals, traffic signal optimization using connected vehicle data, and the joint optimization of CAV trajectories and traffic signals, followed by summarizing the research gaps.

1.2.1 CAV trajectory planning under exogenous traffic signals

In trajectory planning systems, cooperative vehicles are generally controlled to avoid collision for minimal travel delay. The major differences between different studies are how to deal with the traffic signals at intersections.

With the presence of signal controllers, speed guidance systems such as GLOSA (Green Light Optimized Speed Advisory) (Stevanovic et al., 2013; Li et al., 2014a; Stebbins et al., 2017) and Eco-Approach and Departure systems (Altan et al., 2017; Hao et al., 2018; Wang et al., 2019) provide speed advice in the vicinity of signalized intersections. The generated advisory speed is designed to reduce travel delay, vehicle stops, and/or energy consumption, but these systems aim for an individual vehicle rather than a system of multiple vehicles.

CAV trajectories can be directly controlled assuming known signal parameters. The trajectory optimization systems at an isolated signalized intersection take fuel consumption and comfort into account in the objective functions (Jiang et al., 2017; Zhao et al., 2018). The terminal time (i.e., the signal cycle tail), the terminal vehicle position (i.e., the position of stop-line), the terminal speed (i.e., the limit speed), and the terminal acceleration when passing the stop-line (i.e., zero acceleration) can be easily determined at an isolated intersection, and the red phases can be represented by restricting these terminal conditions. However, this red phase representation method regards every intersection as a separate optimal control problem, and thereby fails to yield the global optimal trajectories when vehicles are traveling along a corridor (He et al., 2015).

To resolve this problem, the red phases along a corridor with multiple pre-timing signalized intersections are formulated as tracking the pre-defined

piece-wise speeds or accelerations in the cost terms to reflect the following, stopping, and leading modes of the controlled vehicles (Asadi & Vahidi, 2010; Kamal et al., 2012; HomChaudhuri et al., 2016; Wan et al., 2016). In general, the trajectory optimization systems under pre-timing signals are designed for an individual vehicle, considering multiple criteria in the objective function (Asadi & Vahidi, 2010; Kamal et al., 2012; He et al., 2015; HomChaudhuri et al., 2016; Wan et al., 2016; Jiang et al., 2017).

Furthermore, the autonomous intersection systems assume that the traffic signal controller is eliminated completely, and vehicles are coordinated to depart the intersection with no collision at a signal-free intersection (Lee & Park, 2012; Ahmane et al., 2013; Zohdy & Rakha, 2016; Yu et al., 2019). However, these systems cannot work in the mixed traffic flow of human drivers and cooperative vehicles, which is expected to appear and continue at least for the next decade (Sivak & Schoettle, 2015). The vulnerable road users (e.g., pedestrians and bicyclists) are neglected at the autonomous intersections, which questions the realistic applicability in the near future. Additionally, the autonomous intersection systems require high robustness for vehicle control to guarantee traffic safety, because the conflicting traffic flows are not separated.

1.2.2 Signal optimization using connected vehicle data

Signal optimization systems predict the traffic flow state by utilizing connected vehicles (but not necessarily automated vehicles) information and then generate the optimal signals (Feng et al., 2015; Al Islam & Hajbabaie, 2017; Beak et al., 2017; Li & Ban, 2018). Al Islam & Hajbabaie (2017) distribute the urban network into the intersection level to solve the signal timing optimization problem in real-time. Feng et al. (2015); Beak et al. (2017); Li & Ban (2018) (re)formulate the signal optimization problem in a bi-level structure to enumerate the feasible set of signal parameters in the upper level using the forward and backward recursion. In the lower level, the total vehicle delay or queue length are optimized in Feng et al. (2015); the green allocation at intersections and the offsets on the corridor are optimized iteratively in Beak et al. (2017); the total fuel consumption and travel time are optimized in Li & Ban (2018).

1.2.3 Joint optimization of CAV trajectories and traffic signals

The signal optimization models in section 1.2.2 only use CAVs as sensors without exploring their potential as traffic control actuators. To fill this gap, several research efforts are devoted to the joint optimization of traffic signals and vehicle trajectories.

Traffic signals and vehicle trajectories are mutually dependent in the vicinity of signalized intersections. Owing to the differences in the time scales of the considered dynamics (e.g., slow or fast dynamics, short or long horizon), the joint optimization of signals and trajectories are generally cast into hierarchical models to determine signals and trajectories in the upper and lower levels respectively (Li et al., 2014b; Yang et al., 2016b; Xu et al., 2018; Feng et al., 2018; Yu et al., 2018; Guo et al., 2019b; Niroumand et al., 2020). These bi-level models usually optimize signal parameters using enumeration or the similar forward/backward recursion method, and adopt different approximation methods to decrease control dimensions or to solve the control problems iteratively in a shorter horizon. However, the current joint approaches lose the benefits of integration between vehicle control and signal optimization in a unified framework on account of treating vehicle and signal control separately.

1.2.4 Research gaps

From the discussion above, the research gaps that are addressed in this thesis are detailed by summarizing the limitations of current literature on trajectory control and signal optimization.

G1. *Individual vehicle performance* : Current trajectory optimization systems at signalized intersections are normally designed for an individual vehicle (Asadi & Vahidi, 2010; Kamal et al., 2012; He et al., 2015; HomChaudhuri et al., 2016; Wan et al., 2016; Jiang et al., 2017). The scalability to surrounding vehicles in incorporating platooning of multiple traffic movements have to the best or our knowledge not been demonstrated.

G2. *Simple objective function*: In general, existing trajectory optimization systems consider few criteria in the objective functions. Fuel consumption is optimized in Asadi & Vahidi (2010); Kamal et al. (2012);

He et al. (2015); HomChaudhuri et al. (2016); Wan et al. (2016); Jiang et al. (2017); Zhao et al. (2018), and besides the ride comfort is introduced in HomChaudhuri et al. (2016); Jiang et al. (2017). Additionally, the desired gap penalty term is formulated in Kamal et al. (2012); HomChaudhuri et al. (2016), and the red phase term is designed for stopping vehicles in Asadi & Vahidi (2010); Kamal et al. (2012); HomChaudhuri et al. (2016). However, the designs of cost terms in these objective functions are simple, which cannot reflect the realistic traffic flow at signalized intersections.

G3. *Inflexible red phase representation*: The controlled vehicles that cannot pass the stop-line during the green phase should decelerate or stop confronting the red indication of the traffic light. Currently, there are two methods proposed to represent the red phases, i.e., the terminal condition method and the target speed method. Firstly, the terminal condition method requires vehicles to reach the stop-line at the terminal time (e.g., the arrival time to the stop-line) with specific speed (e.g., the limit speed) and position (e.g., the position of the stop-line). The arrival time of stopping vehicles is designed as the end of the red light, so the basis of this method is the estimation of the vehicle arrival time to the stop-line. Inaccurate arrival time estimation probably leads to inefficient vehicle trajectories (i.e., vehicles stop during the green phase) or infeasible trajectories (i.e., vehicles pass the stop-line during the red phase). The arrival time of an individual vehicle can be easily determined at an isolated intersection, but the arrival times of a platoon are difficult to be accurately calculated especially at the corridor or network level. Therefore, this method is neither scalable to multiple consecutive vehicles nor extendable to a large urban network scale. Secondly, the target speed method designs the vehicle trajectories to reflect signal changes by tracking the pre-defined desired accelerations/deceleration rates or speeds facing the green and red signal indications respectively (Kamal et al., 2012; Wan et al., 2016; HomChaudhuri et al., 2016). The pre-determined target speeds possibly generate unnecessary vehicle stops facing the red phase and dramatic accelerations/decelerations at the red phase starts/ends. Therefore, more attention should be paid when designing the target speeds to avoid such inefficient trajectories.

G4. *Trajectory optimization using exogenous signal parameters*: The ways to utilizing the signal phase and timing (SPaT) information in current trajectory optimization studies to our knowledge cannot be applied under actuated traffic signals. The feed-forward optimal control systems are restricted to be applied in the fixed or pre-timing signals owing to lack of system feedback (He et al., 2015; Wan et al., 2016; Jiang et al., 2017). The feedback systems using the model predictive control (MPC) framework allow for system feedback (Asadi & Vahidi, 2010; Kamal et al., 2012; HomChaudhuri et al., 2016; Zhao et al., 2018), but these studies cannot incorporate actuated signals. The main reason is that SPaT information, which is used for calculating the estimated arrival time or determining the target speed, can be hardly updated in the control systems.

G5. *Computational complexity of jointly optimizing signals and trajectories*: Research efforts on the joint control approaches of signals and trajectories usually adopt the inefficient enumeration method to solve the signal optimization problem of the bi-level models (Li et al., 2014b; Yang et al., 2016b; Xu et al., 2018; Feng et al., 2018; Guo et al., 2019b; Niroumand et al., 2020), which questions the scalability of the computational load to large-scale problems and real-time performance. In addition, the approximation methods in Li et al. (2014b); Yang et al. (2016b); Xu et al. (2018); Feng et al. (2018); Yu et al. (2018); Guo et al. (2019b); Niroumand et al. (2020) oversimplify the signal optimization, and the global optimum of the platoon trajectories are not guaranteed.

1.3 Research objectives

The overall research objective of this thesis is to develop an optimization-based control framework to plan CAV trajectories with multiple signal control approaches in a unified framework. The research aims at not only addressing the trajectory optimization problem under exogenous signal phase and timing (SPaT) information, but also jointly optimizing traffic signal timing and vehicle trajectories for the global optimum. In order to close the research gaps presented in Section 1.2.4 and fulfil the overall research objective, the detailed research sub-objectives are defined as follows.

R1. To design a controller that optimizes the CAV platoon trajectories along a corridor with pre-timing signal controllers, taking throughput, ride comfort, travel delay of passing vehicles, and fuel consumption of stopping vehicles into account. The controller should respect vehicle position constraints when facing the red light and does not need to prescribe vehicle arrival time and terminal conditions of speed and position. *(Chapter 2)*

R2. To design a controller that optimizes CAV platoon trajectories at actuated signalized intersections. The platoon controller should be able to anticipate signal plans and react to actuated signal changes by replanning trajectories. Multi-criteria of safety, efficiency, sustainability, and comfort should be considered in the design. *(Chapter 3)*

R3. To design a bi-level controller that optimizes traffic signal timing at the upper layer and platoon trajectories at the lower layer at standard signalized intersections. *(Chapter 4)*

R4. To design a computationally scalable single-level controller that simultaneously optimizes traffic signals and vehicle trajectories of a full intersection. The signal timing variables should be formulated as the vehicle-level control variables and no terminal conditions on speed and position at the cycle tail need to be pre-specified. *(Chapter 5)*

1.4 Contributions

The main contributions of the thesis are highlighted in this section, considering both theoretical or methodological contributions in Section 1.4.1 and societal contributions and relevance in Section 1.4.2.

1.4.1 Scientific contributions

An optimal CAV platoon trajectory control approach under the pre-timing signals is proposed considering multiple measures of efficiencies (related to R1). The proposed control approach optimizes throughout, ride comfort, travel delay, and fuel consumption, subject to the constraints on admissible accelerations, speeds, and safe gaps. Additionally, the red traffic light under the pre-timing signals is formulated as the position constraint for the

stopping vehicles. The proposed optimal control approach is flexible in incorporating queue discharging, platoon split and merge maneuvers along a corridor of multiple intersections. (see Chapter 2)

A closed-loop control approach is presented for actuated signals to optimize CAV platoon trajectories considering multi-criteria using the model predictive control (MPC) framework (related to R2). The MPC framework is computationally efficient due to the use of an iterative Pontryagin maximum principle approach. The feedback information (such as signal changes) at each time step in the closed-loop is used to re-plan the trajectories under actuated signal plans. The red indication is designed as a position penalty term in the running cost, and signal changes are anticipated by updating signal parameters in the online trajectory optimization problem at each time step. The proposed system is flexible in accounting for queue discharging, platoon split/merge, and stops along a corridor with multiple intersections in an oversaturated traffic flow. (see Chapter 3)

A hierarchical control approach is developed at standard full intersections to simultaneously optimize signals and CAV platoon trajectories (related to R3). The hierarchical control approach is able to incorporate different traffic movements during multiple signal phases. The red phase is formulated as the logic position constraint, which removes the restrictions of the existing terminal condition approach (i.e., prior estimation of vehicle arrival time) and applicability limitation to an isolated intersection. (see Chapter 4)

A new joint optimal control method is proposed at isolated signalized intersections for integrated optimization between traffic signals and CAV platoon trajectories (related to R4). The objective function and the constraints of this joint control problem can be linearized and thereby solved using mixed integer linear programming (MILP) techniques. The reconstructed linear red phase constraints reduce computational complexity by removing the need for calculation of vehicle arrival time. The joint approach is capable of generating the global optimum considering platoons from different movements within the signal cycle. Furthermore, the optimal vehicle trajectory pattern and the optimal traffic signal pattern are discovered. (see Chapter 5)

1.4.2 Practical contributions

This thesis proposes a framework of integrating traffic signals with trajectory planning under multiple signal control approaches. The policymakers can be inspired by the simulation results of the framework in the future CAV environment. The optimal signal and trajectory patterns explored in this framework offer suggestions on signal settings and speed prediction to urban road operators. Furthermore, the benefits of jointly optimizing signals and trajectories over the individual signal or vehicle optimization convince the road administrators to establish such communication systems and requisite infrastructures earlier for better traffic management and operations.

The flexibility and generality of this control framework proposed in this thesis are verified under different signal control approaches and platoon settings. Therefore, this framework is able to: 1) provide recommendations and guidance on developing vehicle controllers to original equipment manufacturers (OEMs) and service providers of cooperative vehicle systems; and 2) provide advice on developing intelligent traffic signal algorithms for traffic signal controller and ITS device manufacturers, and traffic infrastructure designers.

1.5 Thesis outline

The thesis structure consists of six chapters, as outlined in Figure 1.1. Chapter 1 introduces the background and motivation of this thesis. Chapter 2 to Chapter 5 respond to the specific research objectives as in Section 1.3, which are based on published or accepted scientific journal papers. And Chapter 6 concludes the findings of this thesis and further directions for research.

Chapter 2 and 3 focus on vehicle trajectory optimization where the signal phase and timing information is applied as exogenous inputs. Specifically, Chapter 2 aims at designing an optimal platoon trajectory control approach under fixed or pre-timing signals by optimizing accelerations of the controlled CAV platoon. The optimal throughput is determined first, and then comfort, travel delay, and fuel consumption are optimized subject to safe and physical constraints. The red phases are formulated as position constraints for stopping vehicles during the red phases. The control approach is flexible in incorporating multiple intersections with downstream vehicle queues.

Chapter 3 proposes a CAV trajectory control approach under actuated signals using model predictive control (MPC) framework. The actuated sig-

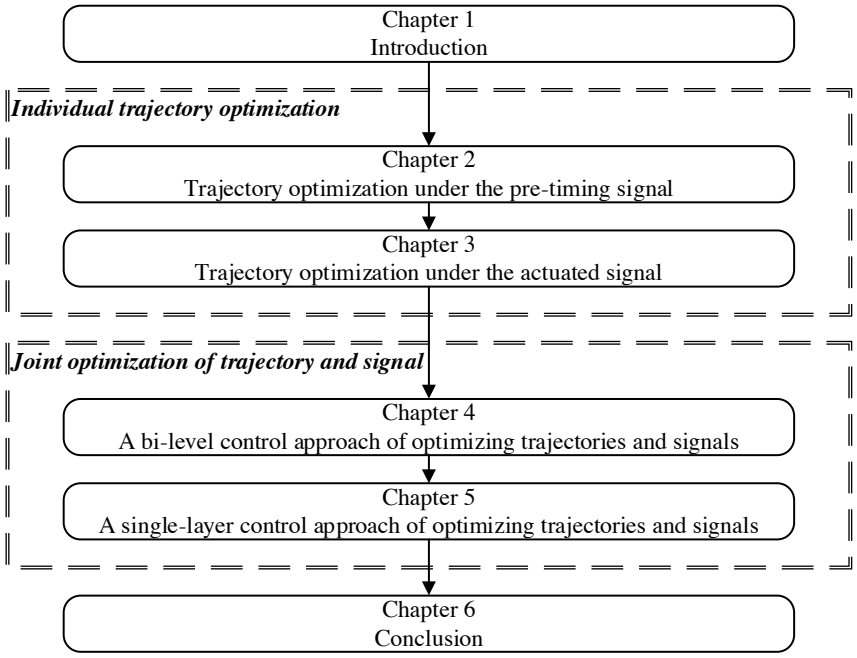

Figure 1.1: Overview of thesis structure

nal information is conveyed to the platoon controller since the beginning of the signal cycle. Unlike the design of safe gap and red phase constraints in Chapter 2, Chapter 3 regards the safe gap requirement as a penalty term in the running cost, and the red phases are represented by penalizing the gap between the stopping vehicles and the virtually stationary vehicles at the stop bar. The proposed MPC framework in Chapter 3 is solved using the receding horizon scheme, i.e., the iterative Pontryagin Maximum Principle (iPMP) approach.

Chapter 4 and 5 develop the optimal control approaches to integrating vehicle trajectories and traffic signals in a unified framework at isolated intersections. In Chapter 4, the two-layer control design is proposed to incorporate different traffic movements of the platoons during multiple signal phases. The signal phase lengths and the CAV platoon accelerations are optimized in the upper and lower layers respectively, considering comfort and travel delay. The red phases are formulated as logic constraints of position to render vehicles responsive to adaptive signal changes. Typical platoon performance and the optimal patterns of trajectories and signals are explored

in Chapter 4.

In order to simplify the hierarchical structure in Chapter 4, the joint control approach presented in Chapter 5 simultaneously optimizes traffic signals and trajectories of cooperative (automated) vehicle platooning in a single layer. The control formulation is linearized and then recast into a mixed integer linear programming (MILP) optimization problem to enable efficient solutions using MILP techniques. The joint control approach incorporates trajectory optimization of the platoons from all incoming traffic movements. The optimal trajectory and signal patterns are further revealed for the optimal traffic control actions at intersections.

Finally, Chapter 6 concludes this thesis by summarizing the findings, implications for practice, and directions for future research.

Chapter 2

Trajectory optimization under the pre-timing signal

In this chapter, we present an optimal control approach to optimize cooperative vehicle trajectories at pre-timing signalized intersections along an arterial. The proposed approach aims to maximize throughput, and subsequently optimize comfort, travel delay and fuel consumption. The red phases are taken into account as position constraints for stopping vehicles. Safety is guaranteed by constraining the inter-vehicle distance to be larger than some desired value. To verify the performance of the controlled platoon, simulation under three different traffic scenarios is conducted, including platoon trajectory control at an isolated intersection with/without vehicle queue, and platoon trajectory control at multiple intersections. The results demonstrate the control approach generates plausible behavior at an intersection and along a corridor with downstream queues. Moreover, the benefits of the proposed approach in mobility and fuel consumption are revealed by comparing with three baseline scenarios without control.

This chapter is an adapted version of the journal paper:

Liu, M., Wang, M. and Hoogendoorn, S., 2019. Optimal platoon trajectory planning approach at arterials. Transportation Research Record, 2673(9), pp.214-226.

2.1 Introduction

From the safety-oriented perspective, setting traffic lights on urban roads is an important traffic control approach (Guler et al., 2014). Unlike highways, vehicles have to decelerate or stop during the red time and accelerate or restart when the green time starts at signalized intersections, resulting in shock waves. Therefore, there are always acceleration and deceleration behaviors - even stops - in the vicinity of signalized intersections, which causes travel delay as well as excessive fuel consumption and emissions (Yang et al., 2016a). With the development of cyber-physical technologies, connected and automated vehicles (CAVs) are able to extend the sensing and anticipation ranges, and coordinate their decisions for a common goal (Wang et al., 2016). They have the potential to improve efficiency, safety, and sustainability at signalized intersections. Thus, the necessity for taking advantage of CAV technologies for effective traffic operations at signalized intersections has become pervasive.

Significant research efforts have focused on CAV platooning on highways (Wang et al., 2014b,c; Han et al., 2017; Fountoulakis et al., 2017), however, less attention has been devoted to design of CAV platoons on urban roads. Vehicle acceleration/deceleration maneuvers in the vicinity of signalized intersections on urban roads produce high levels of emissions and fuel consumption (Li et al., 2011). Thus it is valuable to optimize the fuel efficiency at signalized intersections, in addition to travel delay. Many existing research efforts of optimization-based control framework designs on urban roads applied different microscopic fuel consumption models (Akcelik, 1989; Ahn et al., 2002; Rakha et al., 2004) in simulation to validate the effectiveness in reducing fuel consumption and emission, and/or delay (average stop time) (Kamal et al., 2011; Hu et al., 2016; Rakha & Kamalanathsharma, 2011; Kamalanathsharma & Rakha, 2013; Kamalanathsharma et al., 2015). However, these studies aimed for an isolated intersection and eliminated fuel efficiency and even travel delay in the objective functions, which could not reflect realistic performance of the controlled vehicles.

Reported efforts on trajectory control of CAV systems can be grouped into two categories: V2V-based trajectory control and V2I/I2V-based speed advice/control. As to V2V-based trajectory control, several control algorithms were proposed at an isolated intersection without a traffic signal. Some researchers argued that the application of CAV technologies on traffic control had the potential to remove traditional signal controllers at isolated

intersections, if reliable connectivity of V2V information was provided (Lee & Park, 2012; Lee et al., 2013b; Zohdy & Rakha, 2016; Krajewski et al., 2016). Such control algorithms were proposed aiming at avoiding collision and improving traffic efficiencies, i.e., travel time and total delay. However, these control algorithms could not account for potential conflicts and safety problems of pedestrians and bicyclists, and they only confined to an isolated intersection. These two features rendered these algorithms far away from realistic traffic operations.

As to V2I/I2V-based speed advice systems, a number of efforts were made to investigate optimization-based speed advice algorithms on urban arterials via V2I and I2V communications. Some optimization-based velocity planning algorithms used simplified objective functions, such as maximizing the absolute value of accelerations or minimizing the differences between actual and maximal feasible speeds, when safety constraints were satisfied (Mandava et al., 2009; Asadi & Vahidi, 2010; Xia et al., 2013). Green Light Optimized Speed Advisory (GLOSA) system was proposed to provide drivers with speed advice on urban corridors by calculating travel time to the stop-line (Katsaros et al., 2011b,a; Stevanovic et al., 2013) or by minimizing fuel consumption (Li et al., 2014a; Stebbins et al., 2017; Seredynski et al., 2013) or delay (Stebbins et al., 2017). However, such speed advice systems considered only one criterion in the objective function, ignoring the comprehensive traffic operations in reality.

A few speed advisory or optimization systems were designed under actuated or adaptive signal control approaches. As to the actuated signal control approach (without optimizing signal parameters), speed advisory systems were designed at isolated actuated signalized intersections (Yang et al., 2016a; Altan et al., 2017) or corridors with actuated signal traffic lights (Hao et al., 2018). An optimization-based speed control algorithm was proposed on arterials by combining control effects of isolated intersections together (He et al., 2015). With respect to the integrated optimization of adaptive traffic signals and vehicle trajectories, existing research efforts mainly focused on isolated intersections (Feng et al., 2018; Yu et al., 2018). However, only acceleration fluctuations of platoon leaders were optimized over time for the representative of energy savings and emission reduction of the platoon, which was hard to reveal the optimal eco-driving performance of the platoon. In addition, actuated or adaptive signal control approaches will add computational complexity to optimization-based control approaches. Thus, we design a control system under fixed-timing control approach in this chap-

ter, which only requires fixed-timing signals within the prediction horizon.

From the discussion above, we conclude that the existing control algorithms seldom optimize fuel efficiency and travel delay of the platoon. In addition, it is not evident that existing algorithms are scalable to multiple intersections. This chapter aims at designing an optimal platoon trajectory control method by optimizing accelerations of the controlled CAV platoon when satisfying safe driving requirements. The proposed control approach obtains the optimal throughput first, and then maximizes ride comfort (by minimizing accelerations) and simultaneously minimizes average travel delay (by maximizing vehicle speeds) and fuel consumption rates, subject to admissible constraints on acceleration and speed. Rear-end collisions are avoided by constraining the inter-vehicle distance to be greater than the (minimum) safe gap. The red traffic light is formulated as position constraints to vehicles that cannot pass the stop line during the green phase. The control approach is flexible in incorporating queue discharging features on intersection approaches, as well as the platoon splitting and merging performance. Therefore, the proposed framework is flexible since it can be applied at multiple intersections with queues on signalized intersection approaches under multi-criteria in the objective function. Finally, the performance of the proposed control method is verified by simulation using several scenarios.

The remainder of this chapter is organized as follows: the following section introduces the control formulation for longitudinal driving task, followed by analysis of the simulation results. We summarize the study in the last section.

2.2 Control formulation

The longitudinal platoon control problem is formulated in this section, including design assumptions, control objectives and constraints, system dynamics, and solution approach.

2.2.1 Design assumptions and description of the control problem

The basic assumptions in this optimal trajectory design are described as follows:

1. Fixed signal timing during a cycle at signalized intersections;

2. Signal plan communicated to CAVs via I2V communication;

3. CAVs connected to the signal controllers via V2I communication;

4. Accelerations of all CAVs in the control zone are controlled;

5. No spillback.

We consider 100% CAV environment to demonstrate the workings of the proposed approach. First, we take the isolated intersection without a queue as an example. The longitudinal position of the stop-line is defined as 0. When the leader of the CAV platoon reaches L_0 meters upstream of the stop-line, the platoon trajectory optimization starts, i.e., the beginning of the prediction horizon. The prediction horizon ends with the signal cycle tail. Assuming the signal indication is green when the optimization starts, the prediction horizon length can be described as $T = g_1 + r$. g_1 and r are defined as the lengths of the (remaining) green phase and red phase in the current cycle when control starts. The control problem aims to optimize acceleration trajectories in order to fulfil control objectives and constraints, which will be detailed in the forthcoming subsections.

If the downstream vehicle queues are taken into account, the controlled platoon can be treated similarly to the aforementioned traffic scenario. As shown in Figure 2.1, an approaching platoon is traveling along the corridor when downstream CAVs are queuing behind the stop-lines. L_1 denotes the lane length between the stop-lines of the upstream and the adjacent downstream (second) intersection. The prediction horizon T is considered to start from the time when the leader of the approaching platoon arrives at L_0 meters away from the stop-line in the upstream direction at the first intersection to the end of the green phase at the second intersection.

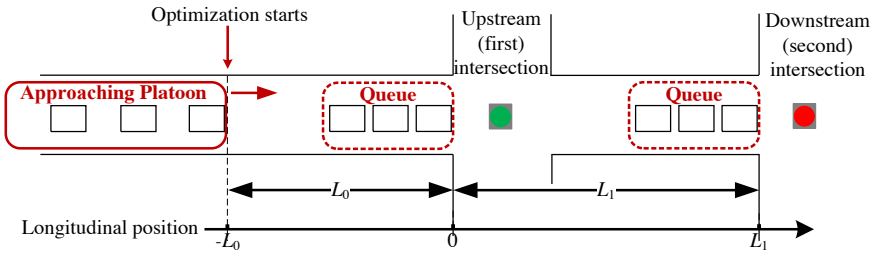

Figure 2.1: Illustration on operations of the control system

2.2.2 Control objectives

Due to the red phase, the platoon may split into two parts in the control design. The first part which can pass the intersection is required to operate with minimum travel delay and depart the intersection as soon as possible. Meanwhile, the maximum number of vehicles that can depart at the intersection is one of the variables that can be optimized. On the other hand, CAVs in the second part that cannot leave the intersection are expected to operate with minimum energy consumption and emission, and decelerate facing the red phase. Furthermore, the ride comfort and safety requirements of the platoon are considered. All these strategies aim to control the CAV platoon efficiently.

The control design is expected to fulfil the following control objectives:

1. To maximize ride comfort (by minimizing accelerations);
2. To minimize the travel delay of passing vehicles (by maximizing vehicle speeds);
3. To maximize the number of vehicles that is able to pass the stop-lines during the (remaining) green phases;
4. To minimize the fuel consumption of vehicles that can not pass the intersection.

In addition, the controller should satisfy the no-collision driving requirements.

2.2.3 System dynamics model

The control input variables include the acceleration, $a_i(t)$, and the maximum number of vehicles that can pass the stop-line, q (veh). i denotes the vehicle sequence number on a single lane, and N is the number of controlled vehicles. State variables $\mathbf{x}$ are considered as the longitudinal position, $x_i(t)$, and the speed, $v_i(t)$, of the controlled vehicle i.

$$\mathbf{x}(t)=(x_1(t),...,x_i(t),...,x_N(t),v_1(t),...,v_i(t),...,v_N(t))^{\mathrm{T}} \tag{2.1}$$

$$\mathbf{u}(t) = (a_1(t),...,a_i(t),...,a_N(t))^{\mathrm{T}} \tag{2.2}$$

The longitudinal dynamics model is described by the following ordinary differential equations:

$$\frac{\mathrm{d}}{\mathrm{d}t}\mathbf{x}(t) = \frac{\mathrm{d}}{\mathrm{d}t}(x_1(t),...,x_i(t),...,x_N(t),v_1(t),...,v_i(t),...,v_N(t))^{\mathrm{T}} = \mathrm{f}(\mathbf{x},\mathbf{u}) \tag{2.3}$$

$$\mathrm{f}(\mathbf{x},\mathbf{u}) = A\mathbf{x} + B\mathbf{u} \tag{2.4}$$

where

$$A = \begin{bmatrix} 0_{N,N} & I_N \\ 0_{N,N} & 0_{N,N} \end{bmatrix}; B = \begin{bmatrix} 0_{N,N} \\ I_N \end{bmatrix}$$

$$0_{N,N} = \begin{bmatrix} 0 & 0 & \cdots & 0 \\ 0 & 0 & \cdots & 0 \\ \vdots & \vdots & \ddots & \vdots \\ 0 & 0 & \cdots & 0 \end{bmatrix}; I_N = \begin{bmatrix} 1 & 0 & \cdots & 0 \\ 0 & 1 & \cdots & 0 \\ \vdots & \vdots & \ddots & \vdots \\ 0 & 0 & \cdots & 1 \end{bmatrix}$$

Here, the subscripts indicate the dimensions of the identity matrix I and the zero matrix 0.

2.2.4 Optimal control problem formulation

From aforementioned discussion, the control problem formulation at an isolated signalized intersection without a queue can be described as:

$$\min_{\mathbf{u},q} J_0 = \min_{\mathbf{u},q} \int_0^T \left(\beta_1 \sum_{i=1}^{N} a_i^2(t) - \beta_2 \sum_{i=1}^{q} v_i(t) - \beta_3 q + \beta_4 \sum_{i=q+1}^{N} f_v(v_i(t), a_i(t)) \right) \mathrm{d}t \tag{2.5}$$

Here, β_1, β_2, β_3, β_4 are positive cost weights. f_v is the instantaneous fuel consumption rate which can capture transient changes in speed and acceleration. For typical vehicles on a flat road, the instantaneous fuel consumption rate f_v (milliliter/s) can be estimated by the 3rd order polynomial with coefficients b_i for all instantaneous accelerations and the 2nd order polynomial with coefficients c_i for only positive accelerations, as follows.

$$f_v(t) = \begin{cases} b_0 + b_1 v(t) + b_2 v^2(t) + b_3 v^3(t) + a(t)\left(c_0 + c_1 v(t) + c_2 v^2(t)\right) & a(t) > 0 \\ b_0 + b_1 v(t) + b_2 v^2(t) + b_3 v^3(t) & a(t) \leqslant 0 \end{cases} \tag{2.6}$$

Detailed parameter values can be found in Kamal et al. (2011). Optimizing instantaneous consumption rates may give the trivial optimal solution of $v = 0$ and $a = 0$, but we overcome this problem by maximizing speeds in the objective function.

In Equation 2.5, the passing q vehicles are optimized to depart in maximal speeds while vehicles that can not leave are expected to operate with minimum fuel consumption rates. In addition, ride comfort for all controlled vehicles is included, as shown in the first cost term of Equation 2.5. Noteworthy is the fact that q is a variable which also needs to be optimized. We define an upper bound for the maximum passing vehicle number in the remaining green time, M_1. M_1 can be obtained as follows

$$M_1 = \lceil \frac{g_1 - L_0/v_{\max}}{t_{\min}} \rceil \tag{2.7}$$

Here, $v_{\max}$ denotes the limit speed on a single lane with signalized intersections. $t_{\min}$ denotes the minimum safe car-following time gap. All the integer values that are not more than M_1 are given to q ($q \leq M_1$), so q is a constant in the objective function. Based on the enumeration of possible q, the biggest value of q is selected in condition that all these q vehicles can pass the stop-line during the green phase. In this way, q is optimized, and then the objective function is minimized with this optimal q value. Although the objective function value will decline with an increase in q value, q is limited by the signal status. There is a position constraint for these q vehicles when the signal status turns red, which means, they are mandatory to pass the intersection during the green phase.

This formulation can also be extended to capture features of queues at multiple intersections on the arterial. Regarding the aforementioned isolated signalized intersection as the most upstream intersection, the control for a corridor applies a different objective function during the prediction horizon, which is detailed in Equation 2.8. The control problem formulation regarding two intersections with queues can be described as:

$$\begin{aligned} \min_{\mathbf{u},q} J_1 = \min_{\mathbf{u},q} \int_0^T \Bigg(& \beta_1 \sum_{i=1}^{N} a_i^2(t) - \beta_2 \sum_{i=1}^{Q_2+q} v_i(t) - \beta_3 q \\ & + \beta_4 \sum_{i=Q_2+q+1}^{N} f_v\left(v_i(t), a_i(t)\right) \Bigg) \mathrm{d}t - \beta_5 \int_{g_1+r}^{T} \left(\sum_{i=Q_2+q+1}^{N} v_i(t) \right) \mathrm{d}t \end{aligned} \tag{2.8}$$

Here, N is the number of vehicles in the controlled platoon, including

the approaching platoon and the vehicles queues at intersections. q can be regarded as the maximum number of vehicles that can pass the stop-line at the most upstream intersection, and Q_2 denotes the queuing vehicle number at the downstream intersection. Assuming no queue spillback occurs, Q_2+q vehicles are supposed to be discharged during the green phases along the corridor. If i denotes the vehicle sequence number on a single lane ($i \geq 0$), vehicles between $i=1$ and $i=Q_2$ are regarded as the vehicle queue on the downstream intersection approach, and the vehicle sequence number of the q passing vehicles at the most upstream intersection is therefore described as $i=Q_2+1$ to $i=Q_2+q$. g_1 and r correspond to the most upstream intersection. In Equation 2.8, the passing q vehicles and queuing Q_2 vehicles are optimized to depart in maximal speeds within the prediction horizon, while vehicles that can not depart the most upstream intersection are expected to operate with minimum fuel consumption rates. Ride comfort is considered in all controlled vehicles. In addition, the fifth cost term shows that the vehicles that can not depart the most upstream intersection are instructed to maximize their speeds during green indication of the next cycle at the most upstream intersection. Herein, the maximum passing vehicle number in the remaining green time at the most upstream intersection considering queue, M, can be obtained as follows

$$M = \lceil \frac{g_1 - L_0/v_{\max}}{t_{\min}} \rceil + Q_1 \tag{2.9}$$

Q_1 denotes the downstream vehicle queue at the most upstream intersection. It should be noted that the optimal value of q can be obtained based on M, which is similar to Equation 2.7.

2.2.5 Controller constraints

The control problem requires the control and state variables to respect some constraints:

1. Admissible acceleration is bounded between the maximum acceleration, $a_{\max}$, and the (negative) maximum deceleration, $a_{\min}$.

$$a_{\min} \leq a_i(t) \leq a_{\max} \tag{2.10}$$

2. Speed is restricted to be no larger than the limit speed, $v_{\max}$, but non-negative.

$$0 \leq v_i(t) \leq v_{\max} \tag{2.11}$$

3. No-collision requirements: Space gap and time gap is required to be greater than or equal to the minimum safe gap within the prediction horizon.

$$x_i(t) - x_{i+1}(t) \geq v_{i+1}(t)t_{\min} + s_0 + l \tag{2.12}$$

l denotes the length of a standard vehicle and s_0 is the minimum space gap at standstill conditions.

4. Red phase position constraint

The red phases within the prediction horizon are regarded as position constraints, which can adapt to deal with queues by adjusting the value of Q_2, q and signal timing parameters , g_1 and r. There are two position constraints regarding the red phase. As to two intersections along a corridor, the (Q_2+q)-th vehicle should be restricted to pass the stop-line during the green time at the most upstream intersection after optimizing the value of q, that is, the longitudinal position of the (Q_2+q)th vehicle should be more than or equal to 0 at the end of green time at the first intersection.

$$x_{Q_2+q}(g_1) \geq 0 \tag{2.13}$$

In addition, the $i = Q_2+q+1$ to $i = N$ vehicles which will encounter the red time at the most upstream intersection should be constrained to stop behind the stop-line during the red phase, which means, the longitudinal positions of $i = Q_2+q+1$ to $i = N$ vehicles should be less than or equal to 0 during the red time at the first intersection, as follows.

$$x_i(t) \leq 0, \text{for } Q_2+q+1 \leq i \leq N, g_1 \leq t \leq g_1+r \tag{2.14}$$

2.2.6 Solution approach

The continuous-time optimal control problem is transformed into a nonlinear programming (NLP) problem by discretizing the control variable of accelerations within the prediction horizon. System dynamics are transcribed as linear equality constraints in the NLP problem. The linear inequality constraints on the control variable, i.e., lower and upper bounds on accelerations, are set to limit admissible control signals. Other linear inequality constraints regarding speed, safe gap and longitudinal position during the red time are described in the form of control variables using the system dynamic equation, as the solver required. Thus, all vehicles in the controlled platoon

within the prediction horizon obey the controller constraints. This optimal control problem is solved with fmincon function in the MATLAB environment, using the SQP algorithm. Hereinafter, we discuss the performance of the controller.

2.3 Simulation results and analysis

In order to verify the platoon performance under different scenarios, ten to fifteen vehicles are simulated in different experiments.

2.3.1 Experiment design

Three scenarios are designed to test the performance of the controlled CAV platoon for different experiment objectives. Table 2.1 describes the experiment design. The parameter values in the simulation settings are detailed in Table 2.2.

Table 2.1: Design of the numerical simulation experiments

	Scenario 1	**Scenario 2**	**Scenario 3**
Scenario design	An isolated intersection without a downstream queue	An isolated intersection with a downstream queue	A corridor of two signalized intersections with downstream queues
Settings	$N = 10$, $g_1 = 30$ s, $r = 30$ s	$N = 15$, $\|Q_1\| = 4$, $g_1 = 30$ s, $r = 30$ s	$N = 10$, $\|Q_1\| = 2$, $\|Q_2\| = 2$, $g_1 = 20$ s, $r = 20$ s, $g_2 = 20$ s, $L_1 = 400$ m
Experiment objectives	To test the validity of the red phase position constraints and to tune the cost weights	To evaluate the workings of a downstream queue and the scalability of the control system	To examine the applicability of the control framework on a corridor and to validate possible deceleration maneuvers

Table 2.2: Parameter and coefficient values

Notation	Parameter/ Coefficient	Value	Unit
-	time step	1	s
-	initial speed of the approaching platoon	8	m/s
-	initial space gap in the approaching platoon	21	m
-	initial space gap in vehicle queues	5	m
N	number of vehicles in the controlled platoon	$10, 15$	-
Q_1	vehicle queue on the first intersection approach	$0, 2, 4$	-
Q_2	vehicle queue on the second intersection approach	$0, 2$	-
g_1	remaining green phase length at the first intersection	$30, 20$	s
r	red phase length at the first intersection	$30, 20$	s
g_2	green phase length at the second intersection	20	s
l	length of every controlled vehicle	3	m
L_0	distance from L_0 meters away from the stop-line in the upstream direction (at the first intersection) to the stop-line at the first intersection	200	m
L_1	lane length between the stop-line at the first and second intersection	400	m
$t_{\min}$	minimum safe car-following time gap	2	s
s_0	minimum space gap at standstill conditions	2	m
$v_{\max}$	limit speed on the urban corridor	15	m/s
$a_{\max}$	allowable maximum acceleration	2	m/s^2
$a_{\min}$	allowable minimum acceleration	-5	m/s^2
β_1	cost weight	1	-
β_2	cost weight	1	-
β_3	cost weight	1	-
β_4	cost weight	34	-
β_5	cost weight	1	-

Scenario 1 represents the situation that the controlled platoon splits into two at an isolated intersection without a downstream queue on the approach within the prediction horizon ($Q_1 = Q_2 = 0$). Scenario 1 is simulated to verify the workings of the optimal control approach when the red phase is included as position constraints. In Scenario 1, the first q vehicles of the

approaching platoon are expected to pass directly and the subsequent $N-q$ vehicles cannot depart due to the red phase. The prediction horizon length T is 60 s ($T = g_1 + r$), including the remaining green phase length ($g_1 = 30$ s) and red phase length ($r = 30$ s). Performance in Scenario 1 can help understand how the control framework works under the weighted sum of different criteria and prove the flexibility of the control approach.

Scenario 2 introduces a downstream vehicle queue at an isolated signalized intersection ($|Q_1| = 4$, $Q_2 = 0$), which provides insights into the effectiveness of the control approach regarding a downstream queue. Apart from the approaching platoon, Q_1 vehicles are set to stop behind the stop-line waiting for the green phase at the start of the optimization. The lengths of the remaining green and red phases are 30 s ($g_1 = 30$ s and $r = 30$ s). In Scenario 2, platoon split and merge and the acceleration behavior of queuing vehicles at the start of the green phase can be tested. In addition, an increase in the number of controlled vehicles ($N = 15$) can validate the scalability of the control system.

Scenario 3 is designed along a corridor of two signalized intersections with downstream queues. The remaining green phase length at the first intersection $g_1 = 20$ s (from $t = 0$ s to $t = 20$ s), the red phase length at the first intersection $r = 20$ s (from $t = 21$ s to $t = 40$ s), and the green phase length at the downstream (second) intersection $g_2 = 20$ s (from $t = 41$ s to $t = 60$ s). The prediction horizon T is 60 s. The controlled N (=10) vehicles includes Q_1 ($|Q_1|$=2) and Q_2 ($|Q_2|$=2) vehicles waiting for the green phases behind the stop-line at the first and the second intersection respectively, and $N - |Q_1| - |Q_2|$ (=6) vehicles approaching from L_0 meters away from the stop-line in the upstream direction at the first intersection. Given a short lane length ($L_1 = 400$ m) between two intersections, q passing vehicles at the first intersection may experience deceleration maneuvers between the first intersection and the second intersection. The q vehicles are expected to pass as soon as possible but decelerate to keep safe gaps. Q_2 vehicles on the second intersection approach keep zero acceleration behind the stop-line during the red phase ($t \in [0, g_1 + r]$). Scenario 3 can help validate the flexible characteristic of the control framework regarding the application on an arterial corridor of multiple signalized intersections with queues.

The results of three designated scenarios can verify the performance of the platoon trajectory control approach. Similar settings (e.g., the number of controlled vehicles, vehicle queues behind the stop-line at intersections, and the number of consecutive intersections along a corridor) can be imple-

mented in the same way. In addition, the communication ranges of V2I, I2V and V2V are limited to about 200 meters in reality, so the control approach starts from L_0 (=200) meters away from the stop-line in the upstream direction at the first intersection. The distance between the upstream intersection and the downstream intersection L_1 is set to be 400 m to verify the possible deceleration maneuvers.

2.3.2 Platoon performance

Three scenarios are simulated to evaluate control effects based on trajectory analysis, as depicted in Figure 2.2 to Figure 2.4. The horizontal red lines in these figures show the red traffic light. Instantaneous fuel consumption rates (see subfigure (d) of Figure 2.2 to Figure 2.4) are calculated based on accelerations and speeds using Equation 2.6. Since speeds are developed from accelerations, fluctuations in instantaneous fuel consumption rate are highly relevant with variations in accelerations (see subfigure (a) of Figure 2.2 to Figure 2.4). Overall, it is evident that vehicle accelerations and decelerations are considerably smooth owing to the cost term of maximizing ride comfort, and the optimal trajectories satisfy the controller constraints, including constraints on the safe gap, allowable acceleration, and limited speed.

The remainder of this section analyzes the platoon performance in different scenarios. Finally, three comparison baseline scenarios are implemented using intelligent driver model (IDM) under the same settings of the designated scenarios. The simulation results can reveal differences and benefits of the proposed control approach in comparison to human drivers.

Tuning cost weights

The cost weights are tuned in Scenario 1 and applied in all scenarios. Firstly, we regard $\beta_1 = 1$ as a baseline. The choice of β_3 (=1) does not influence the optimal solution because q is a constant in the objective function. The cost weight of speed, β_2, is supposed to keep the same order with the cost weight of acceleration β_1, thus $\beta_2 = \beta_1 = 1$. The same also holds for β_5. As to the fuel consumption cost weight β_4, we find that bigger values of β_4 (> 34) will overweight the fuel consumption cost term, causing lower speeds with respect to the first q vehicles when passing the intersection. It is obvious that an overweighted fuel consumption cost weight β_4 has a negative effect on the trajectory performance, especially speeds. Therefore, β_4 is selected to be

34, which reaches its largest value without sacrificing speeds.

Analysis of Scenario 1

In Scenario 1, $M_1 = 9$ and q is optimized to be 7. The optimal trajectories of Scenario 1 are demonstrated in Figure 2.2. Vehicle 1 to 10 represent the vehicle sequence number of the approaching platoon on the lane. In Figure 2.2, only the first q (=7) vehicles are leaving the intersection, while the subsequent $N-q$ (=3) vehicles cannot catch the green phase. The first q vehicles accelerate quickly till the limit speed $v_{\max}$ and then keep it. Only Vehicle 1 reaches the maximum acceleration at the beginning, because it does not have to satisfy the safety constraint as the followers do. Vehicles that cannot pass the intersection decelerate and slowly approach the stop-line, due to an explicit optimization function of fuel consumption rates. Performance in Scenario 1 proves the flexibility of the control approach that multiple criteria in the objective function can be applied, and the control approach works well subject to all constraints and system dynamics.

Analysis of Scenario 2

Platoon performance of Scenario 2 at an isolated intersection with a downstream queue is depicted in Figure 2.3. The first $|Q_1|$ (=4) vehicles in the legend represent the vehicle queue Q_1 on the intersection approach. The maximum number of vehicles that can depart the first intersection, q, is optimized to be 11. It is shown that the last $N-q$ (=4) vehicles cannot catch the green time and decelerate behind the stop-line. Similar trajectories appear in Scenario 1 in terms of the split of the approaching platoon (see Figure 2.2). Using position constraints to express the red phase, it is clear that the implementation of a downstream queue works in the proposed optimal control approach.

Analysis of Scenario 3

The optimal trajectories of Scenario 3 are presented in Figure 2.4. In Scenario 3, q is optimized to be 5. The approaching platoon experiences split and merge with the preceding vehicles (Q_1 and Q_2) when the signal status changes ($t = 20$ s and $t = 40$ s). The vehicle queue Q_2 (Vehicle 1 and 2) accelerates when the signal status turns green at the second intersection ($t = 41$ s). The vehicle queue Q_1 (Vehicle 3 and 4) starts acceleration from

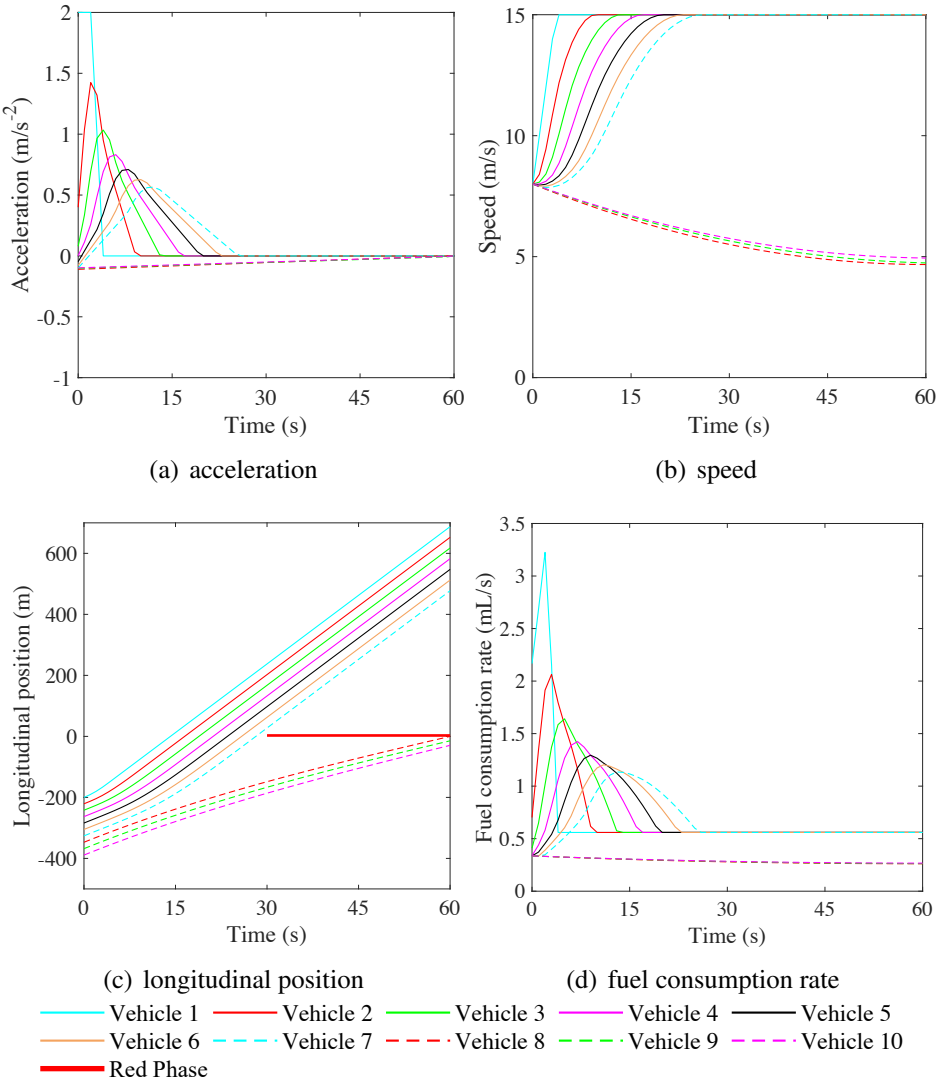

Figure 2.2: Optimal trajectories in Scenario 1

standstill conditions at the beginning of the green time at the first intersection and moves to the second intersection with gradually increasing speeds. While merging, Q_1 vehicles keep the safe gap with Q_2 vehicles. The passing vehicles (Vehicle 3 to 7) accelerate at the beginning and depart the first intersection directly. The leader in the approaching platoon (Vehicle 5) is expected to accelerate till the maximum speed $v_{\max}$ but it cannot, because Vehicle 5 should keep the safe gap with Vehicle 4 on the short lane length

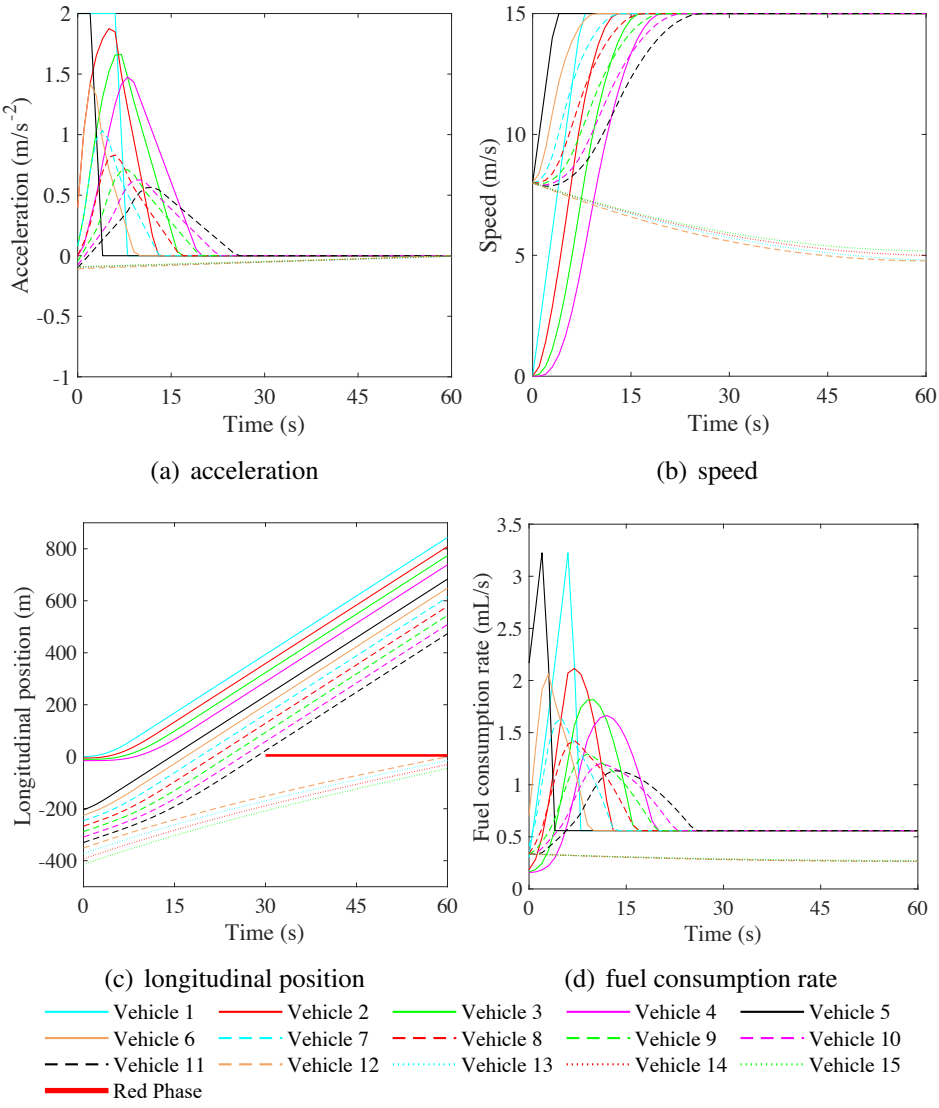

Figure 2.3: Optimal trajectories in Scenario 2

($L_1 = 400$ m). Owing to the red phase constraints, the last 3 vehicles (Vehicle 8 to 10) can pass the first intersection only if the subsequent green phase starts ($t = 41$ s). Vehicle 8 to 10 have to decelerate facing the red phase and then accelerate till the maximum speed after the next green phase starts.

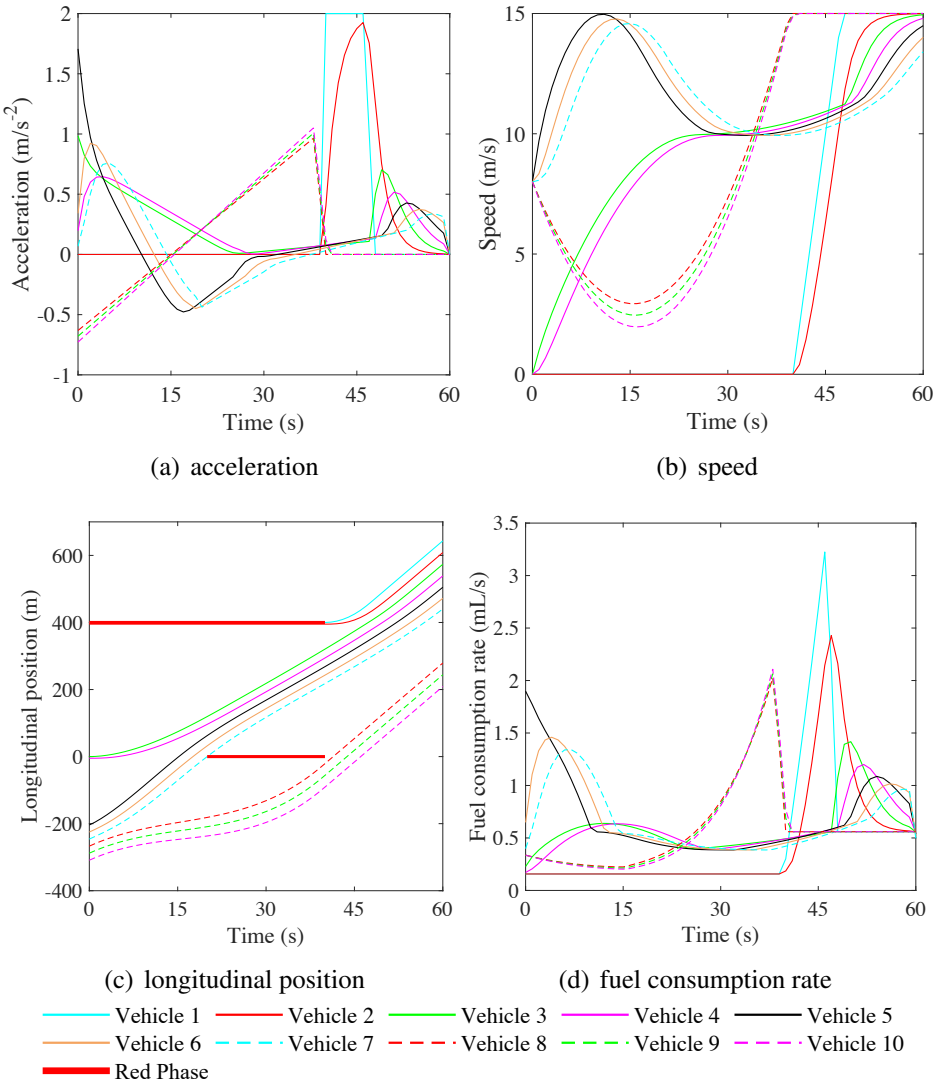

Figure 2.4: Optimal trajectories in Scenario 3

Analysis of comparison scenarios

In order to show the behavioral differences and potentials of the controlled platoon, three comparison baseline scenarios, which apply the intelligent driver model (IDM) (Treiber et al., 2000), are designed using the same settings in Scenario 1 to Scenario 3. The simulation results of the comparison scenarios are shown in Figure 2.5. The maximum number of vehicles that can pass the intersection is evaluated first when implementing the IDM

model. Later, a virtual standstill vehicle (also applicable to the safe gap constraint) is placed at the stop line representing the red phase. After adding the virtual vehicle(s), the IDM model is implemented again to simulate the trajectories under the workings of the red phase constraint (i.e., the safe gap constraint of the virtual vehicle). The virtual vehicle is removed after the green time starts.

Figure 2.5 shows the simulation results under the IDM model. It is obvious that the optimal throughputs in the IDM model are worse than the counterparts in our control approach. Two, two, and one more vehicles are released in our control approach compared with IDM under Scenario 1 to Scenario 3. In addition, the total fuel consumption of all controlled vehicles by integrating the instantaneous fuel consumption rate in time is also an advantage of our approach. For instance, the fuel savings of our control approach are 18.4509 ml in Scenario 3.

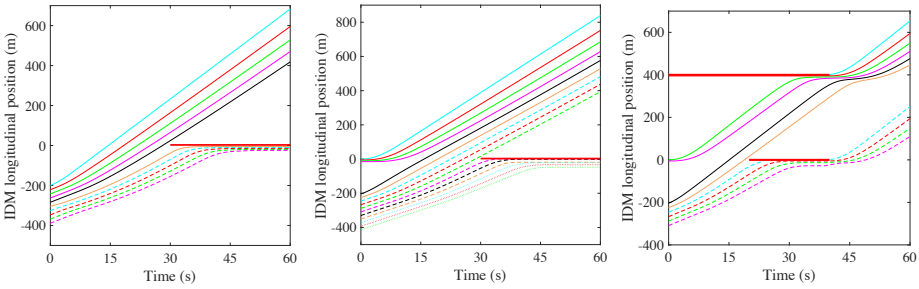

(a) Scenario 1 (b) Scenario 2 (c) Scenario 3

Figure 2.5: Longitudinal trajectories of IDM in Scenario 1, 2 and 3

2.4 Conclusions and future work

In this chapter, we proposed a flexible CAV acceleration control approach on urban roads that optimizes traffic operations with multiple criteria of throughput, ride comfort, travel delay, and fuel consumption, subject to safe and physical constraints. The optimal control-based approach takes downstream vehicle queues into account and can be applied not only at an isolated signalized intersection but on urban arterials as well. The proposed control approach is applied to design the controller, the performance of which is verified by simulation with multiple intersections and downstream vehicle

queues. Simulation results show that the proposed control system is able to achieve control objectives and satisfy constraints.

However, this approach treats the red phases as position constraints without tracking the vehicle in front with desired gaps, and consequently cost weights are required to be selected carefully to avoid unexpected trajectories such like vehicles stop far away from the stop bar to save fuel.

In the next chapter, a platoon trajectory control approach under actuated signal plans will be proposed to improve this limitation in Chapter 2.

Chapter 3

Trajectory optimization under the actuated signal

In this chapter, a platoon trajectory control approach using model predictive control is proposed for cooperative (automated) vehicles under exogenous actuated signals. Real-time signal phase and timing information is available to the platoon Infrastructure-to-Vehicle communication. This control approach optimizes acceleration trajectories of the controlled CAV platoon along a corridor with signalized intersections. The objectives of the proposed approach are to maximize the throughput first, and optimize comfort, travel delay and fuel consumption simultaneously after that. Safety is included by penalizing smaller gaps between CAVs in the running cost. The red phases are represented by virtual vehicles at the stop-line during the red time to force stopping vehicles to decelerate using the safe gap penalty. The acceleration and speed are constrained within the upper and lower bounds. The proposed approach is flexible in dealing with platoon merging, splitting, stopping, and queue discharging maneuvers at signalized intersections. Finally, the proposed approach is verified by simulation under five scenarios, considering a variety of pre-timing and actuated signal settings with/without anticipating red phases. The simulation results show the benefits of the proposed approach in fuel savings, compared with the state-of-the-art approach which used the virtual vehicle term without anticipation. The adjustments of signal parameters in Scenario 3 and 4 demonstrate the applicability of the MPC approach under actuated signals.

This chapter is an adapted version of the journal paper:

Liu, M., Hoogendoorn, S. and Wang, M., 2020. Receding horizon cooperative platoon trajectory planning on corridors with dynamic traffic signal. Transportation Research Record, 2674(12), pp.324-338.

3.1 Introduction

Although considerable amount of work has been done to mitigate urban congestion, traffic delays are still urgent problems on urban roads (Ubiergo & Jin, 2016). In addition, the deceleration and acceleration maneuvers of traditional vehicles in the vicinity of signalized intersections produce high levels of emissions (Li et al., 2011). The current advances in connected and automated vehicle (CAV) technology have the potential to operate vehicles in an efficient, safe and environmental-friendly way (Wang et al., 2014a). CAVs can exchange information under Vehicle-to-Vehicle (V2V) and Vehicle-to-Infrastructure (V2I) communication, which provides possibilities for anticipation and cooperative driving (Guanetti et al., 2018). Thus, numerous research efforts have been conducted to improve traffic operations by using CAV technologies at signalized intersections (Wang et al., 2018).

Current literature on CAV platooning on urban roads can be categorized into four directions, i.e., driver assistant systems, cooperative vehicle intersection control algorithms, CAV trajectory optimization, and the integrated optimization of traffic signals and vehicle trajectories.

Driver assistant systems, such as GLOSA (Green Light Optimized Speed Advisory) (Stevanovic et al., 2013; Li et al., 2014a; Stebbins et al., 2017) and Eco-Approach and Departure systems (Altan et al., 2017; Hao et al., 2018; Wang et al., 2019), are able to provide speed advice to drivers at signalized intersections for eco-driving. The purpose of these systems was to operate vehicles in such a way that vehicles arrived at the stop bar in green phases without stop by calculating the advisory speed based on the predefined rules. Therefore, the travel time and the fuel consumption were reduced at signalized intersections for the single subject vehicle. Although the further applications of actuated signal plans, market penetration rates and the extension to multiple intersections were studied in Stevanovic et al. (2013); Hao et al. (2018); Wang et al. (2019), the traffic and vehicle dynamics models were usually oversimplified, making the results less convincing. Furthermore, the drivers may not comply with the advisory speed and may not control the vehicle speed perfectly as suggested in reality, so the effects of these systems were required to be validated in field experiments. The empirical validation was only tested in few studies (Bodenheimer et al., 2014; Altan et al., 2017). In addition, these systems were designed only for the individual vehicle benefits, rather than the benefits of the platoon or the traffic flow.

A cooperative vehicle intersection is a “signal-free” intersection which

enables the CAVs to communicate with each other and thereby pass the intersection cooperatively without collision (Lee & Park, 2012). Although these intersection control algorithms had the potential to improve the traffic operations of CAVs at a typical four-arm intersection (Ahmane et al., 2013; Lee et al., 2013a; Zohdy & Rakha, 2016; Yu et al., 2019) or along a corridor (Lee et al., 2013b), the driver/user acceptance in relation to safety perception and potential conflicts of pedestrians and bicyclists were neglected, which questions the applicability of this line of research in reality.

With respect to the CAV trajectory optimization by controlling speeds or acceleration rates at fixed-timing intersections, some CAV trajectory control approaches at isolated intersections only applied simple objective functions to optimize the energy consumption and/or ride comfort (Zhao et al., 2018; Jiang et al., 2017). These control algorithms used terminal costs to represent the red phase, assuming that the terminal conditions (time and position) were known at an isolated intersection. However, terminal costs are confined to be applicable at isolated intersections, because it is difficult and suboptimal to combine intersections along an arterial using terminal costs. Several instantaneous fuel consumption and/or emission models (Akcelik, 1989; Rakha et al., 2004; Kamal et al., 2011) were adopted in these control approaches to minimize the fuel usage, or to validate the reduction of fuel consumption and emission in simulation. More sophisticated systems on corridors with multiple pre-timing intersections were designed for an individual vehicle considering multiple criteria (Asadi & Vahidi, 2010; Kamal et al., 2012; He et al., 2015; Wan et al., 2016; HomChaudhuri et al., 2016; Liu et al., 2019). The key in the control design was how to make vehicles stop facing the red phase.

Generally, there are three approaches to represent the red phase, i.e., using the virtual vehicle, tracking the target speed, and constraining the position. The first approach was to apply a virtually preceding vehicle at the stop bar representing the red phase. Together with the safe gap requirement, the followers behind the virtual vehicle were able to stop in order to keep the safe gap with the virtual vehicle. The control approach in Asadi & Vahidi (2010) considered the red phases in constraints by introducing a virtual vehicle in front, but the signal information was implemented with no prediction. The second approach aimed to track the piecewise target speed (including desired deceleration rates/speeds) facing the red phases (Kamal et al., 2012; He et al., 2015; Wan et al., 2016; HomChaudhuri et al., 2016). To track the pre-defined target speed would produce large decelerations once the vehicle

was recognized to miss the green phase, and then accelerate dramatically at the beginning of the next green phase. Therefore, more attention should be paid to design the target speed in an optimal way, and relieve computational burden when tracking the piecewise target speed cost term. The last approach was to regard the red phases as position constraints that the stopping vehicles could not pass (Liu et al., 2019). However, this work was not tracking the preceding vehicles in desired gaps. Therefore, elaborate work on tuning cost weights was necessary to make a trade-off between maximizing speeds and minimizing fuel consumption. Otherwise, the vehicles might stop far away from the stop bar to save fuel.

There were also research interests focusing on the integrated optimization of adaptive traffic signals and vehicle trajectories in a unified framework (Yu et al., 2018; Xu et al., 2018; Feng et al., 2018). The platoons were designed to decelerate but not stop when approaching the intersection during the red phase. However, these control algorithms were designed to optimize simple objective functions of the platoon leader in the vicinity of an isolated intersection for relieving computational load.

From the discussion above, it can be concluded that most current approaches only optimize the trajectories of an individual vehicle using simple objective functions of a few criteria. In addition, it is evident that the existing optimization-based control algorithms under traffic signals mostly focus on design for pre-timing signals, and the current approach to treat the red phases using the piecewise target speed term may result in computational issue. The previous work in Chapter 2 was designed for an arterial by optimizing throughput, ride comfort, travel delay and fuel savings. However, the previous control system was open-loop based on the feed-forward optimal control, and thereby was restricted in fixed-timing signal plan. One advantage of closed-loop control systems over open-loop systems is the fact that the use of feedback allows the system to be insensitive to both external disturbances and internal variations in system parameters (Åström & Murray, 2010), such as changes in signal settings. Although the control approaches allow for system feedback in (Zhao et al., 2018; Asadi & Vahidi, 2010; Kamal et al., 2012; HomChaudhuri et al., 2016), they did not take advantage of it and were thereby confined to pre-timing signals. The reason is that signal information in these approaches is an input when tracking the pre-defined target speed, which excludes signal changes within the control systems. In order to include the actuated signal plan, a closed-loop system is developed to overcome the limitations of open-loop systems. The feedback at each

time step in the closed-loop can re-plan the trajectories under actuated or semi-actuated signals. In addition, the work in Chapter 2 required elaborate work on tuning cost weights to avoid stopping away from the stop-line. An improvement to address the problem is to transform the red phase position constraint to a penalty term and add a desired gap term in the running cost.

In this chapter, a model predictive control (MPC) framework is proposed for urban corridors to overcome the aforementioned limitations of platoon trajectory control approaches. The proposed MPC framework is efficient on computational time using an iterative Pontryagin Maximum Principle (iPMP) approach (Hoogendoorn et al., 2012). An optimal platoon trajectory control algorithm is presented by optimizing accelerations of the controlled CAV platoon. The control algorithm determines the optimal throughput first, and then optimizes multi-criteria including ride comfort (by minimizing accelerations), average travel delay (by maximizing vehicle speeds), safe space gap, and fuel consumption rates, subject to admissible constraints on acceleration and speed. Safety requirements are incorporated by stimulating the inter-vehicle distances larger than the minimum safe gap as a penalty term in the running cost. The red phases are represented by introducing virtual vehicles at the stop bars during the red phases, so the stopping vehicles can avoid departure in red time using the safe gap penalty with the virtual vehicles. The red phases are designed with anticipation by updating the cost terms in the running cost at the beginning of the current signal cycle. The proposed control approach is flexible in accounting for platoon dynamics of merging, splitting, stopping, and queue discharging along a corridor with multiple intersections. The proposed trajectory control approach is not restricted to fixed signal timing. It also works under the actuated signal plan by updating the signal parameters in the closed loop, which reveals the flexibility of the control approach under different signal control approaches. Finally, the performance of the proposed control algorithm is verified by simulation using four scenarios and a baseline scenario, taking the signal settings and the anticipation time of the red phases into account.

The remainder of Chapter 3 is organized as follows: the following section introduces the control formulation for longitudinal driving task, followed by the experiment design and analysis of the simulation results. We conclude the study in the final section.

3.2 Control formulation

The longitudinal platoon control problem is formulated in this section, including control problem, control objectives and constraints, system dynamics, controller formulation, running cost specification, derivation of the optimal control input and solution approach.

3.2.1 Control problem

100% CAV environment and exogenous signal parameters are considered to demonstrate the workings of the proposed algorithm. It is assumed that Signal Phasing and Timing (SPaT) information is available for the platoon controller under Infrastructure-to-Vehicle (I2V) communication, and CAVs can communicate with each other and be controlled via accelerations. The actuator lag and the sensor delay are not considered. Merging behaviors from side streets or adjacent lanes are not taken into account.

The statement of the control problem can be described as a CAV platoon traveling on the corridor with multiple intersections where downstream CAVs are queuing behind the stop-lines. The platoon trajectory control system will be activated if the platoon leader reaches the control zone (e.g., 200 meters upstream of the stop-line at the upcoming intersection). The control objective is to determine the accelerations of the CAV platoon and CAVs in the queue in order to fulfil control objectives and constraints. The maximal throughput is pre-determined, which will be detailed in the forthcoming subsection.

3.2.2 Control objectives

The control design is expected to fulfil (a trade-off between) the following control objectives.

1. To maximize the throughputs during the (remaining) green phases
2. To maximize the ride comfort (by minimizing accelerations)
3. To minimize the travel delay (by maximizing vehicle speeds)
4. To minimize the fuel consumption
5. To maintain the safe gap with the preceding vehicle

6. To decelerate or even stop confronting the red phases if unable to pass the intersection

The throughput is optimized first by determining the maximal number of vehicles that are able to pass the intersection during the green phase. The reason for that is to confirm the first-stopping vehicle facing the red phase, and then the red phase term of the sixth objective will be applied to the first-stopping vehicle.

3.2.3 System dynamics model

To describe the longitudinal dynamics model, a second-order model is proposed in this subsection. The control input variable $\mathbf{u}$ is the acceleration, $u_i(t)$. i $(1 \leq i \leq N)$ denotes the vehicle sequence number on a single lane, and N is the total vehicle number in the controlled platoon. State variables $\mathbf{x}$ are considered as the longitudinal position, $x_i(t)$, and the speed, $v_i(t)$, of the controlled vehicle i. The control and state variables can be defined as:

$$\mathbf{u} = (u_1, ..., u_i ..., u_N)^{\mathrm{T}} \tag{3.1}$$

$$\mathbf{x} = (\mathbf{x}_1, ..., \mathbf{x}_i ..., \mathbf{x}_N)^{\mathrm{T}} \tag{3.2}$$

$$\mathbf{x}_i(t) = \begin{pmatrix} x_i(t) \\ v_i(t) \end{pmatrix} \tag{3.3}$$

The longitudinal dynamics model is described by the following ordinary differential equation:

$$\frac{\mathrm{d}}{\mathrm{d}t}\mathbf{x}_i(t) = \frac{\mathrm{d}}{\mathrm{d}t}\begin{pmatrix} x_i(t) \\ v_i(t) \end{pmatrix} = \mathrm{f}(\mathbf{x}_i, \mathbf{u}_i) \tag{3.4}$$

$$\mathrm{f}(\mathbf{x}_i, \mathbf{u}_i) = A\mathbf{x}_i + B\mathbf{u}_i \tag{3.5}$$

where

$$A = \begin{bmatrix} 0 & 1 \\ 0 & 0 \end{bmatrix}; B = \begin{bmatrix} 0 \\ 1 \end{bmatrix}$$

3.2.4 Controller formulation and running cost specification

If q_j (veh) denotes the maximal number of vehicles able to pass the jth intersection, the cost function J of the control system can be formulated as the following:

$$\min_{\mathbf{u},q_j} J\left(\mathbf{x},\mathbf{u},t,q_j\right) = \min_{\mathbf{u},q_j} \int_0^{T_p} L\left(\mathbf{x},\mathbf{u},t,q_j\right) + G\left(\mathbf{x}\left(T_p\right)\right) \mathrm{d}t \tag{3.6}$$

subject to

1. the system dynamics model of Equation 3.4
2. the initial condition: $\mathbf{x}(\mathbf{0}) = \mathbf{x_0}$
3. the constraints on state and control variables: $\mathbf{x}(t) \in \mathbf{X}$, $\mathbf{u}(t) \in \mathbf{U}$, $t \in [0, T_p]$

where L denotes the running cost and G denotes the terminal cost at the end of the prediction horizon T_p. Although the terminal cost function has an influence on the controller stability and performance, a longer prediction horizon can compensate this impact of G at the cost of computational load (Wang et al., 2012). The terminal cost G (=0) and an appropriate prediction horizon are chosen in this work to guarantee the controller performance. Noteworthy is the fact that the maximal throughput q_j can be pre-determined before the final optimal solution. The value of q_j can be maximized beforehand based on the optimal position trajectory $x_i(t)$ when removing the red phase penalty in the control objectives. In other words, the last vehicle that can depart the jth intersection during the green time is pre-determined as the q_jth vehicle. Here, the first vehicle unable to pass and behind the q_jth vehicle is defined as the first-stopping vehicle ($i = q_j + 1$) at the jth intersection.

In this control design, the running cost of vehicle i, L_i (a constituent of L), is defined as follows (the time t is omitted in order to simplify equations):

$$\begin{aligned} L_i\left(\mathbf{x}_i,\mathbf{u}_i,t,q_j\right) &= \beta_1 {u_i}^2 - \beta_2 v_i + \beta_3 \tfrac{(v_{i-1}-v_i)^2}{x_{i-1}-x_i-l_i} \\ &+ \beta_4 (x_{i-1} - x_i - v_i t_{\min} - s_0 - l_i)^2 + \beta_5 f_v(u_i, v_i) + \beta_6 \tfrac{\left(v_j^{\mathrm{vir}} - v_{q_j+1}\right)^2}{x_j^{\mathrm{vir}} - x_{q_j+1}} \end{aligned} \tag{3.7}$$

$$L\left(\mathbf{x},\mathbf{u},t,q_j\right) = \sum_{i=1}^{N} L_i\left(\mathbf{x}_i,\mathbf{u}_i,t,q_j\right) \tag{3.8}$$

Here, l_i denotes the length of vehicle i, $t_{\min}$ denotes the minimum safe car-following time gap, and s_0 is the minimum space gap at standstill conditions. Turning vehicles to leave intersections can be included in the control approach by setting different values of $t_{\min}$ for different turning movements. To represent the red phase, a virtual standstill vehicle is introduced in the last term of the running cost. v_j^{vir} (=0) and x_j^{vir} are the speed and the position of the virtual vehicle at the jth intersection respectively. β_1, β_2, β_3, β_4, β_5, β_6 are cost weights.

The first cost term in the running cost is designed to maximize ride comfort by minimizing accelerations. The second cost term in the running cost is to maximize speeds in order to minimize travel delay. The third cost term is to track the preceding vehicle and consider the safety as a large penalty if the distance to the predecessor is short. The fourth cost term implies that the gap is stimulated to follow the desired time gap, $t_{\min}$. The fifth cost term represents the minimization of fuel consumption. The last cost term is designed only for the first-stopping vehicle at the jth intersection ($i = q_j + 1$) during the red phase. This term renders the stopping vehicles stay behind the stop-line using the safe gap penalty with the virtual vehicle.

In the fifth term, f_v is the instantaneous fuel consumption rate (ml/s). Detailed parameter values can be found in Kamal et al. (2011). Although f_v is optimized to approach zero accelerations and speeds, other criteria in the running cost trade off with the fuel consumption term to generate optimal trajectories in the vicinity of signalized intersections. For typical vehicles on a flat road, f_v (ml/s) can be estimated as (omitting the time t)

$$f_v = \begin{cases} b_0 + b_1 v + b_2 v^2 + b_3 v^3 + u\left(c_0 + c_1 v + c_2 v^2\right) & u > 0 \\ b_0 + b_1 v + b_2 v^2 + b_3 v^3 & u \leq 0 \end{cases} \tag{3.9}$$

It should be noted that the running cost in Equation 3.7 is a piecewise function according to the vehicle sequence in the platoon, see Equation 3.10. The running cost is categorized into three modes for better illustration, i.e., the leading mode, the following mode, and the first-stopping mode. Leading mode is designed for the platoon leader ($i = 1$), so the third and fourth (safe following and desired time gap) cost terms vanish owing to no preceding vehicle ahead. Following mode is used for the following vehicles, so the sixth (virtual vehicle) term is removed. First-stopping mode is used for the first-stopping vehicle ($i = q_j + 1$), which engages in avoiding collision with the virtual vehicle and anticipating signals facing the red phase, so the fourth

(desired time gap) term is unnecessary.

$$L_i = \begin{cases} \beta_1 {u_i}^2 - \beta_2 v_i + \beta_5 f_v(u_i, v_i) & i = 1 \\ \beta_1 {u_i}^2 - \beta_2 v_i + \beta_3 \frac{(v_{i-1}-v_i)^2}{x_{i-1}-x_i-l_i} + \beta_5 f_v(u_i, v_i) + \beta_6 \frac{\left(v_j^{\text{vir}}-v_i\right)^2}{x_j^{\text{vir}}-x_i} & i = q_j+1 \\ \beta_1 {u_i}^2 - \beta_2 v_i + \beta_3 \frac{(v_{i-1}-v_i)^2}{x_{i-1}-x_i-l_i} + \beta_5 f_v(u_i, v_i) & \text{others} \\ \quad + \beta_4 (x_{i-1} - x_i - v_i t_{\min} - s_0 - l_i)^2 & \end{cases} \tag{3.10}$$

The piecewise running cost of Equation 3.10 can be implemented by updating cost weights, i.e., $\beta_3 = 0$ when $i = 1$, $\beta_4 = 0$ when $i = 1$ and $i = q_j + 1$, and $\beta_6 = 0$ when $i \neq q_j + 1$. In this way, the switch between the leading mode (β_3 and β_4), the first-stopping mode (β_4) and the following mode (β_6) is achieved. Hereinafter, the running cost of Equation 3.7 is still applied but the cost weights of β_3, β_4, and β_6 are replaced using $\hat{\beta}_3$, $\hat{\beta}_4$, and $\hat{\beta}_6^{q_j+1}$ as follows.

$$\hat{\beta}_3 = \begin{cases} \beta_3 & i \neq 1 \\ 0 & \text{others} \end{cases}, \hat{\beta}_4 = \begin{cases} \beta_4 & i \neq 1, q_j+1 \\ 0 & \text{others} \end{cases}, \hat{\beta}_6^{q_j+1} = \begin{cases} \beta_6 & i = q_j+1 \\ 0 & \text{others} \end{cases} \tag{3.11}$$

Assuming the signal cycle starts from the green phase, all cost weights can remain unchanged within the cycle. This is beneficial to apply the proposed control approach under actuated signal plan because the red and green phase lengths are flexible during a signal cycle.

3.2.5 Derivation of the optimal control input

Hereafter, the control problem is solved based on Pontryagin Maximum Principle (PMP). Without providing too much detail, the Hamiltonian H is defined as follows (t is again omitted):

$$\begin{aligned} &H_i\left(\mathbf{x}_i, \mathbf{u}_i, \lambda, t, q_j\right) = L_i\left(\mathbf{x}_i, \mathbf{u}_i, t, q_j\right) + \lambda_i \mathbf{f}_i(\mathbf{x}_i, \mathbf{u}_i, t) \\ &= \beta_1 {u_i}^2 - \beta_2 v_i + \hat{\beta}_3 \frac{(v_{i-1}-v_i)^2}{x_{i-1}-x_i-l_i} + \hat{\beta}_4 (x_{i-1} - x_i - v_i t_{\min} - s_0 - l_i)^2 \\ &+ \beta_5 f_v(u_i, v_i) + \hat{\beta}_6^{q_j+1} \frac{\left(v_j^{\text{vir}}-v_{q_j+1}\right)^2}{x_j^{\text{vir}}-x_{q_j+1}} + \lambda_i^1 v_i + \lambda_i^2 u_i \end{aligned} \tag{3.12}$$

where λ denotes the co-state of the system:

$$\lambda_i(t) = \begin{pmatrix} \lambda_i^1(t) \\ \lambda_i^2(t) \end{pmatrix} \tag{3.13}$$

Thus, the optimal control law can be obtained according to the necessary condition for the optimal control law using Hamiltonian. Therefore, the optimal control law can be described as:

$$u_i^* = \begin{cases} -\frac{\lambda_i^2 + \beta_5\left(c_0 + c_1 v_i + c_2 v_i^2\right)}{2\beta_1} & \lambda_i^2 < -\beta_5\left(c_0 + c_1 v_i + c_2 v_i^2\right) \\ -\frac{\lambda_i^2}{2\beta_1} & \text{otherwise} \end{cases} \tag{3.14}$$

In order to simplify the piecewise feature of the instantaneous fuel consumption model f_v, the Heaviside function h is introduced:

$$h(n) = \begin{cases} 1 & n > 0 \\ 0 & n \leq 0 \end{cases} \tag{3.15}$$

In Equation 3.15, the Heaviside function value is zero for negative and zero arguments ($n \leq 0$), and holds for one under positive arguments ($n > 0$). The co-state dynamics are thereby derived as:

$$\begin{aligned} -\frac{\mathrm{d}\lambda_i^1}{\mathrm{d}t} &= \frac{\partial H}{\partial x_i} = \hat{\beta}_3 \frac{(v_{i-1} - v_i)^2}{(x_{i-1} - x_i - l_i)^2} - 2\hat{\beta}_4 \left(x_{i-1} - x_i - v_i t_{\min} - s_0 - l_i\right) \\ &+ \hat{\beta}_6^{q_j+1} \frac{\left(v_j^{\mathrm{vir}} - v_{q_j+1}\right)^2}{\left(x_j^{\mathrm{vir}} - x_{q_j+1}\right)^2} \end{aligned} \tag{3.16}$$

$$\begin{aligned} -\frac{\mathrm{d}\lambda_i^2}{\mathrm{d}t} &= \frac{\partial H}{\partial v_i} = -\beta_2 - 2\hat{\beta}_3 \frac{v_{i-1} - v_i}{x_{i-1} - x_i - l_i} - 2\hat{\beta}_4 t_{\min} \left(x_{i-1} - x_i - v_i t_{\min} - s_0 - l_i\right) \\ &+ \beta_5 \left(b_1 + 2b_2 v_i + 3b_3 v_i^2 + u_i h(u_i)\left(c_1 + 2c_2 v_i\right)\right) - 2\hat{\beta}_6^{q_j+1} \frac{v_j^{\mathrm{vir}} - v_{q_j+1}}{x_j^{\mathrm{vir}} - x_{q_j+1}} + \lambda_i^1 \end{aligned} \tag{3.17}$$

3.2.6 Controller constraints

The control problem should respect some constraints on control and state variables. Admissible acceleration is restricted between the maximum acceleration, $a_{\max}$, and the minimum (negative) acceleration, $a_{\min}$. Speed should be lower than the limit speed, $v_{\max}$, but nonnegative.

$$a_{\min} \leq u_i(t) \leq a_{\max} \tag{3.18}$$

$$0 \leq v_i(t) \leq v_{\max} \tag{3.19}$$

3.2.7 Solution approach

An iterative Pontryagin Maximum Principle (iPMP) solution approach is applied to solve this control problem, referring to Appendix and Hoogendoorn et al. (2012); Wang et al. (2014b) for details. The continuous-time control problem is discretized in time within the prediction horizon in terms of the control and co-state variables. The iPMP approach solves the state and co-state dynamics forward and backward in time respectively, and then updates the co-state dynamic with a weight factor. The updated co-state will be imported to the next iteration as an input. The optimization converges if the error between the state and co-state dynamics is smaller than the pre-defined threshold, and then the iteration stops. The illustration of the solution approach is depicted in Figure 3.1 .

The model predictive control (MPC) framework is applied, which solves the control problem in a shorter horizon than the optimal control framework in Chapter 2. This shorter horizon of the MPC framework results in an efficient computational time. The MPC framework only selects the first time step of the optimal solution in the iPMP algorithm. The constraints on control and state variables are implemented on restricting control variables based on system dynamics.

Platoon dynamics of merging, splitting, stopping, and queue discharging along a corridor are achieved by switching three modes of the running cost (updating the values of cost weights), which is included within the MPC closed-loop at every time step. In presence of signal anticipation, the red phases can be anticipated by implementing the virtual vehicle term as early as possible, i.e., at the beginning of the current signal cycle or at the moment when the platoon controller receives the updated actuated signal plan. MPC framework allows for system feedback, i.e., signal changes, so actuated signal settings can be incorporated in the MPC closed-loop. In addition to signal anticipation, the signal settings (the green and red time) can be updated in the MPC closed-loop by switching the cost weights in response to the actuated signals. Therefore, this approach can also be applied under the actuated signal control approach.

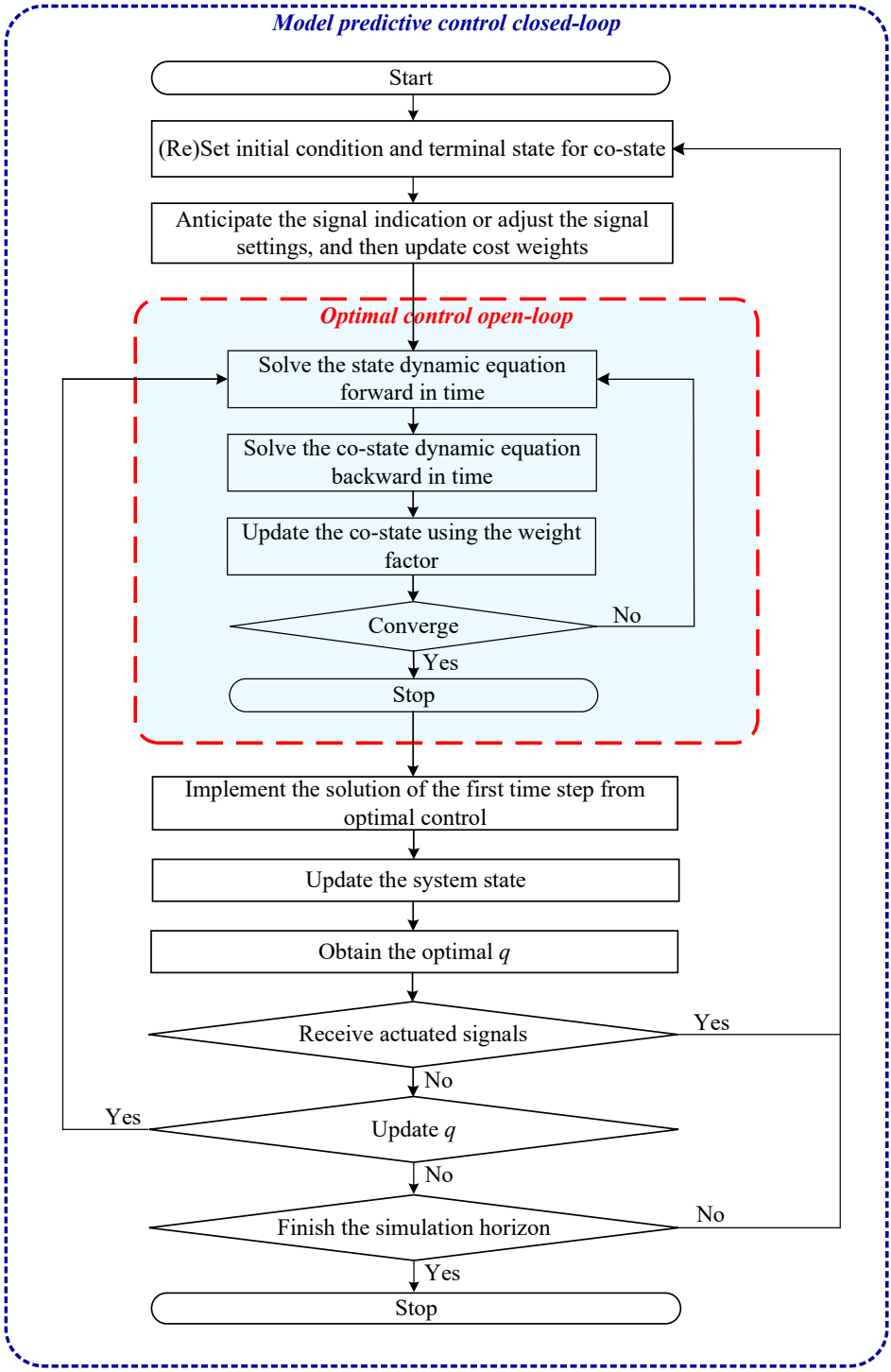

Figure 3.1: Illustration of the solution approach

3.3 Simulation results and analysis

This section verifies the platoon performance of this control algorithm under four scenarios, considering the signal settings and the anticipation time of the red phases. Furthermore, a baseline scenario is presented for comparison.

3.3.1 Experiment design

In order to test the behaviors of the platoons resulting from the proposed control approach, trajectories on a corridor with two signalized intersections are simulated, taking into account the signal settings, the lane length between two adjacent intersections, the speed limit, the numbers of vehicles in the controlled platoon and in the queue. Four scenarios and a baseline scenario are designed to verify the characteristics of platoon splitting, merging, decelerating, accelerating, stopping and queue discharging. The control effects on the fuel savings are revealed by comparing the total fuel consumption of all controlled vehicles within the simulation horizon. Hereinafter, the intersection in the upstream direction on the arterial is referred as the upstream intersection, and the intersection in the downstream direction is considered as the downstream intersection.

Two pre-timing signal settings are designed to test the workings of the red phase term, i.e., the opposite and overlapped signal settings, as shown in Figure 3.2. The effective green phase lengths in both settings are 30 s, and the effective red phase lengths are 30 s and 20 s respectively. Therefore, the simulation horizon lengths are 90 s and 80 s in the opposite and the overlap signal settings. The prediction horizon length is selected to be 10 s, because the influence of the zero terminal cost is negligible with respect to 5 s and larger prediction horizon (Wang et al., 2012).

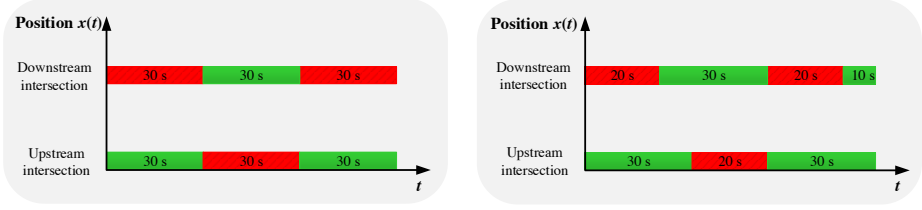

(a) opposite signal setting (b) overlap signal setting

Figure 3.2: Design of signal settings

In reality, the communication ranges of I2V and V2V are about 200 meters, so the control zone starts from 200 m away from the stop bar in the upstream direction at the upstream intersection. The longitudinal position of the stop-line at the upstream intersection is defined as 0. The lane section length between two adjacent intersections is designed as 800 m, so the longitudinal position of the stop-line at the downstream intersection is 800.

In order to test the performance of different signal settings and the anticipation time of the red phases, four scenarios and a baseline scenario are designed aiming to verify the feasibility of the platoon trajectory control approach regarding the applications on an arterial with intersections. The characteristics of platoon splitting, merging, decelerating, accelerating, stopping and queue discharging in all the scenarios provide insights into the effectiveness of the control approach. The benefits on fuel savings are explored in all scenarios. Similar settings (e.g., the number of controlled vehicles, vehicle queues, the number of multiple intersections and the signal timing plans) can be implemented easily in the same way. The cost weights are tuned in Scenario 1 and then are applied in other scenarios. The parameter values in the simulation experiments are detailed in Table 3.1. The choices for the parameter values mostly come from Chapter 2. In our experiment settings, the time step is 1 s, which means delays under 1 s have no effect on the optimal trajectories.

The baseline scenario is presented under the opposite signal setting without anticipating the red phase. Removing the anticipation of the red phases means the virtual vehicle term is added just at the beginning of the red phase. The objective of this baseline scenario is to obtain insights of the validity of the red phase (virtual vehicle) term, which is similar to the application in the previous work of Asadi & Vahidi (2010).

However, the anticipation time of the red phases is the implemented at the beginning of the current signal cycle in Scenario 1 to Scenario4. Anticipating the red indication before the start of the red phases is supposed to outperform the baseline scenario where no anticipation exists (e.g., save more fuel). Scenario 1 is simulated under the pre-timing opposite signal setting. The comparison between the baseline scenario (no anticipation) and Scenario 1 (anticipation from the beginning of the current signal cycle) can explore the benefits of anticipating the red phases in the proposed control approach. Scenario 2 is designed under the pre-timing overlapped signal setting, the objective of which is to prove the workings of the adjustment in signal settings under pre-timing signal control approach.

Table 3.1: Parameter and coefficient values

Notation	Parameter/ Coefficient	Value	Unit
-	time step	1	s
-	prediction horizon	10	s
-	the effective green phase length	30	s
-	the effective red phase lengths	20, 30	s
-	initial speed	0, 15	m/s
-	initial space gap in the nonstatic platoon	35	m
-	initial space gap in vehicle queues	5	m
-	the range of the control zone at the upstream intersection	200	m
-	vehicle queues at the upstream intersection	3	veh
-	the number of vehicles on the lane section between two intersections	8	veh
N	the number of total controlled vehicles	25	veh
Y_j	the position of the stop lines at intersections	0, 800	m
l_i	length of every controlled vehicle	3	m
$t_{\min}$	minimum safe car-following time gap	2	s
s_0	minimum space gap at standstill conditions	2	m
$v_{\max}$	limit speed on the urban corridor	20	m/s
$a_{\max}$	allowable maximum acceleration	2	m/s^2
$a_{\min}$	allowable minimum acceleration	-5	m/s^2
β_1	cost weight	1	-
β_2	cost weight	1	-
β_3	cost weight	1	-
β_4	cost weight	1	-
β_5	cost weight	5	-
β_6	cost weight	5	-

Scenario 3 and 4 include the actuated signals in the MPC closed-loop, aiming to investigate the workings of the proposed control approach under the actuated signals assuming the platoon controller receives the actuated signal plan after the first prediction horizon, i.e., 10 s after the beginning of the signal cycle. In Scenario 3, the green phase lengths increase 5 s and the red phase lengths decrease 5 s based on the initial overlapped signal settings. Scenario 4 updates the signal plan based on the initial overlapped signal setting to reflect the vehicle actuation.

3.3.2 Platoon performance

The aforementioned scenarios are simulated to evaluate control effects based on trajectory analysis, as depicted in Figure 3.3 to Figure 3.7. The vehicle numbers in the legend represent the vehicle sequence of the platoon on a single lane. The horizontal red dashed lines in these figures show the red signal indication at intersections. The longitudinal positions of the stop-line at the upstream and downstream intersections are 0 and 800 respectively. The initial conditions at the beginning of the simulation are as follows: the first eight vehicles are set with initial speed (15 m/s) on the lane section between two adjacent intersections, after that three vehicles stop (0 m/s) at the upstream intersection, and the last 14 vehicles are traveling (15 m/s) from 200 m upstream direction of the upstream intersection (-200 m). The maximal throughputs are determined first for all scenarios when removing the red phase penalty, as discussed in Chapter 3.2.4. Overall, it is obvious that the safe gap penalty and the red phase penalty work, and the controller constraints are satisfied in all scenarios.

The remainder of this section analyzes the platoon performance and spacing gap in each scenario. The advantages of the proposed control approach are discussed in comparison to the baseline scenario.

Tuning cost weights

Firstly, the cost weights are tuned to gain insights of optimal trajectories based on Scenario 1. Considering $\beta_1 = 1$ as a baseline, the cost weight of speed, β_2, the cost weight of safe gap term, β_3, and the cost weight of the desired gap, β_4, keep the same order with the cost weight of acceleration β_1, thus $\beta_2 = \beta_3 = \beta_4 = \beta_1 = 1$. Bigger values of the fuel consumption cost weight, β_5, will result in lower accelerations and speeds, so the maximal throughput cannot be obtained via this overweighed β_5. The biggest value of β_5 (=5) is selected to avoid unnecessary deceleration. Smaller values of virtual vehicle cost weight β_6 are unable to act as the red phase, while vehicles will decelerate and stop near the initial position if β_6 is too large. The appropriate value of the red phase cost weight, $\beta_6 = 5$, is chosen such that vehicles stop just behind the stop-line during the red phase. The selected cost weight values are chosen in Scenario 1 and then applied in all scenarios.

Analysis of the baseline scenario

The baseline scenario provides no anticipation of the red phases under the opposite signal setting, and the optimal trajectories are presented in Figure 3.3. The vehicles in the queue at the upstream intersection (vehicle 9 to 11) start from 0 speed, while other vehicles begin with the initial speed of 15 m/s. Vehicle 1 to 12 that pass the downstream intersection and vehicle 9 to 20 that leave the upstream intersection accelerate till the limit speed $v_{\max}$, so the maximal throughput can be guaranteed. Vehicle 9 decelerates from 38 s to 43 s to keep the safe gap when merging with the preceding platoon. The same also holds for vehicle 12 from 10 s to 13 s.

Since the red phases are not anticipated, vehicle stops during the red traffic light cannot be avoided. The stopping vehicles can stop but with drastic decelerations at the beginning of the red phases (e.g., for vehicle 21 at 30 s and for vehicle 13 at 60 s). Vehicle 1 to 8 decelerate facing the red time and then accelerate suddenly at the beginning of the green phase, which causes more fuel consumption. The total fuel consumption of all vehicles within the simulation horizon is 1888.3 ml (0.0606 ml/m) in this baseline scenario.

Analysis of Scenario 1

Scenario 1 is simulated under the opposite signal setting but with anticipating the red phases at the beginning of the current signal cycle, as shown in Figure 3.4. Vehicle 9 and 12 still decelerate to keep the safe gap with the preceding vehicles while merging, as in the baseline scenario.

However, owing to the anticipation of the red phase starts/ends, two more vehicles are released at the downstream intersection when comparing Figure 3.3 with Figure 3.4. The fluctuations in accelerations and decelerations are smoother in Scenario 1 compared with the baseline scenario. In particular, the first-stopping vehicles (vehicle 15 and 21) react more predictively to the red phases and approach the stop-line slowly in comparison with the baseline scenario.

The differences in trajectory performance between the baseline scenario and Scenario 1 prove the benefits of anticipating the red phases in the proposed control approach. The sharp decelerations and stops facing the red phases are avoidable, and more fuel savings are verified in Scenario 1. The total fuel consumption of all vehicles is 1854.9 ml (0.0579 ml/m) in Scenario 1, which is 12% (calculated using milliliter per meter) smaller than the counterpart in the baseline scenario.

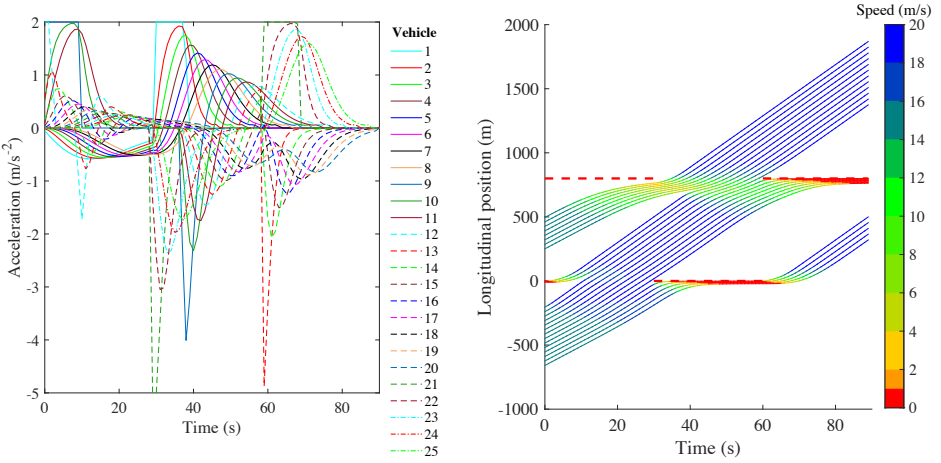

(a) acceleration (b) longitudinal position

Figure 3.3: Optimal trajectories of the baseline scenario

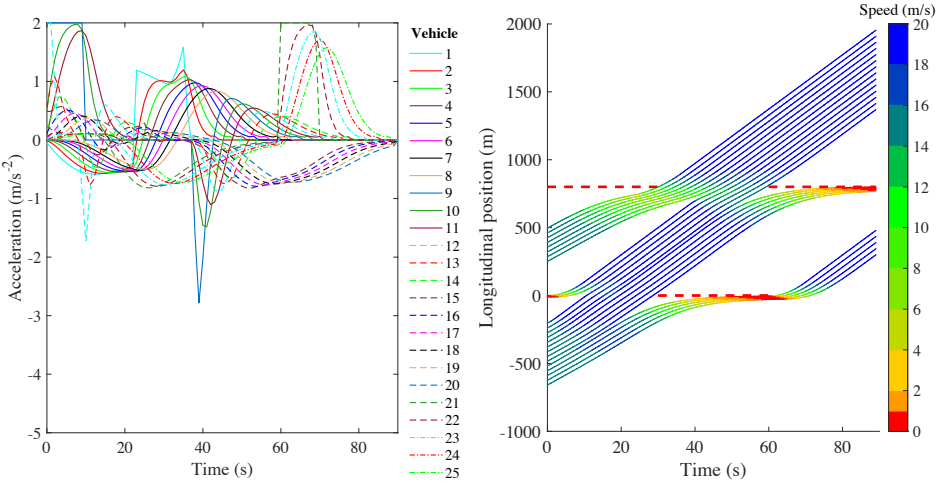

(a) acceleration (b) longitudinal position

Figure 3.4: Optimal trajectories of Scenario 1

Analysis of Scenario 2

The optimal trajectories of Scenario 2 under the overlapped signal setting are depicted in Figure 3.5. The trajectory performance in Scenario 2 have the same features as in Scenario 1. Therefore, Scenario 2 validates the flexibility of the control approach in changes of signal settings under the pre-timing

signal plan. The total fuel consumption of all vehicles are 1736.2 ml (0.0550 ml/m) in Scenario 2.

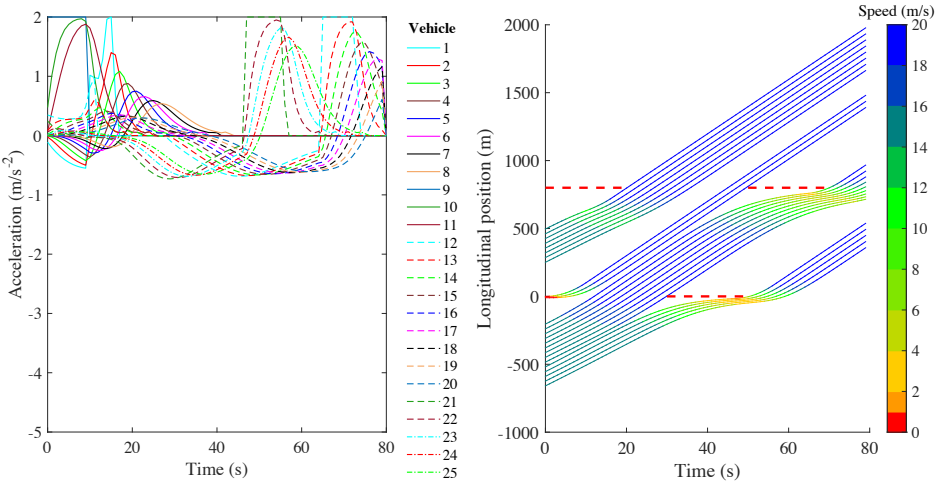

(a) acceleration (b) longitudinal position

Figure 3.5: Optimal trajectories of Scenario 2

Analysis of Scenario 3

Scenario 3 explores the potentials to implement the proposed approach under the actuated signal plan. The signal plan is the overlapped signal setting initially, and then is updated in the MPC closed loop after the first prediction horizon finishes (10 s). The lengths of green phases change with an increase of 5 s, and the lengths of red phases varies with a decrease of 5 s. The total fuel consumption of all vehicles is 1879.2 ml (0.0550 ml/m) in Scenario 3. The optimal trajectories depicted in Figure 3.6 prove the feasibility of the control approach in terms of application in actuated or adaptive signal plans.

Analysis of Scenario 4

Scenario 4 provides more insights for the proposed control approach being applied with the actuated signal approach. The initial signal plan is the overlapped setting, and then signal parameters are adjusted to accommodate changes in the traffic flow. At the downstream intersection, the red time starts from 0 s to 17 s and from 35 s to 59 s. At the upstream intersection, the red time starts from 27 s to 45 s and from 62 s to 80 s. The total fuel

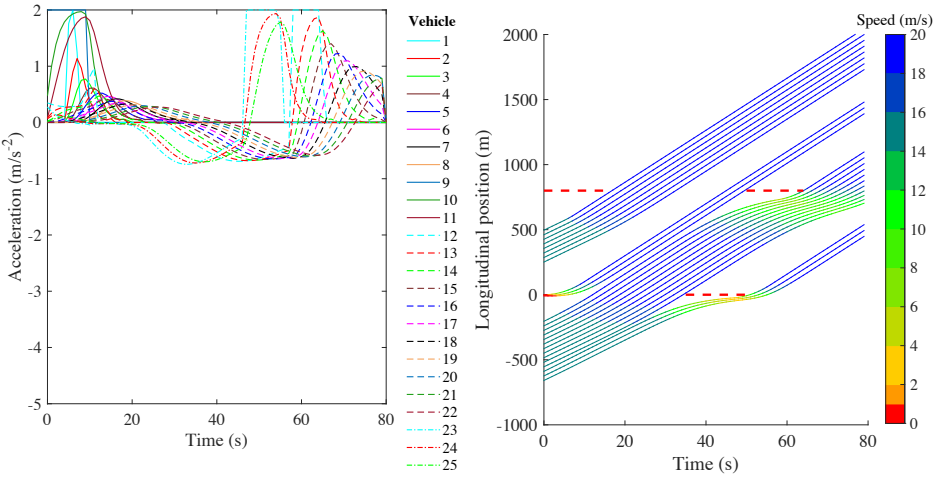

(a) acceleration (b) longitudinal position

Figure 3.6: Optimal trajectories of Scenario 3

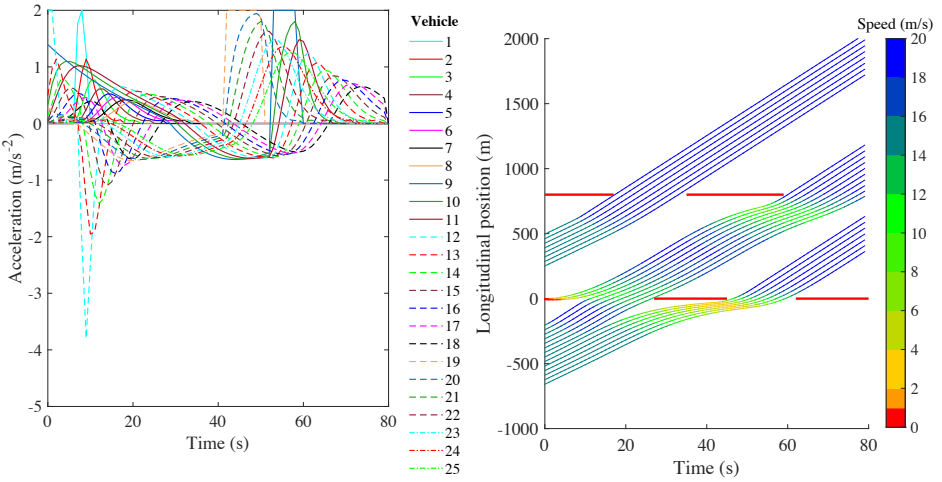

(a) acceleration (b) longitudinal position

Figure 3.7: Optimal trajectories of Scenario 4

consumption of all vehicles is 1885.1 ml (0.0592 ml/m) in Scenario 4. The optimal trajectories in Figure 3.7 further validate the workings under actuated signals.

Table 3.2: Vehicles sequence number considering splitting gaps and stopping gaps

Vehicle Type		First-stopping vehicle	Splitting gap	Stopping gaps
Downstream intersection	Scenario 1	V15	V14, V15	V15 to V20
	Scenario 2	V12	V11, V12	V12 to V20
	Scenario 3	V12	V11, V12	V12 to V22
	Scenario 4	V9	V8, V9	V9 to V18
Upstream intersection	Scenario 1	V21	V20, V21	V21 to V25
	Scenario 2	V21	V20, V21	V21 to V25
	Scenario 3	V23	V22, V23	V23 to V25
	Scenario 4	V19	V18, V19	V19 to V25

Analysis of spacing gap

The spacing gaps of all controlled vehicles can be categorized into four groups, i.e., the splitting gaps, the stopping gaps, the following gaps and the merging/catching gaps. The splitting gaps aim to reflect the increases in gaps resulted from the red indication, i.e., the gaps between the first-stopping vehicles and the immediately preceding vehicles. For other stopping vehicles behind the first-stopping vehicles, the stopping gaps can describe the gaps between two adjacent stopping vehicles. Table 3.2 details the vehicle sequence number (represented by V) regarding the first-stopping vehicles, the splitting gaps and the stopping gaps under four scenarios at two intersections. The following gaps account for gaps between vehicles that can pass the downstream intersection during the first green phase. The merging or catching gaps are proposed to capture declines in spacing owing to the signal settings and the initial position settings. The differences between the merging gaps and the catching gaps are whether the gaps drop into the following gaps within the horizon. It is noted that the merging/catching gap and the splitting gap may occur on a certain vehicle sequentially under different signal phases, e.g., in Scenario 2, Scenario 3 and Scenario 4.

In order to explore the performance of spacing, the gaps between two adjacent vehicles under four scenarios are illustrated in Figure 3.8. The vertical ordinates of the spacing subfigures are presented compactly in the way of logarithmic scale. Four spacing gap categories are depicted in different colors and line types. It can be concluded that the spacing gaps are in ac-

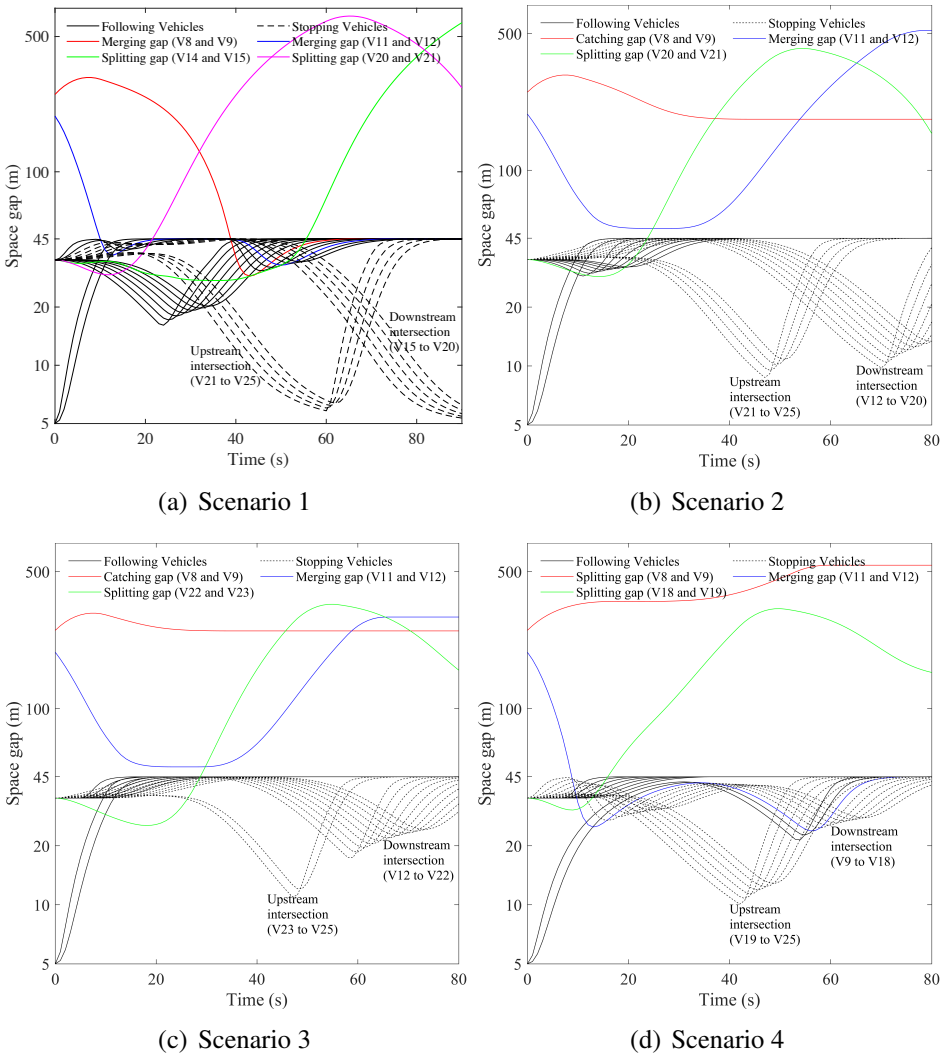

(a) Scenario 1 (b) Scenario 2

(c) Scenario 3 (d) Scenario 4

Figure 3.8: Spacing gap under four scenarios

cordance with the system design, because the space gaps satisfy the safe requirement over the simulation horizon in all scenarios, and the spacing gaps fluctuate with changes in splitting and merging performance and signal changes.

There are general characteristics in all scenarios. The initial space gaps are 5 meters for queuing vehicles at the standstill condition, and 35 meters for the nonstatic vehicles. The maximal following gap is 45 meters, which is calculated using $v_{\max} t_{\min} + s_0 + l_i$. Taking into account the speed constraint

which limits the controlled speeds being equal to or lower than the maximal speed, the following and stopping gaps cannot exceed the maximal following gap (45 m). The stopping gaps of stopping vehicles decline during the red phases at the upstream and downstream intersections, as the two declined trends of dashed lines in subfigures (a) to (d) of Figure 3.8. The depths of the declines in stopping gaps vary under different scenarios as a result of various red phase lengths. Longer red phase lengths, such as under pre-timing signals in Scenario 1 and 2, give rise to deeper drops. In addition, the merging gaps between vehicle 8 and 9 increase slightly at the beginning of the horizon in all scenarios, because vehicle 9 needs accelerations to pass the upstream intersection from the stationary condition while vehicle 8 is moving forward.

Taking Scenario 1 as example, the merging gaps between vehicle 8 and 9 and between 11 and 12 fall below the maximal following gap (45 m), which means vehicle 9 and 12 merge with the predecessors into platooning. As shown in the subfigure (a) of Figure 3.8, the splitting gap between vehicle 14 and 15 rises when vehicle 15 confronts the red indication at the downstream intersection. Vehicle 21 decelerates facing the red time at the upstream intersection, resulting in the splitting gap, and then accelerates to catch up with the vehicles in front during the subsequent green phase, causing the catching gap. Same explanation holds for other scenarios.

3.4 Conclusions and future work

In this study, a flexible CAV trajectory control approach is proposed on arterial with signalized intersections based on model predictive control framework. The throughput is firstly maximized during the green phase, and multiple criteria of ride comfort, travel delay, and fuel consumption are optimized after that, subject to linear constraints on acceleration and speed. The safe following requirement is formulated as a penalty in the running cost function to regulate vehicles to follow the predecessor at a safe gap . The red phases are represented by keeping the safe gap with a virtually stationary vehicle at the stop bar, and it can also be anticipated by the first-stopping vehicle since the beginning of the signal cycle. The control approach is flexible in incorporating platoon merging, splitting, stopping, and queue discharging characteristics. Simulation under four scenarios verified the performance of the approach.

The simulation results show that the red phase term with anticipation works better than the case where no anticipation is provided. The performance of the control approach also demonstrates its flexibility regarding application in different settings, i.e., changes in signal parameters under pretimed signal plan and actuated signal plan. Future work can be directed to remove the piecewise feature of the running cost function and the switch of cost weights.

In the next chapter, a bi-level control approach to optimize traffic signals and cooperative vehicle trajectories in a unified framework will be presented.

Chapter 4

A bi-level control approach of optimizing trajectories and signals

This chapter proposes a bi-level control approach for optimizing traffic signals and cooperative vehicle trajectories at urban intersections. The upper layer determines the optimal signal timing parameters using enumeration method, and the lower layer optimizes vehicle trajectories under each feasible signal plan. In the lower layer, the accelerations of the platoons are optimized considering ride comfort and travel delay, while satisfying physical motion constraints and safe driving requirements. The red phase is enforced as a logic constraint, which restricts vehicles to stay behind the stop-line during the red phase. Typical platoon maneuvers at intersections such as split, merge/approach, acceleration/deceleration can be included in the lower layer. The integrated control approach is adaptive to traffic demands, and is flexible in incorporating different traffic movements during multiple signal phases. Simulation is performed to verify the performance of the integrated control approach. Three scenarios are designed and simulated to demonstrate the advantages on throughput and fuel consumption, delay and vehicle stops, compared with two baseline scenarios of trajectory-only optimization and signal-only optimization respectively. Analysis of the simulation results reveals insights into the optimal patterns on signals and vehicle trajectories.

This chapter is an adapted version of the journal paper:

Liu, M., Zhao, J., Hoogendoorn, S. and Wang, M., 2021. An optimal control approach of integrating traffic signals and cooperative vehicle trajectories at intersections. Transportmetrica B. https://doi.org/10.1080/21680566.2021.1991505

4.1 Introduction

The suboptimal setting of traffic lights is considered to be one of the leading causes of travel delay as well as excessive fuel consumption and emissions on urban roads (Ubiergo & Jin, 2016). Considerable numbers of studies have been conducted to relieve this problem at urban intersections from design, control, and management perspectives (Zhao et al., 2020; Guler et al., 2014). Connected and automated vehicle (CAV) technology enables the roadside infrastructure to communicate with the onboard vehicle control algorithms (Wang et al., 2014a). The promise of further optimizing traffic conditions has led to a surge in the number of studies devoted to enhancing traffic operations at signalized intersections by improved and integrated design of traffic signals and/or CAV trajectories.

Four directions have been explored with respect to CAV platooning at urban intersections, i.e., cooperative intersection systems, speed advisory algorithms, CAV trajectory planning and the optimization of traffic signals and vehicle trajectories. The cooperative intersection algorithms develop a signal-free intersection to coordinate CAVs to depart the intersection without collision (Lee & Park, 2012; Ahmane et al., 2013; Lee et al., 2013a; Zohdy & Rakha, 2016; Yu et al., 2019), but the challenges of this line of research are how to consider the safety requirements of pedestrians and cyclists. Speed advisory systems such as GLOSA (Green Light Optimized Speed Advisory) (Stevanovic et al., 2013; Li et al., 2014a; Stebbins et al., 2017) and Eco-Approach and Departure systems (Altan et al., 2017; Hao et al., 2018; Wang et al., 2019) aim at providing speed advice to avoid stops when passing signalized intersections, causing less stops and energy consumption. However, only individual vehicles are considered in these systems, neglecting the benefits of operating the vehicle platoons. CAV trajectory planning systems optimize vehicle trajectories at isolated intersections (Zhao et al., 2018; Jiang et al., 2017) or along a corridor (Asadi & Vahidi, 2010; Kamal et al., 2012; He et al., 2015; Wan et al., 2016; HomChaudhuri et al., 2016; Liu et al., 2019), whereas the signal phase and timing information is used as exogenous inputs to the optimization model and consequently the superiority of integrated information between vehicles (i.e., speed and position) and infrastructures (i.e., signal parameters) is hampered for lacking signal optimization.

The integrated approaches of optimizing traffic signals and vehicle trajectories in Li et al. (2014b); Yang et al. (2016b); Xu et al. (2018); Feng et al. (2018); Guo et al. (2019b) generally adopt a two-layered structure to solve the problem. In the signal optimization layer, the enumeration method (Li et al., 2014b; Xu et al., 2018) and the similar forward/backward recursion method (Feng et al., 2018; Guo et al., 2019b) are applied, whereas the signals are not explicitly optimized in a few studies (Li et al., 2014b; Yang et al., 2016b; Yu et al., 2018). The red phase in the signal layer is considered as constraining the arrival time in Xu et al. (2018); Feng et al. (2018); Guo et al. (2019b), which requires estimation of vehicle arrival time at the stop bar. In the vehicle trajectory layer, as opposed to trajectory optimization of the vehicle platoon, the trajectories of the platoon leader (Feng et al., 2018; Yu et al., 2018) or an individual vehicle (Xu et al., 2018) are optimized to reduce the computational load. Alternatively, the rule-based trajectory planning methods are used to simulate trajectories (Li et al., 2014b; Yang et al., 2016b). The red indication in Xu et al. (2018); Feng et al. (2018); Yu et al. (2018) is regarded as terminal condition constraints on position and/or speed. This unfortunately restricts the applicability on a corridor with multiple intersections, due to the difficulties in determining the terminal conditions at each intersection.

To conclude, current studies are confined to a single subject vehicle in the trajectory optimization models, excluding the potential benefits of considering the vehicle platoons. With respect to signal optimization, the red phases in existing research are presented by constraining the arrival time and/or terminal conditions, causing additional calculation of arrival time and the restricted application scope of isolated intersections. Therefore, the necessity of proposing an approach to integrating signal optimization with platoon trajectory planning that is not restricted at isolated intersections arises.

To fill the scientific gaps, this chapter proposes an integrated control approach of optimizing signals and trajectories for CAV platoons at standard full intersections. In the upper layer, all feasible signal plans are enumerated provided the signal cycle length, and each feasible signal plan is transferred to the lower layer iteratively. The lower layer determines accelerations of the CAV platoons under each feasible signal plan, optimizing ride comfort (by minimizing accelerations) and average travel delay (by maximizing speeds) , subject to the constraints on admissible accelerations, speed bounds, and safe driving requirements. The red phase is formulated as a logic position constraint so that vehicles can react to signals accordingly. The optimal sig-

nal plan is determined in the upper layer by finding the minimal objective function value among all feasible signal plans. The queue discharging and the transmissions from low speeds to high speeds (or vice versa) are taken into account in the lower layer.

The integrated signal and trajectory control approach is flexible owing to design of the logic red phase constraint. Unlike the existing terminal condition constraints of red phases which require prior knowledge of the arrival time of every vehicle, our formulation applies the logic constraint and thereby is not limited at an isolated intersection. The proposed trajectory optimization layer can also work under adaptive signals without predetermining stopping vehicles, which lifts one of the limitations in Chapter 2 and Chapter 3. The integrated approach is scalable to incorporate different traffic movements during multiple signal phases. Finally, the performance of the integrated control approach is validated by simulation of three scenarios and two baseline scenarios. Simulation results demonstrate the benefits of the proposed control approach.

The rest of this chapter is structured as follows. First, the control architecture is introduced, followed by the integrated control formulation for the vehicle trajectories and the traffic signals. The experiment design and simulation analysis are discussed after that. The last section provides conclusions and directions of future work.

4.2 Control architecture

In this section, the hierarchical control problem is specified, which determines the signal parameters in the upper layer and optimizes the vehicle trajectories in the lower layer. Later, the operational assumptions (e.g., minimum and maximum admissible vehicle accelerations) are illustrated.

4.2.1 Control problem description

Without loss of generality, CAV platoons are considered to approach the signalized intersection from four arms, and downstream CAVs are queuing behind the stop-lines, as shown in Figure 4.1 (a). The longitudinal trajectory control algorithm will be triggered when the approaching platoon leader at any direction enters the control zone, which is the interior region of the circle in Figure 4.1 (a). The center of the control zone is the signal controller, and

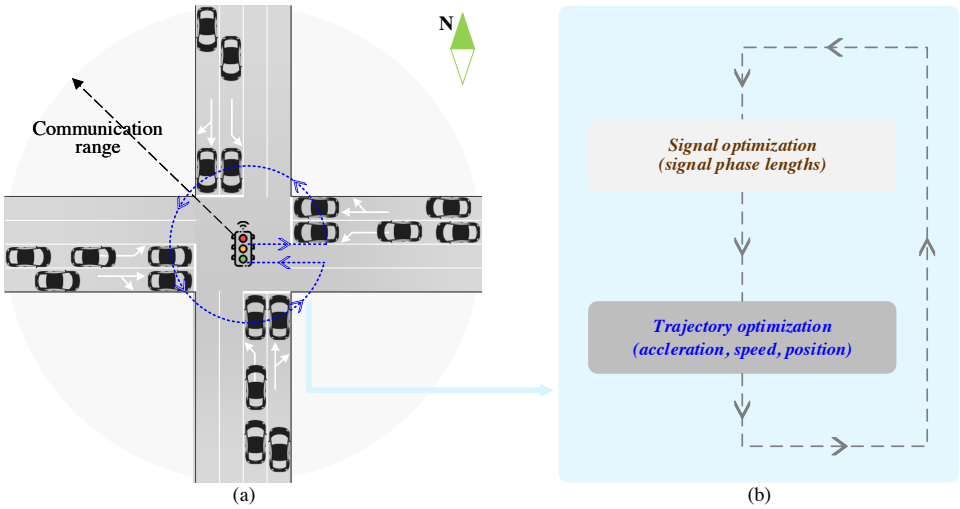

Figure 4.1: Illustration on operations of the control system

the radius of the control zone is the communication range (normally 200 meters).

The control objectives are to determine the optimal signal plan in the upper layer and to optimize accelerations of all CAVs in the lower layer, subject to safety and comfort constraints, as shown in Figure 4.1 (b). In the upper layer, the feasible signal plans are generated and iteratively imported to the lower layer. In the lower layer, the ride comfort is maximised by minimizing accelerations and the travel delay is minimised by maximizing vehicle speeds under each iterative signal plan. The control designs of the upper and lower layers are detailed in the forthcoming section.

4.2.2 Design assumptions

The assumptions of the integrated control algorithm are described as follows:

1. The signal phases are arranged in a pre-defined sequence at the considered intersection. The phase lengths are controlled under the assumption of a constant cycle length;

2. All vehicles in the control zone are cooperative and controlled via their accelerations within the admissible range. They exchange position and speed information with each other via V2V communication;

3. Signal Phasing and Timing (SPaT) information is delivered to the platoon controller via I2V communication;

4. The sum of feedback information and vehicle actuation delay is smaller than 1 second. Hence delays can be omitted in formulation with an acceleration sampling time interval of 1 second.

5. Lane changing behavior is not taken into account in the control zone.

Under these assumptions, different geometry configurations of multiple lanes at intersections are able to be accommodated by regarding the traffic movements released during the same green phase but on multiple lanes as multiple platoons of one traffic movement.

4.3 Control problem formulation

The integrated control problem of trajectories and signals is formulated in this section, including control objectives and constraints, system dynamics, controller formulation and solution approach.

4.3.1 Upper layer

Let J denote the total number of green phases for different traffic movements within the signal cycle, and j ($\in J$) is the green phase sequence number in the current cycle. The movement(s) released in the jth green phase refers as the jth movement(s). The yellow change intervals and the all-red clearance time are converted to the effective green and red time. The decision variables in the upper layer are the green phase lengths, g_j, ($j \in J$), the summation of which are equal to the fixed signal cycle length, C:

$$\mathbf{g} = [g_1, g_2, \ldots, g_J]^{\mathrm{T}} \tag{4.1}$$

$$\sum_{j=1}^{J} g_j = C \tag{4.2}$$

If $g_j^{\min}$ and $g_j^{\max}$ are the minimal and maximal green time of the jth green phase, the bounds on green phase lengths are

$$g_j^{\min} \leq g_j \leq g_j^{\max}, \forall j \in J \tag{4.3}$$

The feasible set of control variables in the upper layer mainly depends on the constraints of green phase lengths. The signal parameters can be optimized based on enumerating the feasible set. Each feasible signal plan is transferred to the lower layer that will determine vehicle trajectories and simultaneously calculate the objective function. The objective function values under all feasible signal plans are recorded and compared to find the optimal signal plan in the upper layer. In other words, the objective functions in the upper and lower layer are the same.

The integration between the upper layer and the lower layer is reflected in the objective function and the constraints. To this end, the upper layer decision variables are conveyed to the lower layer as parameters, which will be detailed in the forthcoming subsection.

4.3.2 Lower layer

The vehicle trajectories are optimized in the lower layer. The control variable in the lower layer is the acceleration of vehicle i in jth movement, $a_{ij}(t)$, and the state variables are the longitudinal position, $x_{ij}(t)$, and the speed, $v_{ij}(t)$. Here, i denotes the vehicle sequence number and N_j is the total number of controlled vehicles in the jth movement ($1 \leq i \leq N_j$). The control and state variables are defined as:

$$\mathbf{u}(t) = (a_{11}(t), a_{21}(t), ..., a_{N_1 1}(t), ..., a_{1J}(t), a_{2J}(t), ..., a_{N_J J}(t))^{\mathrm{T}} \tag{4.4}$$

$$\begin{aligned} &\mathbf{x} = (\mathbf{x}_{11}, \mathbf{x}_{21}, ..., \mathbf{x}_{N_1 1}, ..., \mathbf{x}_{1J}, \mathbf{x}_{2J}, ..., \mathbf{x}_{N_J J})^{\mathrm{T}}, \\ &\mathbf{x}_{ij}(t) = \left(x_{ij}(t), v_{ij}(t)\right) \end{aligned} \tag{4.5}$$

The following ordinary differential equation is used to describe the system dynamics model of a single vehicle:

$$\frac{\mathrm{d}}{\mathrm{d}t}\mathbf{x}_{ij}(t) = \frac{\mathrm{d}}{\mathrm{d}t}\begin{pmatrix} x_{ij}(t) \\ v_{ij}(t) \end{pmatrix} = \mathrm{f}(\mathbf{x}_{ij}, \mathbf{u}_{ij}) \tag{4.6}$$

$$\mathrm{f}(\mathbf{x}_{ij}, \mathbf{u}_{ij}) = A\mathbf{x}_{ij} + B\mathbf{u}_{ij} \tag{4.7}$$

where

$$A = \begin{bmatrix} 0 & 1 \\ 0 & 0 \end{bmatrix}; B = \begin{bmatrix} 0 \\ 1 \end{bmatrix}$$

If T ($\geq C$) is the prediction horizon, the control problem formulation is described as:

$$f = \min_{\mathbf{u}} \sum_{j=1}^{J} \sum_{i=1}^{N_j} \int_0^T \beta_1 a_{ij}^2(t) - \beta_2 v_{ij}(t) \mathrm{d}t \tag{4.8}$$

Here, β_1 and β_2 are positive cost weights. β_1 is unitless and the unit of β_2 is defined as m/s^3. The first cost term in Equation 4.8 is designed to maximize ride comfort by minimizing accelerations. The second cost term represents the minimization of travel delay by maximizing speeds.

In addition, the control and state variables are required to obey some constraints in the lower layer.

1. Admissible acceleration
   The control variable, acceleration, should be bounded between the maximal acceleration, $a_{\max}$, and the minimal acceleration, $a_{\min}$.

$$a_{\min} \leq a_{ij}(t) \leq a_{\max} \tag{4.9}$$

2. Speed bounds
   The state variable of speed should be restricted between the limit speed, $v_{\max}$, and 0.

$$0 \leq v_{ij}(t) \leq v_{\max} \tag{4.10}$$

3. Safe driving requirements
   The following vehicles are required to track the vehicles in front with the safe space and time gaps, which should not be less than the minimum safe gap.

$$x_{ij}(t) - x_{(i+1)j}(t) \geq v_{(i+1)j}(t) t_{\min} + s_0 + l_{ij} \tag{4.11}$$

   Here, l_{ij} denotes the length of vehicle i in the jth movement, $t_{\min}$ is the minimum safe car-following time gap, and s_0 is the minimum space gap at standstill conditions.

4. Red phase constraint
   The red phases can be represented as position constraints in the lower layer. In order to react to the red phase, the logic constraint is applied to generate trajectories facing the signals. Whether vehicles can pass

or not is determined by the active of the logic decision. In this way, the vehicles can be responsive to the adaptive signal changes, without pre-determining the first-stopping vehicles as in Chapter 2 and 3.
Assume the longitudinal position at the stop bar is x_{stop}. If vehicle i in the jth movement cannot pass the intersection during the jth green phase, it cannot leave within the signal cycle either. The red phase is formulated as the logic position constraint, i.e., if the vehicle position at the jth green phase tail is behind the stop-line, the vehicle position at the signal cycle tail is also behind the stop-line.

$$x_{ij}(C) \leqslant x_{\text{stop}}, \text{ if } x_{ij}\left(\sum_{k=1}^{j} g_j(k)\right) \leqslant x_{\text{stop}} \tag{4.12}$$

Here, k represents the sequence number of green phases no later than the jth green phase, $k = \{1, 2, ..., j\}$. The implication of Equation 4.12 is that, for the subject vehicle i in the jth movement, it cannot leave the intersection within the signal cycle ($x_{ij}(C) \leqslant x_{\text{stop}}$) if it is behind the stop-line at the jth green phase tail (i.e., $x_{ij}\left(\sum_{k=1}^{j} g_j(k)\right) \leqslant x_{\text{stop}}$), otherwise $x_{ij}(C) > x_{\text{stop}}$.

The lower layer optimization problem can be solved by applying the upper layer decision variables as parameters. To integrate the lower layer with the upper layer, the lower layer optimization problem is cast as a constraint to the upper layer optimization problem.

4.3.3 Solution approach

The lower layer is a parametric optimization problem which applies the upper layer decision variables as parameters. Therefore, the upper and lower layers can be integrated by implementing the lower layer optimization problem as a constraint to the upper layer optimization problem. As discussed above, the objective function for the upper layer F is the same as the objective function for the lower layer f as in Equation 4.8, thus

$$F = \min_{\mathbf{u}} \sum_{j=1}^{J} \sum_{i=1}^{N_j} \int_0^T \beta_1 a_{ij}^2(t) - \beta_2 v_{ij}(t) \mathrm{d}t \tag{4.13}$$

The two-layered problem is formulated as follows:

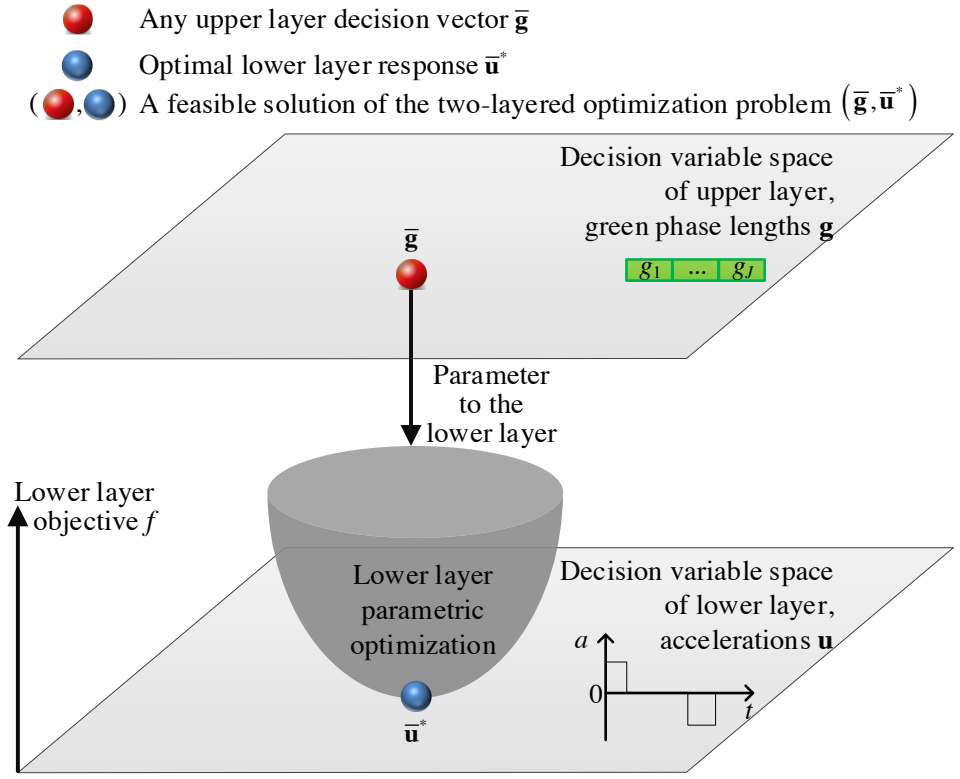

Figure 4.2: Illustration of the two-layered problem

$$\min_{\mathbf{g},\mathbf{u}} F(\mathbf{g},\mathbf{u}) \tag{4.14}$$

s.t.

$$\mathbf{u} \in \arg\min_{\mathbf{u}} \{ f(\mathbf{g},\mathbf{u}) : h(\mathbf{g},\mathbf{u}) \leq 0 \} \tag{4.15}$$

$$G(\mathbf{g},\mathbf{u}) \leq 0 \tag{4.16}$$

G and h correspond to the upper layer constraint and the lower layer constraint respectively, i.e., Equation 4.2, 4.3, 4.7, 4.9 to 4.12. The relationship between the upper layer and the lower layer is depicted in Figure 4.2. In Figure 4.2, the parametric lower layer optimization problem can be solved given any upper layer decision vector $\bar{\mathbf{g}}$. Then, the lower layer provides the optimal response considering the lower layer $\bar{\mathbf{u}}^*$ to the upper layer. This parametric flow is defined as an enumeration step of the upper layer.

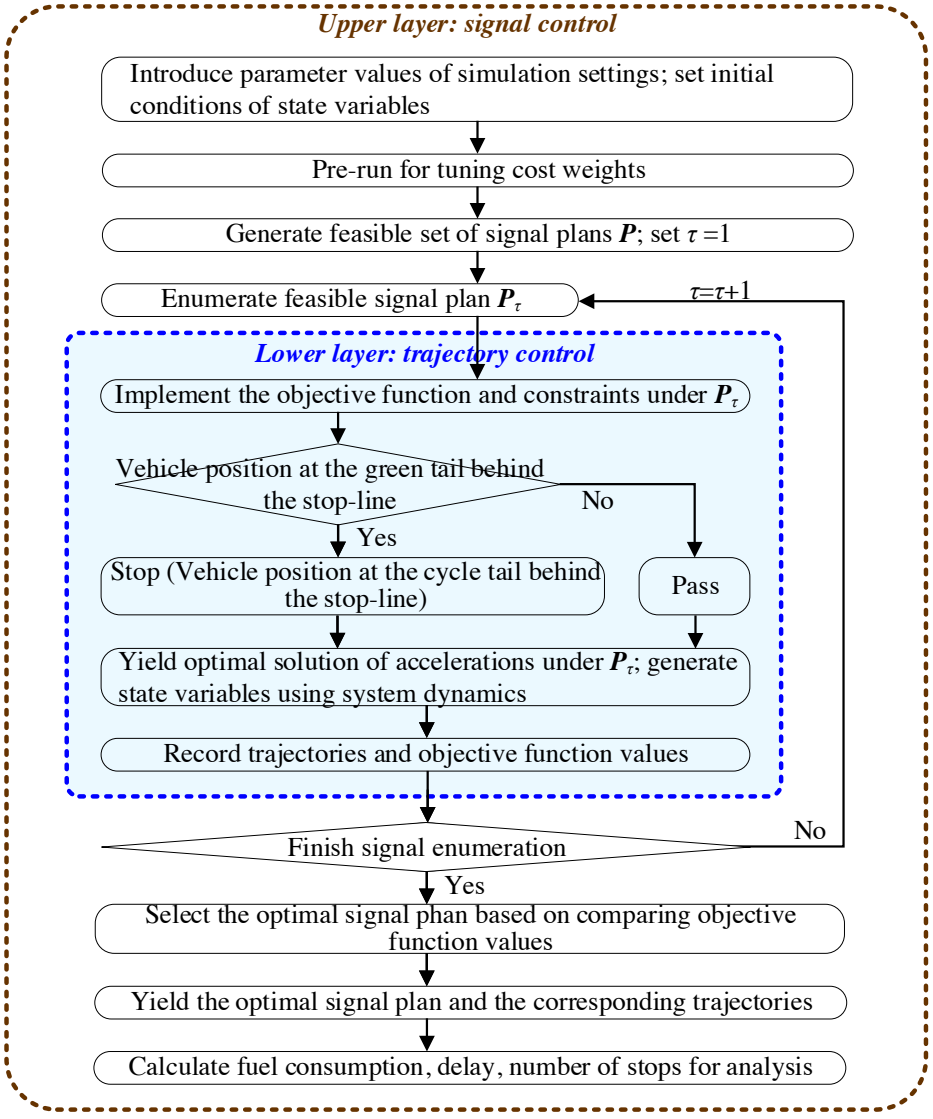

Figure 4.3: Illustration of the solution approach

The solution approach is illustrated in Figure 4.3. In the upper layer, an enumeration method is adopted to evaluate all feasible signal plans, in other words, to solve the equality constraint of Equation 4.2. Let $\boldsymbol{P}$ and Λ denote the upper layer feasible region (i.e., the feasible signal phase lengths) and the number of all feasible signal plans respectively. If τ ($\in [1,2,\ldots,\Lambda]$) implies the enumeration step sequence of the upper layer, $\boldsymbol{P}_\tau$ is defined as the

feasible signal plan at the τth enumeration step, which is conveyed to the lower layer for trajectory control. The algorithm starts with $\tau = 1$, and then the feasible signal plan $\boldsymbol{P}_1$ is transferred to the lower layer for trajectory optimization. In the lower layer, the accelerations are optimized and recorded at each enumeration step, together with the corresponding value of the objective function f. The enumeration continues ($\tau = \tau + 1$) until all feasible signal plans are evaluated ($\tau = \Lambda$). Finally, the optimal signal plan is selected by comparing values of the objective function in the upper layer F. The outputs of the integrated control approach are the optimal signal parameters and the vehicle trajectories.

In the lower layer, the control variable (i.e., acceleration) is discretised in time to solve the continuous-time optimal control problem using nonlinear optimization techniques (Rao, 2009). System dynamics of Equation 4.7 are transformed as linear equality constraints. The control variables, accelerations, are bounded within the admissible range. The linear inequality constraints on state variables, such as the speed bound and the no-collision requirement, are transformed to restrict the control variable using the system dynamics equation. The logic red phase constraint is enforced as the position constraint, under which the vehicles can stop if they cannot pass during the current green phase, as shown in the diamond of the lower layer in Figure 4.3. The vehicles are thereby able to react to the instant changes in the phase lengths, which is beneficial to the applications under adaptive and actuated signal control approaches. The logic red phase constraint is implemented as nonlinear positon constraints for all vehicles. This optimal control problem is solved in MATLAB using fmincon solver. The performance of the controller is simulated and analyzed in the following section.

4.4 Simulation results and analysis

In this section, three scenarios and two baseline scenarios are designed to validate the platoon performance of this control algorithm.

4.4.1 Experiment design

The vehicle trajectories are simulated at a typical four-arm intersection (and each arm is indexed by j) when optimizing the signal parameters. The right-turn, through, and left-turn movements are not differentiated. The queuing

and approaching vehicles on arm j are regarded as the jth movement and are released in sequence during the jth green phase (corresponding to the arm index). Therefore, four signal phases are considered in a signal cycle ($J = 4$). The longitudinal position of the stop-line x_{stop} is set to 0 m. The control zone starts from -200 m to 200 m, considering the fact that the realistic communication ranges of I2V and V2V are around 200 m.

In this experiment settings, the signal cycle length is given ($C = 50$ s) when optimizing four green phase lengths ($j = 1,2,3,4$) within the cycle. The prediction horizon T is 60 s, longer than the signal cycle length to test the accelerating characteristics at the beginning of the subsequent green phase in the next cycle. The time step is 1 s, so delays under this time step have no effect on trajectories. The initial speed of the approaching vehicles in the first movement is 10 m/s to catch the first green phase ($j = 1$), while the counterparts of other movements are 8 m/s. The various initial speeds are designed to test the feasibility of the control approach under different initial conditions. The signal phase lengths are enumerated from the minimal green phase to the maximal green phase with an increase of 2 s. The choice is motivated by the minimum safe car-following time gap $t_{\min}$, which implies the throughput remains unchanged within 2 s during the green time. Other parameter values are detailed in Table 4.1, most of which come from the previous work in Liu et al. (2019). Similar settings (e.g., the vehicle number, the green phase number and signal cycle length) can be simulated in the same way.

In order to test the performance of the integrated control approach, three scenarios and two baseline scenarios are designed. Hereinafter, the symmetric traffic flow refers to the situation that vehicle actuations are the same in all movements, and otherwise it is referred as the asymmetric traffic flow.

In Scenario 1, two queuing vehicles behind the stop-line and three approaching vehicles from the boundary of the control zone (-200 m) are set on each arm. Scenario 1 is designed to validate the optimal signal performance under the symmetric traffic flow and the platoon characteristics such as the decelerations of stopping vehicles facing the red phase and the accelerations of passing and queuing vehicles during the green phase. Scenario 2 is also simulated under the symmetric traffic flow but one more vehicle is added at the approaching platoon tail. The trajectory performance in Scenario 2 helps explore the trajectory pattern generated by the control approach. Scenario 3 aims to investigate the workings under the asymmetric traffic flow. The vehicles are set as follows: two, three, four, and five approaching vehicles in

Table 4.1: Parameter and coefficient values in the experiment

Notation	Parameter/ Coefficient	Value	Unit
-	time step	1	s
-	initial speed of approaching vehicles	10,8,8,8	m/s
-	initial space gap of approaching vehicles	35	m
-	initial position of the leader in the approaching vehicles	-200	m
-	initial space gap of queuing vehicles	5	m
-	initial position of the leader in the queuing vehicles	-5	m
-	control zone range	200	m
J	green phase number within the signal cycle	4	-
$g_j^{\max}$	the maximal green phase, $\forall j$	20	s
$g_j^{\min}$	the minimal green phase, $\forall j$	4	s
C	signal cycle length	50	s
T	prediction horizon length	60	s
x_{stop}	the position of the stop lines at intersections	0	m
l_{ij}	length of vehicle i in the jth movement	3	m
$t_{\min}$	minimum safe car-following time gap	2	s
s_0	minimum space gap at standstill conditions	2	m
$v_{\max}$	limit speed	20	m/s
$a_{\max}$	allowable maximum acceleration	2	m/s^2
$a_{\min}$	allowable minimum acceleration	-5	m/s^2
β_1	cost weight	1	-
β_2	cost weight	1	m/s^3

the first, second, third, and fourth movement respectively, with two queuing vehicles on each arm.

Baseline Scenario 1 and 2 have the same settings as Scenario 1 and 2, but they apply different methods of optimizing either signals or trajectories. In Baseline Scenario 1, the traffic signals are optimized in the same way as Scenario 1 does (using Equation 4.13), while the vehicle trajectories are represented using the intelligent driver model (IDM) (Treiber et al., 2000). The comparisons between Scenario 1 and Baseline Scenario 1 provide insights into the optimal signal pattern of the integrated control approach. In Baseline Scenario 2, the signal controller is assumed to allocate the green time based on the traffic demand, so only vehicle trajectories are optimized but signal

parameters are not. According to the vehicle settings of Baseline Scenario 2, the signal timing plan is 12 s, 13 s, 12 s, and 13 s, for the first to the fourth movements. The comparisons between Scenario 2 and Baseline Scenario 2 can help explore the optimal trajectory pattern.

The following pseudo-code in Algorithm 4.1 shows the implementation procedure of the simulation experiments. *UP* and *LW* represent the upper layer and the lower layer respectively. In the simulation experiments, all parameter values and the initial conditions of state variables are first set. Later, the cost weights are tuned under Scenario 1 and then applied in all scenarios. The cost weights of ride comfort and speed, β_1 and β_2, are supposed to keep the same order, thus $\beta_1 = 1$ and $\beta_2 = 1$ m/s^3. The selected cost weights are appropriate to stimulate vehicles for reaching the maximal speed while unnecessary fluctuations in accelerations are evitable. Detailed discussion on tuning cost weights and parameter values can be found in Chapter 2. Then, the objective function and all constraints are transcribed in matrix as the fmincon solver required. After optimization, the optimal solution of accelerations is generated, and thereby the state variables of position and speed can be determined using the system dynamics model. Furthermore, the fuel consumption, delay, and number of stops in all scenarios are calculated to verify the benefits of the integrated control approach. The instantaneous fuel consumption rate f_v (ml/s) could be estimated using

$$f_v = \begin{cases} b_0 + b_1 v + b_2 v^2 + b_3 v^3 + a\left(c_0 + c_1 v + c_2 v^2\right) & a > 0 \\ b_0 + b_1 v + b_2 v^2 + b_3 v^3 & a \leqslant 0 \end{cases} \tag{4.17}$$

Here, v and a represent $v_{ij}(t)$ and $a_{ij}(t)$ for simplification. Detailed parameter values can be found in Kamal et al. (2011).

4.4.2 Platoon performance

In this section, the designed scenarios and baseline scenarios are simulated and analyzed to illustrate the control effects. As in Figure 4.4 to Figure 4.8, we select the representative speed and position figures to present the trajectories concisely. The vehicle numbers N_j, the signal phase lengths, throughputs during the green time, fuel consumption, delay, and the number of stops are revealed in all scenarios, as detailed in Table 4.2. The travel delay is calculated by the vehicle arrival time at the stop-line minus the minimal traveling time to the stop bar, i.e., the distance from the initial position to the

Algorithm 4.1 Pseudo-code of implementing the simulation experiments

Introduce parameter values of simulation settings [*UP*]
Set initial conditions of state variables [*UP*]
Pre-run for tuning cost weights [*UP*]
Set the enumeration step $\tau = 1$ ($\tau \in [1, 2, \cdots, \Lambda]$) [*UP*]
Generate the feasible set of signal plans $\boldsymbol{P}$ ($\boldsymbol{P}_\tau \in [\boldsymbol{P}_1, \boldsymbol{P}_2, \cdots, \boldsymbol{P}_\Lambda]$) [*UP*]
Convey $\boldsymbol{P}$ to the lower layer as parameters [*UP*]
while $\tau \leq \Lambda$ **do**
    Solve the lower-layer control problem under $\boldsymbol{P}_\tau$ [*LW*]
    if Vehicle position at the green phase tail is behind the stop-line $x_{ij}\left(\sum_{k=1}^{j} g_j(k)\right) \leq x_{\text{stop}}$ **then**
        Add constraints on vehicle position at the cycle tail $x_{ij}(C) \leq x_{\text{stop}}$ [*LW*]
    end if
    Yield the optimal solution of accelerations under $\boldsymbol{P}_\tau$ [*LW*]
    Generate state variables of position and speed using system dynamics [*LW*]
    Record trajectories and the objective function value under $\boldsymbol{P}_\tau$ [*LW*]
end while
Select the optimal signal plan by comparing all objective function values, $\forall\tau$ [*UP*]
Yield the optimal signal plan and the corresponding trajectories [*UP*]
Calculate fuel consumption, delay, number of stops [*UP*]

stop-line divided by the limit speed $v_{\max}$. The fuel consumption (ml/m) is calculated according to the instantaneous fuel consumption model in Kamal et al. (2011) and the traveling distance within the prediction horizon.

Overall, all controller constraints are satisfied, and the indicators can further explore the advantages of the proposed control approach, but the computational times of all scenarios are infeasible in real time, normally more than 100 seconds. Hereinafter, all scenarios are analyzed and compared in detail.

Analysis of Scenario 1 and Baseline Scenario 1

The trajectories of Scenario 1 and Baseline Scenario 1 are analyzed in this subsection to derive the optimal signal pattern. The indicators of throughput,

Table 4.2: Indicators in all scenarios (S and BS represent Scenario and Baseline Scenario)

Indicator	S1	S2	S3	BS1	BS2
Vehicle number of the jth ($j = 1,2,3,4$) movement, N_j (veh)	5,5, 5,5	6,6, 6,6	4,5, 6,7	5,5, 5,5	6,6, 6,6
Optimal/ Pre-timed green phase lengths of the jth ($j = 1,2,3,4$) movement (s)	6,13, 13,18	6,15, 15,14	6,13, 15,16	6,16, 12,16	12,13, 12,13
Throughputs of the jth ($j = 1,2,3,4$) movement (veh)	2,5, 5,5	2,6, 6,5	2,5, 6,6	2,5, 5,5	2,5, 5,5
Fuel consumption (ml/m)	0.0804	0.0837	0.0841	0.1091	0.0830
Number of stops	3	4	2	9	4
Delay (s)	21.49	24.36	22.76	23.29	29.32

delay, vehicle stops, and fuel consumption are calculated and compared after that. Speed trajectories of each movement are presented in Figure 4.4. The vehicle sequence numbers from 1 to 5 are depicted as V1 to V5 in all subfigures of Figure 4.4, where V1 and V2 are queuing vehicles (0 speed when $t = 0$ s) and V3 to V5 are approaching vehicles (10 or 8 m/s when $t = 0$ s). In general, the constraint on speed bounds is respected. The following vehicles in Scenario 1 reach the maximal speed later than the predecessors because of the no-collision requirement, and the queuing vehicles accelerate from the standstill condition at the beginning of the green phases to pass the intersection.

In Scenario 1, the optimal green phase lengths are 6 s, 13 s, 13 s, and 18 s in sequence, releasing 2 vehicles, 5 vehicles, 5 vehicles and 5 vehicles respectively. The signal parameters are optimized to release as many vehicles as possible thanks to the travel delay cost term. In the first movement, as shown in Figure 4.4 (a), the signals are optimized to terminate the first green phase after two queuing vehicles pass the intersection (t =6 s); the approaching vehicles experience stops confronting the long red phase length of 44 s, and start accelerations when $t = 30$ s to catch the next green phase ($t = 51$ s to $t = 60$ s). On the contrary, the approaching vehicles in the latter three movements react to the signal changes by accelerating to catch the green phase (see Figure 4.4 (b)) or decelerating facing the red phase (see Figure 4.4 (d)). In addition, the safe driving constraint and the red phase constraint are satisfied in Scenario 1, see Figure 4.5.

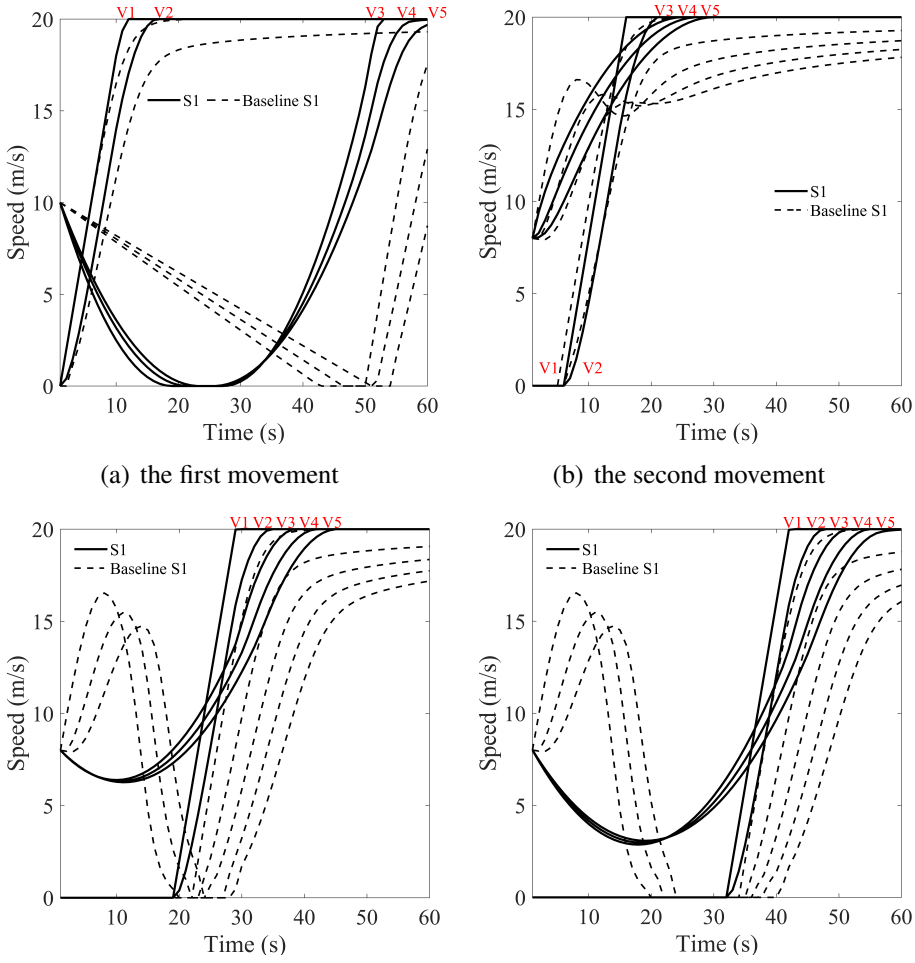

(a) the first movement

(b) the second movement

(c) the third movement

(d) the fourth movement

Figure 4.4: Speed trajectories under Scenario 1 (S1) and Baseline Scenario 1 (BS1)

Baseline Scenario 1 optimizes signals in the same way as Scenario 1 does based on the trajectories generated by IDM. The red phase is represented using the logic constraint of Equation 4.12 when implementing IDM. The speed trajectories of IDM model are illustrated in Figure 4.4, as depicted in the dashed lines. The green phase lengths are optimized to be 6 s, 16 s, 12 s, and 16 s. The optimal signals in Baseline Scenario 1 shorten the first green phase to release more vehicles from the latter movements. Together with the optimal signals in Scenario 1, the optimal signal pattern can be concluded as switching signal phases in time to release as many vehicles as possible.

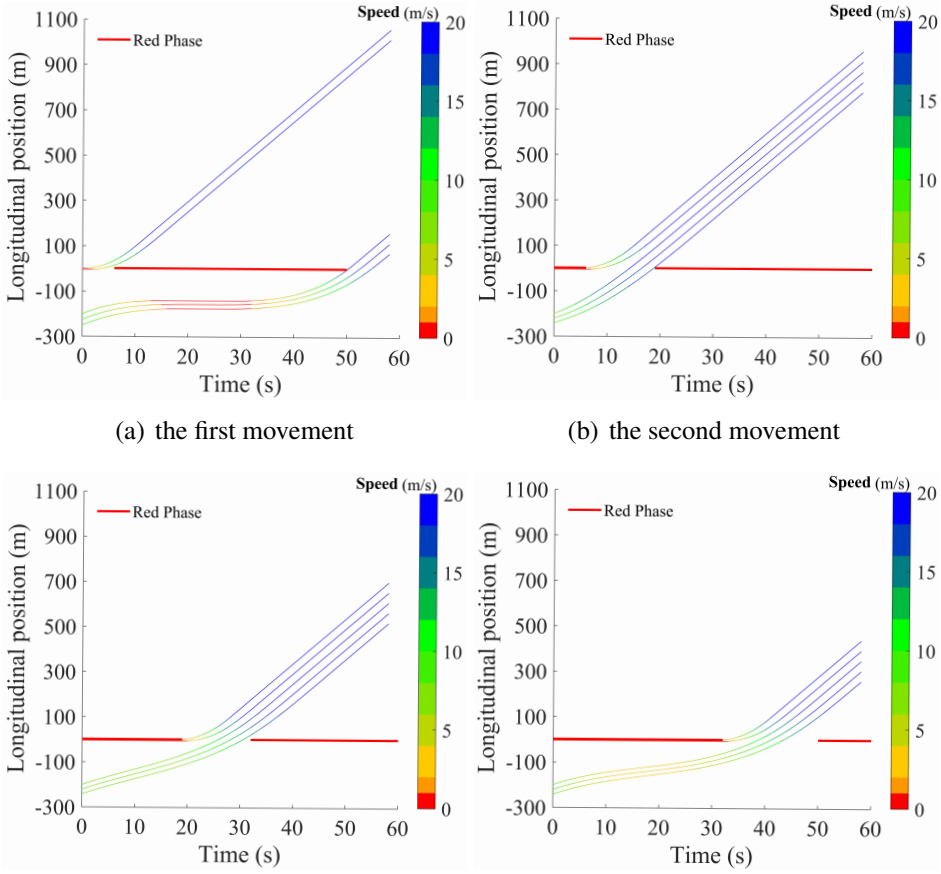

(a) the first movement (b) the second movement

(c) the third movement (d) the fourth movement

Figure 4.5: Longitudinal position under Scenario 1

The tuning procedure in Scenario 1 is simple, while IDM model in Baseline Scenario 1 requires elaborate calibration of parameters to smooth fluctuations in trajectories and adapt to all traffic scenarios. In this chapter, we apply the parameter values of the original IDM model (Treiber et al., 2000), and the generated trajectories sometimes are unsmooth or fail to reach the maximal speed (see Figure 4.4 (b)). On the contrary, the optimal speeds in Scenario 1 are considerably smooth when climbing to the maximal speed owing to the ride comfort cost term. Furthermore, unnecessary vehicles stops during the red time are often unavoidable using IDM (66.67 % more than Scenario 1), which also causes more fuel consumption. The integrated approach in Scenario 1 saves 0.0287 ml/m (26.31 %) compared to the IDM model. The vehicles speeds generated using IDM ascend slowly, which dete-

riorates the traffic delay of Baseline Scenario 1 (7.73 % worse than Scenario 1). These indicators and features highlight the benefits of the integrated control approach in trajectory optimization.

Analysis of Scenario 2 and Baseline Scenario 2

Scenario 2 introduces one more vehicle at the platoon tail, including two queuing vehicles and four approaching vehicles in every movement. For concise illustration, the speed and position trajectories in the second movement are selected to demonstrate the performance under Scenario 2 and Baseline Scenario 2 (see Figure 4.6 and 4.7, which prove the safe following requirement, the speed bounds and the red phase constraint are respected). The other movements show similar trajectories and the same features. Hereinafter, the optimal trajectory pattern is concluded in this subsection, and the indicators such as fuel consumption, throughput, and delay are evaluated.

The optimal green phase lengths under Scenario 2 are 6 s, 15 s, 15 s, and 14 s, with 2 vehicles, 6 vehicles, 6 vehicles and 5 vehicles passing the intersection respectively. Compared to Scenario 1, two more vehicles are released in Scenario 2, which explores the benefits of signal optimization in the upper layer. In Scenario 2, the first green phase length is still 6 s, switching signals after releasing the queuing vehicles in the first movement; the second and third green phases are longer than in Scenario 1 because one more vehicle is optimized to depart the intersection; the last vehicle in the fourth movement cannot pass.

The speed trajectories in Figure 4.6 have the similar features as under Scenario 1 in Figure 4.4 (b). The approaching vehicles V3 to V6 (see red lines under Scenario 2 and red dashed lines under Baseline Scenario 2) climb to the maximal speed over time and the queuing vehicles V1 and V2 are depicted as the black lines under Scenario 2 and black dashed lines under Baseline Scenario 2. The differences in speeds between Scenario 2 and Baseline Scenario 2 result from the first green phase lengths (6 s versus 12 s). The passing vehicles accelerate quickly facing a shorter red phase (6 s) in Scenario 2. However, facing a longer red phase (12 s) in Baseline Scenario 2, the passing vehicles accelerate slowly during the red phase to keep the safe gap and then climb to the maximal speed after merging with the preceding vehicles during the green phase. The trajectory differences in other movements between Scenario 2 and Baseline Scenario 2 are negligible.

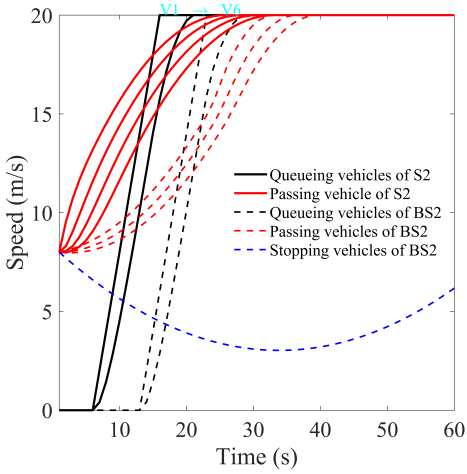

Figure 4.6: Speed trajectories of the second movement under Scenario 2 (S2) and Baseline Scenario 2 (BS2)

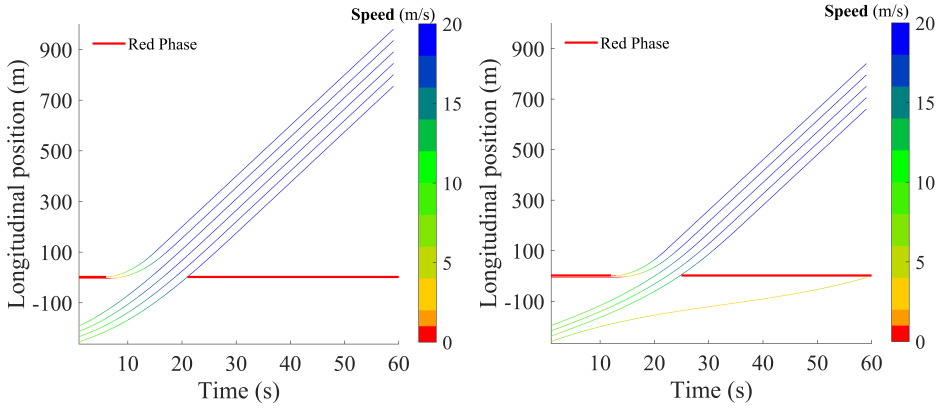

(a) Scenario 2 (b) Baseline Scenario 2

Figure 4.7: Longitudinal position of the second movement under Scenario 2 (S2) and Baseline Scenario 2 (BS2)

The optimal trajectory pattern can be summarized into three categories based on the trajectories under Scenario 1, Scenario 2 and Baseline Scenario 2, as shown in Figure 4.4 to Figure 4.7. Firstly, the queuing vehicles accelerate from the stationary condition at the beginning of the green phases, aiming to reach the maximal speed as soon as possible. Secondly, the passing vehicles, normally the first multiple vehicles in the approaching platoon, accelerate but slower than the predecessors to keep the safe gaps when facing

a shorter red phase (e.g., $j = 2$), or otherwise decelerate first and then accelerate smoothly to avoid stops and arrive at the stop-line with higher speeds (e.g., $j = 3,4$). Thirdly, the stopping vehicles, normally the last several vehicles in the approaching platoon, decelerate first and subsequently accelerate to leave at the beginning of the next green phase.

In Baseline Scenario 2, two vehicles, five vehicles, five vehicles and five vehicles are optimized to depart the intersection. Scenario 2 outperforms Baseline Scenario 2 in throughputs because signal phases are pre-determined according to traffic demand on each arm under Baseline Scenario 2, which neglects the real-time information of vehicle position and speed. Furthermore, Baseline Scenario 2 optimizes vehicle trajectories for each movement, unlike the integrated optimization of four movements in Scenario 2.

As shown in Table 4.2, the overall throughputs in Scenario 2 and Baseline Scenario 2 are 19 and 17, respectively. Two more vehicles are released in Scenario 2 (11.76 % more than in Baseline Scenario 2), which partly explains the almost identical values of fuel consumption between Scenario 2 and Baseline Scenario 2. In addition, more travel time is proved to be saved in Scenario 2 (16.92 %), which demonstrates the superiority of the integrated control approach on signal optimization.

Analysis of Scenario 3

The longitudinal position of all movements under Scenario 3 are depicted in Figure 4.8, with the red lines indicating the optimal signal plan. The signal phase lengths are optimized as 6 s, 13 s, 15 s, and 16 s respectively, and 2 vehicles, 5 vehicles, 6 vehicles and 6 vehicles depart the signalized intersection.

In Scenario 3, the trajectories obey the optimal trajectory pattern, as discussed above, and the signal optimization tends to shorten the first green phase for releasing as many vehicles as possible in the latter movements, as concluded in the optimal signal pattern. Based on Scenario 3, it is verified that signal optimization can react to different traffic demand levels and switch signals for the optimal performance. The fuel consumption (ml/m) under Scenario 3 is 0.0841 ml/m.

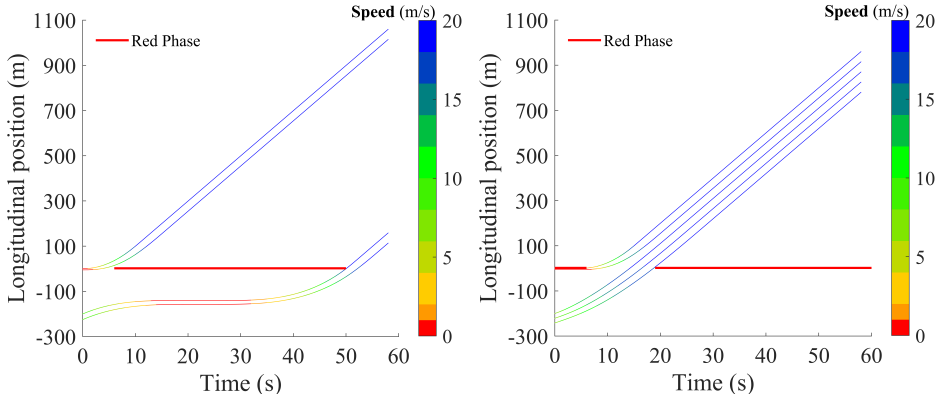

(a) the first movement (b) the second movement

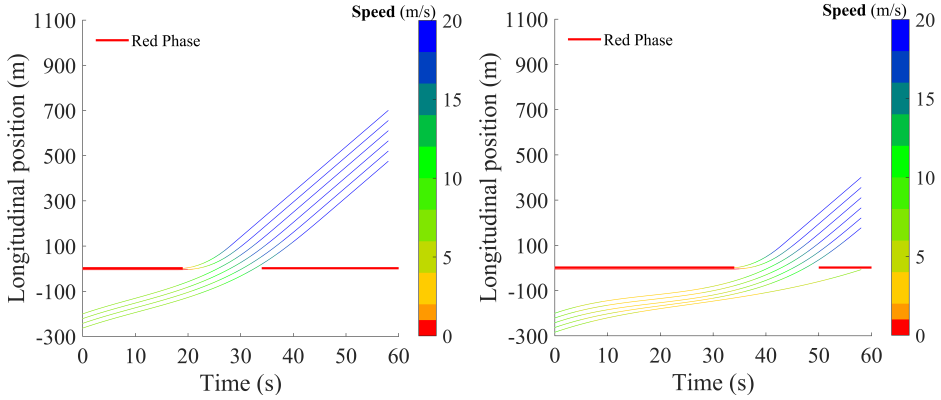

(c) the third movement (d) the fourth movement

Figure 4.8: Longitudinal position under Scenario 3

4.5 Conclusions and future work

In this chapter, we proposed an integrated approach for controlling traffic signals and vehicles trajectories at intersections. The problem is formulated as a two-layer optimization model. The upper layer enumerates all feasible signal plans and sends to the lower layer iteratively. The lower layer determines the accelerations of the platoons at each signal enumeration step, until completing the signal enumeration. The ride comfort and average travel delay are optimized, subject to safe and physical constraints. To be noted, the red phase is represented using the logic constraint, which enables vehicles to respond to the adaptive signal indication. The upper layer finds the

optimal signal plan after enumeration, by searching the minimal objective function value among all enumeration steps. The proposed control approach is feasible in incorporating multiple traffic movements and signal phases, and the benefits of optimizing the vehicle platoons from all incoming traffic movements are taken into account. Simulation under three scenarios and two baseline scenarios demonstrated the performance of the proposed approach.

The simulation results show the potentials of the throughput improvement and environmental benefits. Based on analyzing performance of all scenarios, the optimal signal pattern and the optimal trajectory pattern are derived.

The enumeration method in the signal optimization layer results in intensive computational time, which requires further improvement. In the next chapter, a single-layer design approach that is computationally scalable will be presented.

Chapter 5

A single-layer control approach of optimizing trajectories and signals

In this chapter, a joint control approach that simultaneously optimizes traffic signals and trajectories of cooperative (automated) vehicle platooning at urban intersections is presented. The signal parameters and the accelerations of the controlled platoons are optimized to maximize comfort and minimize travel delay subject to motion constraints on speeds, accelerations and safe gaps. The red phases are recast as several linear constraints to enable efficient solutions. This joint control approach is flexible in incorporating multiple platoons and traffic movements under different traffic demand levels. The performance of the proposed control approach is verified by simulation at a standard four-arm intersection with balanced/unbalanced arrival rates from different arms, taking the released traffic movement numbers, turning proportions, signal cycle lengths and the controlled vehicle numbers into account. The simulation results demonstrate the platoon performance (such as split, merge, acceleration and deceleration maneuvers) under optimal signals. Based on the simulation results, the optimal patterns of trajectories and signals are explored. Furthermore, the computational performance of the proposed control approach is analyzed, and the benefits of the proposed approach on the average travel delay, throughput, fuel consumption, and emission are proved by comparing with the two-layer approaches using the car following model, the signal optimization models, and the state-of-the-art approach.

This chapter is an adapted version of the journal paper:

Liu, M., Zhao, J., Hoogendoorn, S. and Wang, M., 2022. A single-layer approach for joint optimization of traffic signals and cooperative vehicle trajectories at isolated intersections. Transportation Research Part C: Emerging Technologies. https://doi.org/10.1016/j.trc.2021.103459

5.1 Introduction

Traffic lights are one of the fundamental elements on urban roads for traffic management. The red phases are beneficial to separate conflicting traffic movements at intersections, but they also cause substantial travel delay, fuel consumption and emissions on urban roads (Zhao et al., 2020). To relieve these problems, the recent advances in connected and automated vehicle (CAV) technology have attracted considerable attention. CAVs can communicate with each other and the roadside infrastructures via Vehicle-to-Vehicle (V2V) and Vehicle-to-Infrastructure (V2I) communications (Wang et al., 2015), and consequently vehicles can be operated in an efficient, safe and sustainable way in a CAV environment, taking the real-time traffic signals into account (Feng et al., 2018). Therefore, numerous studies have investigated the cooperative design of traffic signals and/or CAV trajectories at signalized intersections taking advantage of CAV technology.

There are mainly three research directions for improving traffic operations at urban intersections using CAV technology: the classical control (e.g., signal control algorithms), guiding or controlling vehicular speeds and paths (e.g., cooperative intersection methods, speed guidance systems and CAV trajectory planning), and the joint control approaches of both traffic signals and vehicle trajectories.

As to classical control, the signal control algorithms with connected vehicles (not necessarily automated vehicles) aim to generate the optimal signal parameters at an isolated intersection (Feng et al., 2015; Chen & Sun, 2016), along a corridor (Beak et al., 2017; Li & Ban, 2018), or at the network level (Le et al., 2015; Al Islam & Hajbabaie, 2017), based on the prediction of future traffic flow states, such as vehicle speeds, arrival time and queue lengths (Guo et al., 2019a). These signal control algorithms do not optimize CAV trajectories but use connected vehicle information for state estimation and prediction. They are usually integer nonlinear programming problems and/or bi-level optimization models, which are difficult to solve. Dynamic programming (DP) (Feng et al., 2015; Chen & Sun, 2016; Beak et al., 2017; Li & Ban, 2018) and the distributed control (Le et al., 2015; Al Islam & Hajbabaie, 2017) are frequently adopted to formulate and approximate the control problems.

The cooperative intersection controller organizes the sequence of CAVs to discharge vehicles without collision at a signal-free intersection in a fully CAV environment (Lee & Park, 2012; Ahmane et al., 2013; Zohdy & Rakha,

2016; Yu et al., 2019). Vehicle trajectories before arrivals of the intersection are usually not considered in these methods. Therefore, complete and sudden stops of CAVs are sometimes inevitable in the vicinity of the intersection in order to avoid crashes, and the optimality of vehicle platooning is not guaranteed in this line of research (Yu et al., 2018). Furthermore, ignoring other road users (e.g., pedestrians, cyclists and human drivers) also challenges the realistic applications of the cooperative intersection controllers.

Individual speed guidance systems provide advisory speeds to individual vehicles for fewer vehicle stops, travel delay and/or energy consumption in the vicinity of urban intersections, such as GLOSA (Green Light Optimized Speed Advice) (Stevanovic et al., 2013; Li et al., 2014a; Stebbins et al., 2017) and Eco-Approach and Departure systems (Altan et al., 2017; Hao et al., 2018; Wang et al., 2019). The generated speed advice can also be implemented in automated vehicles, resulting in the reduction of uncertainties caused by human drivers and thereby better control performance. However, these speed guidance systems are dedicated to an individual vehicle rather than the vehicle platoon(s), implying that the effects on the overall platoon or the traffic flow are ignored.

The cooperative CAV trajectory planning algorithms optimize vehicle accelerations at an isolated intersection or along a corridor, assuming that signal timings are known to the optimization models as exogenous inputs. As to the trajectory planning systems at isolated intersections, the objective functions simply consider comfort and/or fuel consumption (Jiang et al., 2017; Zhao et al., 2018; Li et al., 2018; Typaldos et al., 2020). Providing a fixed signal cycle length, the red phases at isolated intersections are normally represented as constraining the terminal conditions of vehicle position, speed and acceleration using terminal costs and/or equality constraints. These terminal conditions are normally estimated as the position of stopline, the maximal speed and zero acceleration respectively. On the other hand, the trajectory planning systems along a corridor are usually designed for an individual vehicle such as Asadi & Vahidi (2010); Kamal et al. (2012); He et al. (2015); Wan et al. (2016); HomChaudhuri et al. (2016), apart from the control approaches in Liu et al. (2019, 2020) which consider the vehicle platooning. This line of research lacks signal optimization, so the full utilization of vehicle information (e.g., speed and position) and infrastructure information (e.g., signal timings) is hindered.

Based on previous research findings, we conclude that it is difficult to integrate traffic signal optimization with vehicle trajectory planning in a uni-

fied framework, because signal optimization and vehicle control are mutually dependent. Signals affect vehicle maneuvers and performance such as energy consumption and delay, and vehicle trajectories are of vital importance when adjusting signals in return. Therefore, the joint control approaches of traffic signals and vehicle trajectories can be solved by casting the problem in a bi-level optimization model to solve the problem iteratively (Li et al., 2014b; Yang et al., 2016b; Xu et al., 2018; Feng et al., 2018; Guo et al., 2019b; Niroumand et al., 2020; Liu et al., 2021). The vehicle arrival time at the stop-line is normally required to be estimated first and then be constrained in the terminal conditions of position and speed to represent the red indication (Xu et al., 2018; Feng et al., 2018; Guo et al., 2019b; Yu et al., 2018). In the traffic signal optimization, the enumeration method (Li et al., 2014b; Xu et al., 2018; Liu et al., 2021) and the similar forward/backward recursion method (Feng et al., 2018; Guo et al., 2019b) are usually adopted to evaluate all feasible signal parameters, while signals are not explicitly optimized in Li et al. (2014b); Yang et al. (2016b); Yu et al. (2018). Furthermore, some approximation methods are adopted for relieving computational load in vehicle trajectory optimization. The rule-based trajectory patterns are designed to approximate trajectories in Li et al. (2014b); Yang et al. (2016b); the following vehicles are simulated using car following models, while only the platoon leader is controlled (Feng et al., 2018; Yu et al., 2018); each vehicle is optimized individually in Xu et al. (2018), as opposed to trajectory optimization of the platoon; the receding horizon scheme is adopted to update trajectories and signals (Li et al., 2014b; Yang et al., 2016b; Feng et al., 2018) or update trajectories more frequently than signal timing variables (Niroumand et al., 2020), which benefits the computational load but unfortunately causes suboptimum owing to the shortsighted prediction.

This chapter presents a joint control approach to simultaneously optimize traffic signals and vehicle trajectories of all CAV platoons in the vicinity of signalized intersections. The vehicle accelerations and signal phase lengths are jointly optimized aiming to maximize ride comfort and minimize travel delay, subject to motion constraints. The red indication is first formulated as a logic constraint and then reconstructed as a series of linear position constraints. This red phase constraint formulation in this chapter is generic as it requires neither the prescribed terminal conditions of speed/position nor the additional estimation of vehicle arrival time. To further relieve the computational burden, the joint control problem is solved using mixed integer linear programming (MILP) techniques after the linearization of the objec-

tive function. The outputs of the proposed approach are the optimal signal phase lengths and the optimal acceleration trajectories of CAV platoons, so the global optimum considering all platoons is guaranteed within the signal cycle. This approach is scalable to incorporate multiple platoons from different movements under various traffic demand levels. To demonstrate the performance of the proposed approach, simulations under the balanced and unbalanced arrival rates from each arm are conducted, based on which the optimal vehicle trajectory pattern and the optimal traffic signal pattern are found. Finally, the comparison with the Intelligent Driver Model, the signal optimization models, and a state-of-the-art approach (Xu et al., 2018) is made, the results of which show the proposed approach generates higher throughput and less delay, energy consumption, and emission.

The contributions of this study are threefold. First, our approach simultaneously optimizes signal timing and vehicle trajectories of all platoons from multiple traffic movements. It does not require bi-level programming, nor simplifications of vehicle trajectories when optimizing signal timing, which results in nonlinear problems in general. Our formulation in mixed integer linear programming form ensures the global optimum of the control problem. Second, this chapter formulates the joint problem in a single layer other than in a bi-level structure. The nonlinear formulation of this joint control problem is recast in a linear formulation, which reduces the computational load substantially. The red phases are formulated into four linear constraints, which can avoid specifying the terminal conditions of speed and position beforehand. Thereby the infeasible solutions stemming from the inaccurate arrival time estimation are bypassed. Finally, the controller performance of the proposed approach is thoroughly verified in simulation and compared with the state-of-the-art approaches, based on which the optimal signal and trajectory patterns are derived.

The rest of this chapter is structured as follows. Section 5.2 formulates the joint optimal control problem of traffic signals and vehicle trajectories, and then the control formulation is reconstructed and linearized. In Section 5.3, the solution approach is introduced. The controller performance is validated by simulation in Section 5.4, and both the optimal vehicle trajectory pattern and the optimal traffic signal pattern are explored after that, in addition to the analysis on computational performance and the comparison with the car following model, the signal optimization models, and the state of the art. Finally, conclusions and future work are delivered in Section 5.5.

5.2 Control formulation

In this section, the joint optimal control problem of traffic signals and vehicle trajectories is formulated, including problem description, specifications of control and state variables, system dynamics, the objective function and controller constraints. Finally, the control formulation is linearized in this section.

5.2.1 Problem description

In this chapter, a standard signalized intersection is considered under a given signal phase sequence. The left-turn movements are separate from the through and right-turn movements from the perspective of signal and intersection designs. The example research scenario and the pre-defined signal plan are illustrated in Figure 5.1.

The control zone at the signalized intersection is restricted by V2V, V2I and I2V (Infrastructure-to-Vehicle) communication ranges (normally a few hundred meters), where the lane changing behavior is not considered. Vehicles in the control zone are assumed to be cooperative and thereby can be controlled via their (admissible) accelerations. Based on V2V and I2V communication, vehicle position and speed information as well as Signal Phasing and Timing (SPaT) information can be exchanged among each vehicle and the signal controller. The sum of feedback and vehicle actuation delays is

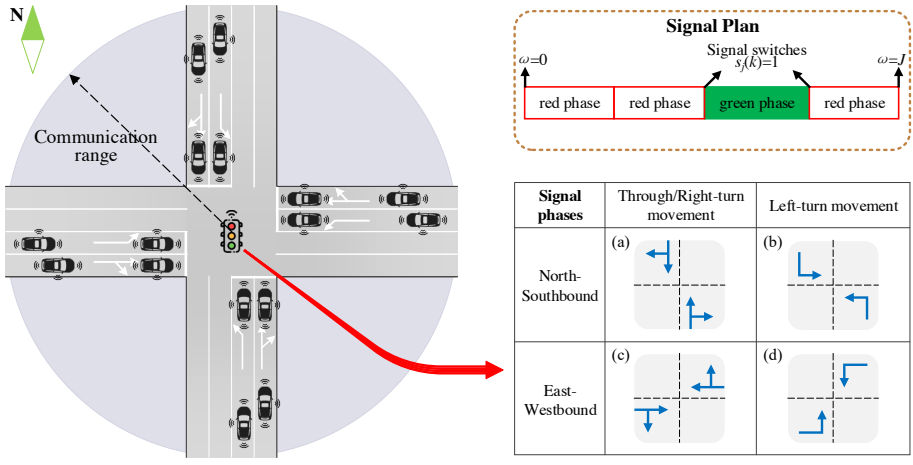

Figure 5.1: Illustration on operations of the control system

assumed to be less than 1 second and hence can be neglected in the control formulation when we choose a discrete time step size of 1 second.

Table 5.1: List of notations

General variables and parameters	
$\mathbb{R}$	Set of real numbers
$\mathbb{Z}$	Set of integers
$\mathbb{Z}^+$	Set of positive integers
$C \in \mathbb{Z}^+$	Signal cycle length, s
$\Delta t = 1$	Time step size, s
$K = \frac{C}{\Delta t} \in \mathbb{Z}^+$	Total number of time steps, i.e., prediction horizon
$k \in \mathbb{Z}^+$	Time index, $k \in \{1, 2, \ldots, K\}$
$J \in \mathbb{Z}^+$	Total number of signal phases in a signal cycle
$j \in \mathbb{Z}^+$	Sequence number of signal phase, $j \in \{1, 2, \ldots, J\}$
$\omega \in \mathbb{Z}^+$	Sequence number of signal switch in a signal cycle, $\omega \in \{0, 1, \ldots, J\}$
k_ω	The moment of the ωth signal switch, s
$N^j \in \mathbb{Z}^+$	Vehicle number in the jth movement
$N \in \mathbb{Z}^+$	Total vehicle number in a signal cycle
(i, j)	Vehicle sequence number i in the jth movement
β_1, β_2	Cost weights
H	Objective function
M	A large value
$A^j(\omega)$	Attached moment of signal switch, s
l_{ij}	The length of the ith vehicle in the jth movement, m
x^j_{stop}	Longitudinal position of the stop-line regarding the jth movement, m
$a_{\min}$	The minimal acceleration, $\mathrm{m/s^2}$
$a_{\max}$	The maximal acceleration, $\mathrm{m/s^2}$
$v_{\max}$	The maximal speed, $\mathrm{m/s}$
$t_{\min}$	The minimum safe car-following time gap, s
s_0	The minimum space gap at standstill conditions, m
$T_{\text{m}}^{\max}$	Maximal number of the released traffic movements
T_{m}	Released traffic movement sequence, $T_{\text{m}} \leq T_{\text{m}}^{\max}$
P_j	The jth optimal signal phase length, s
f_v	The instantaneous fuel consumption rate, ml/s
Control variables	

Table 5.1: List of notations (continued)

$a_{ij}(k)$	Discrete control variable, acceleration of the ith vehicle in the jth movement
$s_j(k)$	Discrete control variable, signal switch in the jth movement
$\gamma_{ij}(\omega)$	Auxiliary control variable, binary variable of passing the intersection or not at the moment of the ωth signal switch
$q_{ij}(k)$	Auxiliary control variable for linearization
$r_{ij}(k)$	Auxiliary control variable for linearization
$\mathbf{u}^{\mathbf{V}}$	Control variable vector of vehicle trajectory optimization for all vehicles in all movements
$\mathbf{u}^{\mathbf{S}}$	Control variable vector of traffic signal optimization for all vehicles in all movements
$\mathbf{u}$	Control variable vector of the joint controller for all vehicles in all movements
Γ	Control variable vector of $\gamma_{ij}(\omega)$ for all vehicles in all movements
State variables	
$x_{ij}(k)$	Discrete state variable, position of the ith vehicle in the jth movement
$v_{ij}(k)$	Discrete state variable, speed of the ith vehicle in the jth movement
$p_j(k)$	State variable, binary variable of traffic signal indication in the jth movement
$\mathbf{x}^{\mathbf{V}}$	State variable vector of vehicle trajectory optimization for all vehicles in all movements
$\mathbf{x}^{\mathbf{S}}$	State variable vector of signal optimization for all vehicles in all movements

The control objective is to jointly determine each signal phase length and vehicle acceleration trajectories from all traffic movements. In the proposed approach, the ride comfort and the travel delay are optimized subject to safety and physical motion constraints, and the vehicle positions during the red signal indication are also constrained when optimizing signal parameters. The main variables and parameters are summarized in Table 5.1.

5.2.2 Control and state variables

The *control variables* of the joint optimal control problem are the accelerations and the signal phase switches of the signal controller, which are detailed in this subsection. The prediction horizon is the signal cycle $C \in \mathbb{Z}^+$, which is an input of the joint controller. $k \in \mathbb{Z}^+$ is the time step within the prediction horizon, and Δt is the time step size. With the choice of $\Delta t = 1$ s and $K = \frac{C}{\Delta t}$, we have $k \in \{1,2,\ldots,K\}$. Let J denote the total signal phase number within a signal cycle and j represent the signal phase sequence number, $j \in \{1,2,\ldots,J\}$. J can respond to the vehicle actuation by skipping certain phase(s) if no vehicle is detected. For simplification, we refer the movement(s) that is released during the jth green phase as the jth movement(s). If i and N^j are the vehicle sequence number and the total vehicle number in the jth movement respectively, the pair of (i,j) can thereby describe the vehicle sequence number i in the jth movement ($i \in \{1,2,\ldots,N^j\}$). N is the total vehicle number within a cycle, which can be calculated by

$$N = \sum_{j=1}^{J} N^j \tag{5.1}$$

For vehicle trajectory planning, the control variable for vehicle i in jth movement $\mathbf{u}_{ij}^V$ is acceleration (vehicle decelerations are represented as negative accelerations), as follows:

$$\mathbf{u}_{ij}^V(k) = a_{ij}(k), k \in \{1,2,\ldots,K\} \tag{5.2}$$

The state variables of the subject vehicle, $\mathbf{x}_{ij}^V$, are the longitudinal position, $x_{ij}(k)$, and the speed, $v_{ij}(k)$. The state variables of trajectory planning are

$$\mathbf{x}_{ij}^V(k) = \begin{bmatrix} x_{ij}(k) \\ v_{ij}(k) \end{bmatrix}, k \in \{1,2,\ldots,K\} \tag{5.3}$$

The control variable vector of vehicle trajectory within the signal cycle, $\mathbf{u}^V$, is defined by $\mathbf{u}_{ij}^V(k)$, as in Equation (5.4). The same also holds for the state variable vector $\mathbf{x}^V$ in Equation (5.5).

$$\mathbf{u}^V(k) = \left[\underbrace{a_{11}(k), a_{12}(k), \cdots, a_{1J}(k)}_{i=1, j\in\{1,2,\ldots,J\}}, \cdots, \underbrace{a_{N^J1}(k), a_{N^J2}(k), \cdots, a_{N^JJ}(k)}_{i=N^J, j\in\{1,2,\ldots,J\}} \right]^{\mathrm{T}} \tag{5.4}$$

$$\mathbf{x}^V(k) = \left[\underbrace{\mathbf{x}_{11}^T(k), \mathbf{x}_{12}^T(k), \cdots, \mathbf{x}_{1J}^T(k)}_{i=1, j\in\{1,2,\ldots,J\}}, \cdots, \underbrace{\mathbf{x}_{N^J1}^T(k), \mathbf{x}_{N^J2}^T(k), \cdots, \mathbf{x}_{N^JJ}^T(k)}_{i=N^J, j\in\{1,2,\ldots,J\}} \right]^{\mathrm{T}} \tag{5.5}$$

With respect to the signal optimization, the control variable is the signal state of whether or not switching the signal phase to release the jth movement at each time step, $s_j(k)$. $s_j(k)$ is defined as a binary variable, setting $s_j(k)$ equal to 1 if shifting the signal at the time step k and 0 otherwise, as shown in Equation (5.6) and Equation (5.7).

$$\mathbf{u}_j^S(k) = s_j(k), k \in \{1, 2, \ldots, K\} \tag{5.6}$$

$$s_j(k) = \begin{cases} 1 & \text{switching signal of movement } j \\ 0 & \text{otherwise} \end{cases} \tag{5.7}$$

The state variable of signal optimization is the color indication of the traffic light in the jth movement at each time step $p_j(k)$. $p_j(k) = 1$ if the signal controller indicates red and otherwise $p_j(k) = 0$, as can be seen in Equation (5.8) and Equation (5.9).

$$\mathbf{x}_j^S(k) = p_j(k), k \in \{1, 2, \ldots, K\} \tag{5.8}$$

$$p_j(k) = \begin{cases} 1 & \text{red signal indication} \\ 0 & \text{green signal indication} \end{cases} \tag{5.9}$$

The control and state variable vectors of signal optimization regarding all traffic movements within the cycle, $\mathbf{u}^S$ and $\mathbf{x}^S$, are defined by $\mathbf{u}_j^S(k)$ and $\mathbf{x}_j^S(k)$ in time ($k \in \{1, 2, \ldots, K\}$, $j \in \{1, 2, \ldots, J\}$). It is also noted that the control variable vector of the joint controller is defined by $\mathbf{u}^V$ and $\mathbf{u}^S$, thus

$$\mathbf{u} = \begin{bmatrix} \mathbf{u}^V \\ \mathbf{u}^S \end{bmatrix} \tag{5.10}$$

5.2.3 System dynamics

The system dynamics model of the joint optimal control problem is presented separately for trajectory planning (as Equation (5.11)) and signal optimization (as Equation (5.12)). For the trajectory optimization subproblem, the system dynamics model is described using the following second-order equation.

$$\mathbf{x}_{ij}^{V}(k+1) = A\mathbf{x}_{ij}^{V}(k) + B\mathbf{u}_{ij}^{V}(k) \tag{5.11}$$

where

$$A = \begin{bmatrix} 1 & \Delta t \\ 0 & 1 \end{bmatrix}; B = \begin{bmatrix} \frac{1}{2}\Delta t^2 \\ \Delta t \end{bmatrix}$$

Here, Δt denotes the time step size. In addition, the dynamics equation of signal optimization is

$$p_j(k+1) = \left| p_j(k) - s_j(k) \right| \tag{5.12}$$

5.2.4 Objective function

Within the prediction horizon ($k \in \{1, 2, \ldots, K\}$), the ride comfort and travel delay of all controlled vehicles from all traffic movements are taken into account by minimizing the absolute value of accelerations and maximizing speeds. The objective function is designed as follows:

$$H = \min_{\mathbf{u}} \sum_{j=1}^{J} \sum_{i=1}^{N^j} \sum_{k=1}^{K} \left[\beta_1 |a_{ij}(k)| - \beta_2 v_{ij}(k) \right] \tag{5.13}$$

Here, β_1 and β_2 are cost weights. The unit of β_1 is defined as second and β_2 is unitless. The first cost term of ride comfort is designed to reduce fluctuations in accelerations. The second cost term of travel delay aims at stimulating vehicles to speed up, departing the intersection as soon as possible.

5.2.5 Controller constraints

The joint optimal controller requires the control and state variables to respect certain constraints, i.e., admissible accelerations, maximum speed bounds,

safe driving requirements, signal switch limitation and the red phase position constraints.

For vehicle trajectory planning, the accelerations of all vehicles are bounded within the admissible range between the maximal acceleration, $a_{\max}$, and the minimal acceleration (i.e., the negative of the maximal deceleration), $a_{\min}$.

$$a_{\min} \leq a_{ij}(k) \leq a_{\max} \tag{5.14}$$

The speeds of all vehicles are restricted to be nonnegative but not larger than the limit speed, $v_{\max}$.

$$0 \leq v_{ij}(k) \leq v_{\max} \tag{5.15}$$

As to the safe driving requirements, the following vehicles should keep at least the minimal safe gap with the vehicles in front. If l_{ij} denotes the length of vehicle i in the jth movement, $t_{\min}$ is the minimum safe car-following time gap, and s_0 is the minimum space gap at standstill conditions, the safety requirements can be represented as:

$$x_{i-1,j}(k) - x_{ij}(k) - v_{ij}(k)t_{\min} - s_0 - l_{ij} \geq 0, i \geq 2 \tag{5.16}$$

In terms of signal optimization, the signal cycle is supposed to contain at least a green phase and a red phase for each traffic movement, so the signal indication should switch at most twice within the prediction horizon. The total signal switch number of the jth movement is constrained as follows.

$$\sum_{k=1}^{K} s_j(k) \leq 2 \tag{5.17}$$

Vehicles are required to respond to signal changes when jointly optimizing traffic signals and vehicle trajectories. In order to connect vehicle positions with signal indications, auxiliary variables are introduced to represent the red phases. Let ω ($\in \{0, 1, \ldots, J\}$) denote the sequence number of signal switches. In the simple signal plans, such as Figure 5.1, $\omega = 0$ refers to the beginning of the signal cycle, $\omega = J$ corresponds to the signal cycle tail, and $\omega = j$ means the end of signal phase j. However, the signal switch ω and the signal phase j may be different in sophisticated signal plans.

Furthermore, the auxiliary binary variable of vehicle position condition, $\gamma_{ij}(\omega)$, is introduced to represent whether or not the ith vehicle in the jth movement can pass the intersection when switching the ωth signal. At the

specific moment of the ωth signal switch, $\gamma_{ij}(\omega)$ is defined as 1 if the subject vehicle cannot pass, and $\gamma_{ij}(\omega) = 0$ if it can pass the stop-line. To reflect the ωth signal switch in time, we refer to k_ω as the time step of the ωth traffic signal switch, i.e., the time when the ωth signal phase ends. Therefore, vehicle position condition $\gamma_{ij}(\omega)$ is represented using state variables of $x_{ij}(k_\omega)$ and $p_j(k_\omega)$. As in Equation (5.18), $\gamma_{ij}(\omega)$ is a step function, in which $\gamma_{ij}(\omega)$ becomes to 1 when $x_{ij}(k_\omega) \leq 0$ until $p_j(k_\omega - 1) \neq p_j(k_\omega)$ and drops to 0 if the ith vehicle in the jth movement passed the intersection.

$$\gamma_{ij}(\omega) = \begin{cases} 1 & x_{ij}(k_\omega) \leq 0, \text{until } p_j(k_\omega - 1) \neq p_j(k_\omega) \\ 0 & \text{afterwards} \end{cases} \tag{5.18}$$

5.2.6 Linear formulation of red phase constraints

The dimension of the joint control problem can be significantly large under high traffic demand levels. In order to relieve the excessive computational load, the control formulation is reconstructed. The red phase representation using the logic constraint of Equation (5.18) is first linearized, followed by linearization of the objective function.

The red phase representation of Equation (5.18) are a logic constraint, which is difficult to solve. To bypass this issue, the auxiliary variable of vehicle position condition $\gamma_{ij}(\omega)$ is introduced as additional control variables. If Γ is defined by $\gamma_{ij}(\omega)$ (see Equation 5.19), the control variable vector of the joint controller is replaced by Equation (5.20).

$$\Gamma = \Bigg[\underbrace{\overbrace{\gamma_{11}(1), \cdots, \gamma_{1J}(1)}^{\omega=1}, \cdots, \overbrace{\gamma_{11}(J-1), \cdots, \gamma_{1J}(J-1)}^{\omega=J-1}}_{i=1, j\in\{1,2,\ldots,J\}}, \cdots, \underbrace{\overbrace{\gamma_{N^J 1}(1), \cdots, \gamma_{N^J J}(1)}^{\omega=1}, \cdots, \overbrace{\gamma_{N^J 1}(J-1), \cdots, \gamma_{N^J J}(J-1)}^{\omega=J-1}}_{i=N^J, j\in\{1,2,\ldots,J\}} \Bigg]^{\mathrm{T}} \tag{5.19}$$

$$\mathbf{u} = \begin{bmatrix} \mathbf{u}^S \\ \mathbf{u}^V \\ \Gamma \end{bmatrix} \tag{5.20}$$

The problem arises when representing the additional system dynamics of the position condition $\gamma_{ij}(\omega)$, owing to its logical and binary features. However, the relationship between the position condition and the original control and state variables can be described as a series of inequality equations, as discussed below.

In the joint optimization of signals and trajectories, the vehicle position conditions $\gamma_{ij}(\omega)$ are known at the beginning and the tail of the signal cycle (i.e., $\omega = 0$ and $\omega = J$), but unknown at the intermediate signal switches when $\omega \in \{1, 2, \ldots, J-1\}$. Nevertheless, the unknown intermediate $\gamma_{ij}(\omega)$ values can be exploited using the known position conditions $\gamma_{ij}(0)$ and $\gamma_{ij}(J)$, because the vehicle position condition remains constant during any red phase, either behind or beyond the stop bar. In other words, we can convert the known position condition values to the uncertain position conditions when switching the ωth ($\in \{1, 2, \ldots, J-1\}$) signal, i.e., $\gamma_{ij}(\omega) = \gamma_{ij}(0)$ if the ωth signal switches to the green phase, and $\gamma_{ij}(\omega) = \gamma_{ij}(K)$ if the ωth signal switches to the red phase in the current signal cycle.

Although the phase lengths are jointly optimized and thereby unknown in the control formulation, $\gamma_{ij}(\omega)$ stays unchanged within the red signal indication, as discussed previously. Hereinafter, the red phase logic constraint of Equation (5.18) is reformulated by introducing the piecewise time moment $A^j(\omega)$ ($\omega \in \{1, 2, \ldots, J-1\}$). $A^j(\omega)$ is designed to attach the moment of the certain signal switch to the beginning or the end of the signal cycle ($k = 1, K$), as in Equation (5.21). The illustration of the signal switch and the attached moment $A^j(\omega)$ within a signal cycle are explained in Figure 5.2. The first (or the second) red time can be removed if the signal cycle starts (or ends) with the green phase. In Equation (5.21), the attached moment equals to the time step of either the beginning or the end of the current cycle, i.e., $A^j(\omega) = 1$ if the ωth signal switches to the green phase and $A^j(\omega) = K$ otherwise.

$$A^j(\omega) = \begin{cases} 1 & \text{until } p_j(k_\omega - 1) = 0, p_j(k_\omega) = 1 \\ K & \text{afterwards} \end{cases}, \omega \in \{1, 2, \ldots, J-1\} \tag{5.21}$$

Furthermore, four linear constraints of Equation (5.22) to Equation (5.25) are proposed to restrict vehicle positions during the red phase(s) without specific signal parameters. Let x^j_{stop} imply the longitudinal position of the stop bar in the jth movement, and M is a large value. Under the workings of these four constraints, the known position condition values can be trans-

ferred from the beginning/end of the signal cycle to the unspecific moments of signal switches.

The constraints of Equation (5.22) and Equation (5.23) demonstrate the position condition at the ωth signal switch equal to the position condition at the attached moment (either the beginning or the end of the signal cycle). Taking Figure 5.2 as an example, if the vehicle can pass the intersection during the green phase ($\gamma_{ij}(J-1)=0$), Equation (5.22) and Equation (5.23) require the vehicle position to be larger than or equal to the position of the stop bar at the end of the current signal cycle, $x_{ij}(A^j(J)) \geq x^j_{\text{stop}}$. Similarly, the terminal position condition of stopping vehicles that cannot depart the intersection ($x_{ij}(K) \leq x^j_{\text{stop}}, \gamma_{ij}(J)=1$) is also conveyed to the $(J-1)$th signal switch via $A^j(\omega)$, thus $\gamma_{ij}(J-1)=1$. If the subject vehicle is behind the stop bar at the beginning of the signal cycle, i.e., $\gamma_{ij}(0)=1$, this position condition is transferred to the first signal switch by the attached moment, thus $\gamma_{ij}(1)=1$. In this way, the vehicle position remains unchanged during the red phase(s) in the signal cycle under indefinite signal parameters.

$$x_{ij}(A^j(\omega)) - x^j_{\text{stop}} \leq (1-\gamma_{ij}(\omega))M \tag{5.22}$$

$$-x_{ij}(A^j(\omega)) + x^j_{\text{stop}} \leq \gamma_{ij}(\omega)M \tag{5.23}$$

Regarding the remaining time within the signal cycle, the vehicle position constraints are elaborated in Equation (5.24) and Equation (5.25). As denoted above, k_ω is the time step of the ωth signal switch, and thus $s_j(k_\omega)=1$ means that the traffic signal is switched at $t=k_\omega$ and otherwise

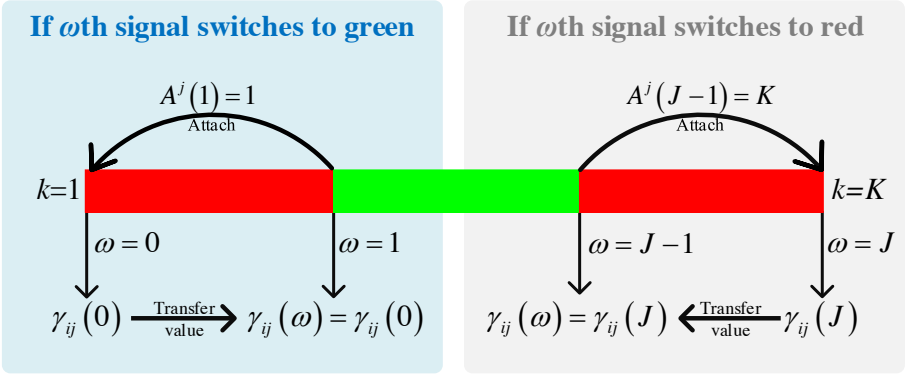

Figure 5.2: Illustration of signal switches and attached moments

$s_j(k_\omega) = 0$. Therefore, the position condition $\gamma_{ij}(\omega)$ is unchanged until the traffic signal is switched (i.e., $s_j(k_\omega) = 1$).

$$x_{ij}(k) - x^j_{\text{stop}} \leq (1 - \gamma_{ij}(\omega))M + (1 - s_j(k_\omega))M \tag{5.24}$$

$$x_{ij}(k) - x^j_{\text{stop}} \geq -\gamma_{ij}(\omega)M - (1 - s_j(k_\omega))M \tag{5.25}$$

In this way, the red phase logic constraint of Equation (5.18) is replaced by a series of linear constraints.

5.2.7 Linearization of the objective function

To simplify this control formulation, the first cost term in the objective function of Equation (5.13) should be linearized. Two auxiliary non-negative variables $q_{ij}(k)$ and $r_{ij}(k)$ are introduced as follows:

$$q_{ij}(k) = \frac{|a_{ij}(k)| + a_{ij}(k)}{2}, q_{ij}(k) \geq 0 \tag{5.26}$$

$$r_{ij}(k) = \frac{|a_{ij}(k)| - a_{ij}(k)}{2}, r_{ij}(k) \geq 0 \tag{5.27}$$

Therefore, the accelerations and the ride comfort cost term can be represented as

$$a_{ij}(k) = q_{ij}(k) - r_{ij}(k), q_{ij}(k) \geq 0, r_{ij}(k) \geq 0 \tag{5.28}$$

$$|a_{ij}(k)| = q_{ij}(k) + r_{ij}(k), q_{ij}(k) \geq 0, r_{ij}(k) \geq 0 \tag{5.29}$$

The auxiliary variables of $q_{ij}(k)$ and $r_{ij}(k)$ can be regarded as additional control variables in the controller, subject to the above linear equality constraints. After replacing the ride comfort cost term in the objective function using Equation (5.29), the control problem is reformulated as:

$$H = \min_{\mathbf{u}} \sum_{j=1}^{J} \sum_{i=1}^{N^j} \sum_{k=1}^{K} [\beta_1 (q_{ij}(k) + r_{ij}(k)) - \beta_2 v_{ij}(k)] \tag{5.30}$$

subject to constraints of Equation (5.11), (5.12), (5.14) to (5.17), (5.22) to (5.25), and (5.28).

5.3 Solution approach

The control variables contain integer variables of signal state $s_j(k)$ and position condition $\gamma_{ij}(\omega)$, so the optimal control problem can be solved using mixed integer linear programming (MILP) techniques. The system dynamics of Equation (5.11) and (5.12) and the linearization equation via auxiliary variables Equation (5.28) are implemented as linear equality constraints. The state variables of speeds and positions can be represented using accelerations via the system dynamic equation. Therefore, all linear inequality constraints of Equation (5.14) to (5.17) and Equation (5.22) to (5.25) are transformed to restrict the control variable acceleration. This optimal control problem is solved using intlinprog solver in MATLAB.

To be noted, the optimization solver intlinprog is warm-started to expedite the runtime. The initial guess of the signal plan is assumed to divide the signal cycle evenly into average signal phases. The initial guess of accelerations is the maximal acceleration until reaching the maximal speed at the beginning of green phases. The initial guess of position condition $\gamma_{ij}(\omega)$ is estimated by the vehicle positions at the end of green phases under the initial acceleration guess, i.e., whether the vehicles can pass the intersection. The joint optimal control algorithm yields the optimal signal parameters and the optimal vehicle trajectories. In the forthcoming section, the outputs of this control algorithm are presented and analyzed before the optimal patterns of trajectories and signals are explored.

5.4 Simulation results and analysis

In order to demonstrate the performance of this controller, the simulation results are discussed after designing several experiments in this section. The optimal results have the single optimum due to the linearity feature of the control formulation.

5.4.1 Experiment design

In simulation experiments, traffic movements on multiple lanes are designed to be released during the same green phase. To make it clear, the notations of J and j are consequently replaced by $T_{\mathrm{m}}^{\max}$, the maximal number of the released traffic movements, and T_{m} ($\leqslant T_{\mathrm{m}}^{\max}$), the released traffic movement sequence. In other words, each green phase (e.g., jth) discharges two

movements, so the jth movement in control formulation corresponds to two movements (i.e., $T_{\mathrm{m}} = j, j+J$) from two opposite arms within one green phase in simulation settings.

Multiple simulation experiments are designed to validate the performance of the control algorithm, taking into account the controlled vehicle number N, the maximal number of the released traffic movements $T_{\mathrm{m}}^{\max}$ (corresponding to each arm during every signal phase), and the signal cycle length C. The controlled vehicles include the queuing vehicles at the stop-line and the approaching vehicles from the boundary of the control zone. To verify the flexibility of the joint control approach in incorporating various signal designs, the controlled vehicles are released into multiple movements within the cycle lengths from 40 s to 60 s respectively.

When $T_{\mathrm{m}}^{\max} = 4$, the turning movements are indistinct at the intersection, so the traffic movements of (a) and (b) (see Figure 5.1) are regarded as two movements from two opposite arms which are released during the first phase, and movements of (c) and (d) are released during the other phase. When $T_{\mathrm{m}}^{\max} = 6$, the turning movements from one pair of the two opposite arms (either movements of (a) and (b) in the northbound/southbound direction or movements of (c) and (d) in the eastbound/westbound direction) are not differentiated at the intersection, which means they are released together in one green phase. The remaining movements of (c) and (d) (or (a) and (b)) are discharged separately during two green phases with the distinction of left-turning movements. When $T_{\mathrm{m}}^{\max} = 8$, traffic movements (a) to (d) depart the intersection in sequence respectively within four signal phases. To be noted, the signal phase(s) can be skipped based on the vehicle actuation if no queuing and incoming vehicles are detected. In other words, the signal phase number J can be optimized according to vehicle actuation.

If the other cost weight is constant, the magnitude of ride comfort cost weight β_1 affects the fluctuations of accelerations. Smaller values of β_1 result in more frequent variations on accelerations, while vehicles may not reach the maximal speed if β_1 is overweighted, causing lower traffic efficiencies because of unable to fully utilize the green phases. The cost weights of β_1 and β_2 are tuned based on the scenario with the largest dimension of control variables, and then applied in all scenarios. First, β_2 is fixed to be 1, and then β_1 is increased from 1 until the variations of accelerations/decelerations are smooth facing the red phases and most vehicles can reach the maximal speed after the green phase. Finally, β_1 is selected to be 7 when $\beta_2 = 1$, under which the acceleration trajectories are smooth without any unnecessary

fluctuation, and the vehicle speeds are able to reach the maximal speed when passing the intersection.

The parameter and coefficient values are detailed in Table 5.2, which mainly come from our previous work (Liu et al., 2020). The designed initial conditions in Table 5.2 are representative. In addition, similar settings and initial conditions add no difficulty on implementation. Delays under 1 s can be ignored because the time step is 1 s.

5.4.2 Operational performance analysis

To verify the feasibility of the control algorithm, the performance of the proposed approach is simulated under different traffic demand levels, signal cycle lengths and the maximal released traffic movement numbers, as detailed in Table 5.3. First, the controller performance is explored thoroughly under the balanced vehicle arrival rates from different arms, i.e., the uniform vehicle settings of Case 1, 2 and 3 (see Table 5.2) per movement released into at most 4, 6 and 8 traffic movements ($T_{\mathrm{m}}^{\max} = 4, 6, 8$) within the cycle lengths from 40 s to 60 s. For concise demonstration, only two scenarios under the balanced vehicle arrival rates are selected to present the optimal trajectories and the optimal signals (Scenario 1 and 2). In addition, Scenario 3 and 4 are designed under the unbalanced vehicle arrival rates from each arm considering the signal phase sequences and turning proportions. The objectives of Scenario 1 to Scenario 4 aim to not only explore the controller performance of the optimal trajectories when platoons react to the optimal signals, but prove the feasibility of the proposed approach in integrating the oversaturated traffic flow and the balanced/unbalanced arrival rates, considering various signal plans and turning proportions under different cycle lengths and the maximal released movements.

The traffic demand levels and the vehicle arrival rates under all scenarios are detailed as follows. The total controlled vehicle numbers are different under four scenarios in order to test the performance of the proposed approach under various traffic demand levels, such as in Scenario 2 and 4 where the controlled vehicle numbers are larger than the maximal vehicle numbers to be released while fewer vehicles are included in Scenario 1 and 3. The controlled vehicle numbers of each movement are balanced in Scenario 1 and 2, i.e., 4 queuing vehicles at the stop bar and 4 approaching vehicles from the upstream direction of the intersection (referring to Case 3). However, the vehicle arrival rates from each arm are unbalanced in Scenario 3 and

Table 5.2: Parameter and coefficient values

Notation	Parameter/ Coefficient	Value	Unit
-	Initial speed of approaching vehicles	10	m/s
-	Initial space gap of approaching vehicles	25	m
-	Initial position of the leader in the approaching vehicles	-200	m
-	Initial space gap of queuing vehicles	5	m
-	Initial position of the leader in the queuing vehicles	-5	m
-	Control zone range	200	m
Δt	Time step size	1	s
M	A large value	100000	-
l_{ij}	Length of the ith vehicle in the jth movement	3	m
x^j_{stop}	Position of the stop line	0	m
$a_{\min}$	Allowable minimum acceleration	-5	m/s^2
$a_{\max}$	Allowable maximum acceleration	2	m/s^2
$v_{\max}$	Limit speed	20	m/s
$t_{\min}$	Minimum safe car-following time gap for the right-turn, through and left-turn movements respectively	3,2,2.5	s
s_0	Minimum space gap at standstill conditions	2	m
β_1	Cost weight	7	s
β_2	Cost weight	1	-
-	Queuing vehicle number per movement in Case 1, 2, 3	2,3,4	-
-	Approaching vehicle number per movement in Case 1, 2, 3	2,3,4	-
N^j	Total vehicle number per movement in Case 1, 2, 3	4,6,8	-
$T_{\text{m}}^{\max}$	Maximal number of the released traffic movements within the signal cycle	4,6,8	-
C	Signal cycle length	40,41,...,60	s

4, which means the compositions of the queuing and approaching vehicle platoons from 8 movements are randomly generated, just like determining

the number of balls in each basket when throwing N balls into 16 baskets randomly.

The turning movements and signal designs under all scenarios are hereinafter disclosed. Scenario 1 and 2 do not distinguish the turning movements, and thereby the desired time headways are 2 s for all vehicles. However, the movements of right turning, through and left turning can be reflected by adopting different values of the minimal safe car-following time gap $t_{\min}$ (see Table 5.2). Scenario 3 and 4 make a distinction between the different signal phase sequences and the turning proportions. In Scenario 3, the left-turn movements ($T_{\mathrm{m}} = 1,3,5,7$) are released prior to the through/right-turn movements ($T_{\mathrm{m}} = 2,4,6,8$), while things are opposite under Scenario 4. The left-turn movements have exclusive lanes and signal phases, so the left-turn proportions are equal to 1. For the through/right-turn shared movements, the right-turn proportions in movements of $T_{\mathrm{m}} = 2,4,6,8$ are 0.3 under Scenario 3, while the right-turn proportions under Scenario 4 are 0.3, 0.4, 0.5 and 0.6 in movements of $T_{\mathrm{m}} = 1,3,5,7$ respectively. In addition, the vehicle compositions of through and right-turn vehicles in the through/right-turn shared movements are produced at random.

In general, the simulation results of Scenario 1 to Scenario 4 show that vehicles are able to respond to the optimal signals via smooth trajectories and all constraints are satisfied. The passing vehicles reach the maximal speed as soon as possible and the stopping vehicles perform to decelerate from the initial speed, smoothly approaching the stop-line with lower speeds. When the green phase starts, vehicles behind the stop bar accelerate to pass but still keep the safe following gaps with the vehicles in front. Overall, it can be concluded that the control approach is feasible under different traffic demand levels, vehicle arrival rates and signal designs. In addition, the joint controller is flexible in accounting for multiple platoons from various traffic turning movements, including queuing and approaching vehicles at the intersection. The optimal trajectories under Scenario 1 to Scenario 4 and the optimal signals are explored and discussed below.

Vehicle trajectory pattern

The optimal performance of longitudinal position trajectories under all scenarios are depicted in Figure 5.3 to Figure 5.6. In Figure 5.3 and 5.4, the trajectories of movements $T_{\mathrm{m}} = 5,6,7,8$ are not presented under Scenario 1 and 2, because they are the same as the trajectories of movements $T_{\mathrm{m}} = 1,2,3,4$

Table 5.3: Scenario design

Scenario design	Scenario 1	Scenario 2	Scenario 3	Scenario 4
Cycle length (s)	C=50	C=60	C=50	C=40
Maximal released movements	$T_{\mathrm{m}}^{\max} = 6$	$T_{\mathrm{m}}^{\max} = 8$	$T_{\mathrm{m}}^{\max} = 8$	$T_{\mathrm{m}}^{\max} = 8$
Total controlled vehicle number (veh/cycle)	$N = 48$	$N = 64$	$N = 44$	$N = 48$
Maximal vehicle number to be released (veh/cycle)	50	60	50	40
Controlled vehicle number per movement (veh/movement)	8 (Case3)	8 (Case3)	Random	Random
Vehicle arrival rates per movement	Balanced	Balanced	Unbalanced	Unbalanced
Signal phase sequence	-	-	Left-turn first	Right-turn first
Turning proportions of the right-turn movements	-	-	0.3, 0.3, 0.3, 0.3	0.3, 0.4, 0.5, 0.6

under the balanced vehicle arrival rates. Other scenarios of the balanced vehicle arrival rates that are not presented here have the significantly similar performance as Scenario 1 and 2. The speed information is displayed in color, as shown in the colorbar of Figure 5.3 (c). The optimal red phase lengths are depicted as black dashed lines at the stop bar in these figures, and the vehicle sequence number in the legend of Figure 5.4 (h) starts from the queuing vehicle with the largest initial position (Vehicle 1) to the approaching vehicle in the platoon tail.

The trajectories under all scenarios demonstrate that all vehicles are able to react to the signal changes, as the longitudinal position subfigures in Figure 5.3 to 5.6. Thus, the red phase constraints of Equation (5.22) to Equation (5.25) are proved to be effective in the joint control formulation. In addition, typical vehicle trajectories such as accelerations/decelerations of stopping, passing and queuing vehicles are considerably smooth, as can be seen in the acceleration subfigures of Figure 5.4 (e) to (h).

The optimal trajectory pattern of vehicles' approach/exit, acceleration, merge, and platoon stability can be summarized from the optimal perfor-

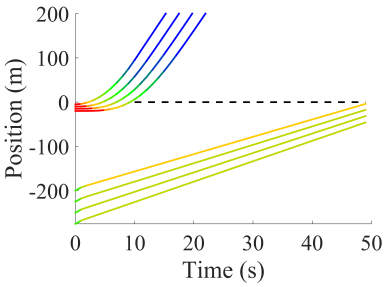

(a) trajectories of movement $T_{\mathrm{m}} = 1$ $(j = 1)$

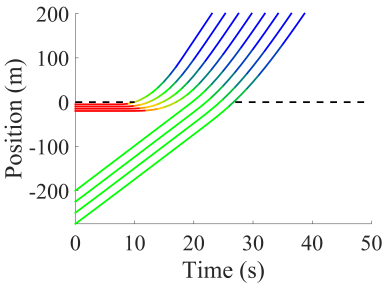

(b) trajectories of movement $T_{\mathrm{m}} = 2$ $(j = 2)$

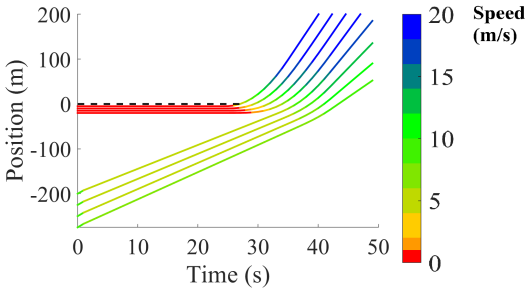

(c) trajectories of movement $T_{\mathrm{m}} = 3$ $(j = 3)$

Figure 5.3: Optimal performance under Scenario 1

mance under all scenarios in Figure 5.3 to 5.6. Vehicles tend to avoid stops and try to exit the intersection with higher speeds. At the beginning of the green phase, the queuing vehicles accelerate dramatically from the stationary condition, aiming to exit the intersection as soon as possible. This acceleration pattern of queuing vehicles is evident when we look at the accelerations of Vehicle 1 in Figure 5.4. When merging, vehicles may decrease the acceleration rates a little bit to keep the safe gap with the preceding vehicles. With respect to the acceleration fluctuations, the following vehicles always perform smaller changes than the predecessors, which proves the platoon stability.

In Scenario 3 and 4, the turning movements are distinguished using the minimal safe car-following time gap t_{min}, i.e., setting $t_{\mathrm{min}} = 3$ s for the right-turn movement, $t_{\mathrm{min}} = 2$ s for the through movement and $t_{\mathrm{min}} = 2.5$ s for the left-turn movement. The turning movements are depicted as the solid lines for the through movement, the dotted lines for the right-turn movement and the dashed lines for the left-turn movement in Figure 5.5 to 5.6. The differ-

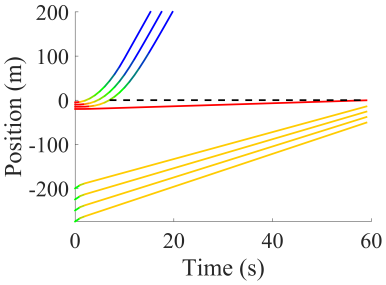

(a) position of movement $T_{\mathrm{m}} = 1$ $(j = 1)$

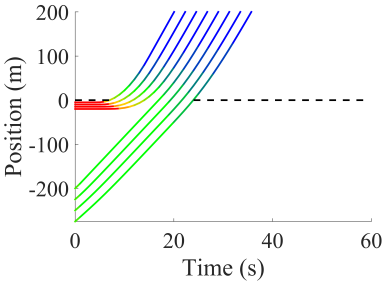

(b) position of movement $T_{\mathrm{m}} = 2$ $(j = 2)$

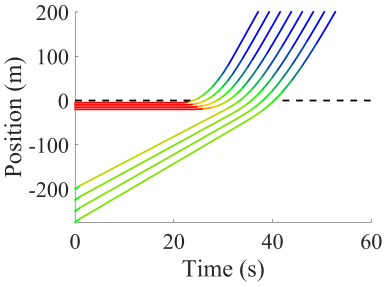

(c) position of movement $T_{\mathrm{m}} = 3$ $(j = 3)$

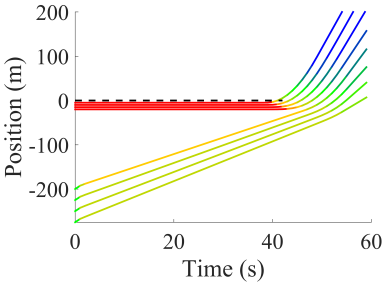

(d) position of movement $T_{\mathrm{m}} = 4$ $(j = 4)$

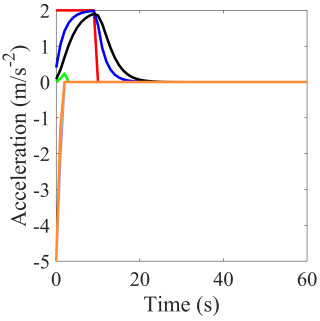

(e) acceleration of movement $T_{\mathrm{m}} = 1$ $(j = 1)$

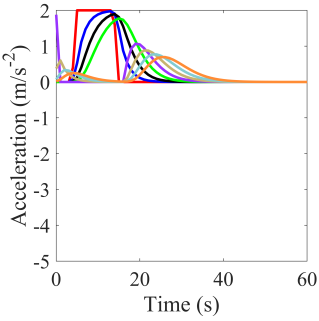

(f) acceleration of movement $T_{\mathrm{m}} = 2$ $(j = 2)$

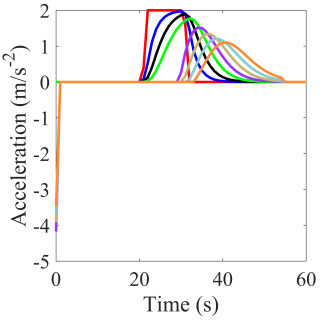

(g) acceleration of movement $T_{\mathrm{m}} = 3$ $(j = 3)$

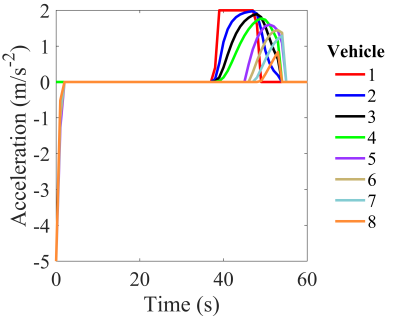

(h) acceleration of movement $T_{\mathrm{m}} = 4$ $(j = 4)$

Figure 5.4: Optimal performance under Scenario 2

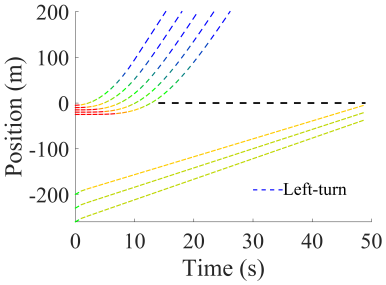

(a) trajectories of movement $T_{\mathrm{m}} = 1$ $(j = 1)$

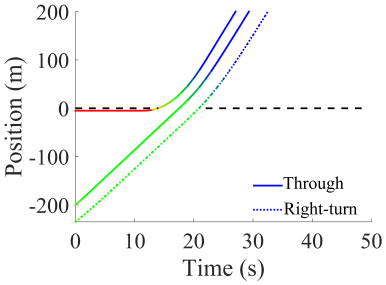

(b) trajectories of movement $T_{\mathrm{m}} = 2$ $(j = 2)$

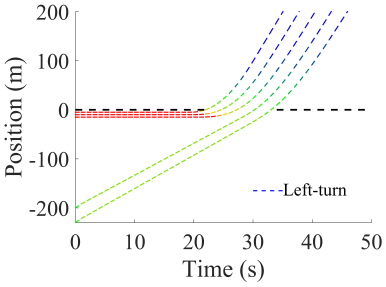

(c) trajectories of movement $T_{\mathrm{m}} = 3$ $(j = 3)$

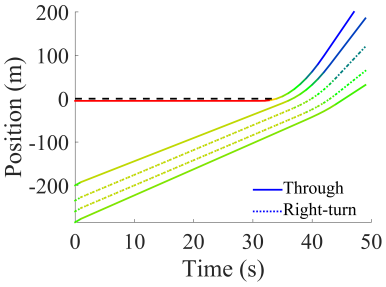

(d) trajectories of movement $T_{\mathrm{m}} = 4$ $(j = 4)$

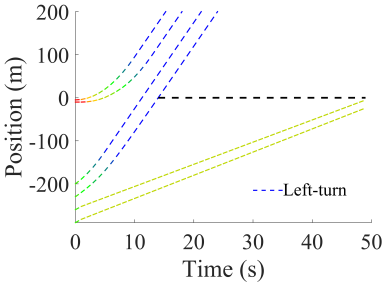

(e) trajectories of movement $T_{\mathrm{m}} = 5$ $(j = 1)$

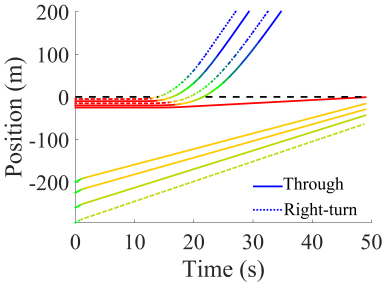

(f) trajectories of movement $T_{\mathrm{m}} = 6$ $(j = 2)$

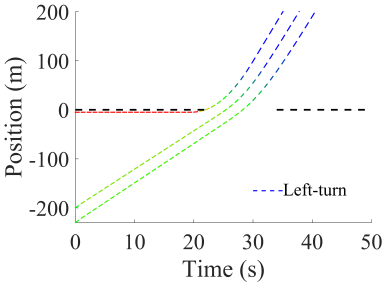

(g) trajectories of movement $T_{\mathrm{m}} = 7$ $(j = 3)$

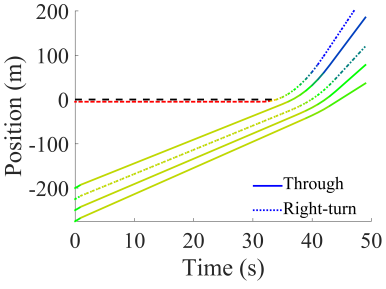

(h) trajectories of movement $T_{\mathrm{m}} = 8$ $(j = 4)$

Figure 5.5: Optimal performance under Scenario 3

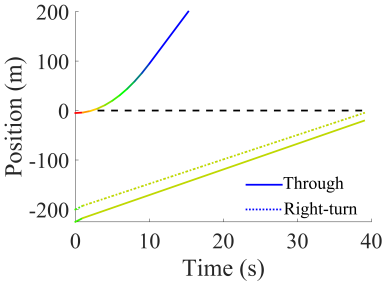

(a) trajectories of movement $T_{\mathrm{m}} = 1$ $(j = 1)$

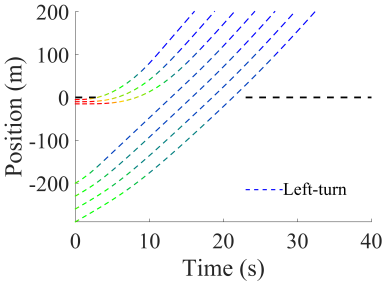

(b) trajectories of movement $T_{\mathrm{m}} = 2$ $(j = 2)$

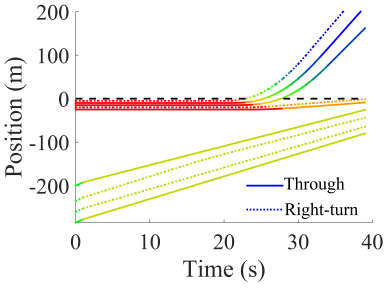

(c) trajectories of movement $T_{\mathrm{m}} = 3$ $(j = 3)$

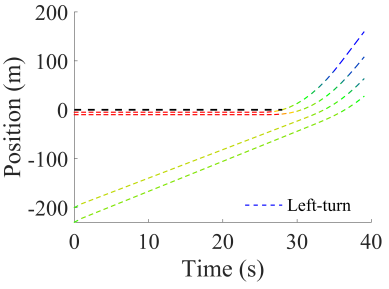

(d) trajectories of movement $T_{\mathrm{m}} = 4$ $(j = 4)$

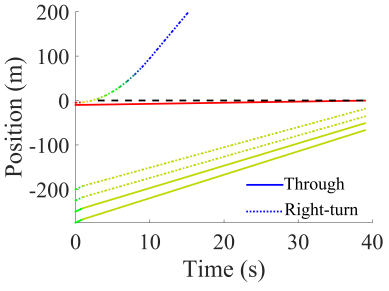

(e) trajectories of movement $T_{\mathrm{m}} = 5$ $(j = 1)$

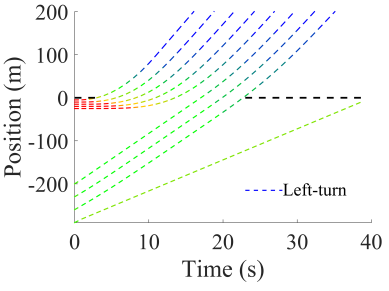

(f) trajectories of movement $T_{\mathrm{m}} = 6$ $(j = 2)$

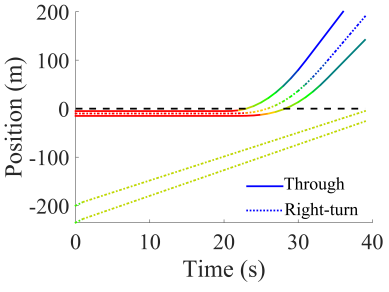

(g) trajectories of movement $T_{\mathrm{m}} = 7$ $(j = 3)$

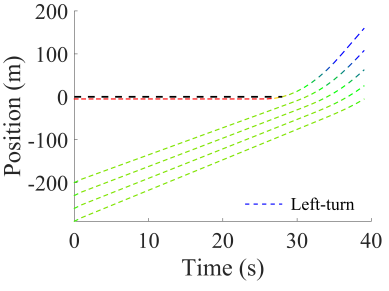

(h) trajectories of movement $T_{\mathrm{m}} = 8$ $(j = 4)$

Figure 5.6: Optimal performance under Scenario 4

ences in the gaps between the right-turn and through movements are obvious (see the second and third vehicles in Figure 5.5 (b), for instance). The optimal trajectory pattern is still respected under Scenario 3 and 4 considering various turning proportions and signal phase sequences, as can be seen in Figure 5.5 to 5.6. Therefore, the flexibility of the proposed control approach in incorporating different signal designs and turning movements is verified.

Furthermore, the approaching vehicles in the movements of $T_{\mathrm{m}} = 4, 8$ confront a long preceding red phase, so they have to decelerate and arrive at the stop-line with relatively low speeds. For instance, the arrival speeds of approaching vehicles in movements of $T_{\mathrm{m}} = 2$ and 4 are normally 12 m/s and 4 to 5 m/s respectively. Therefore, the traffic efficiency of releasing vehicles in movements of $T_{\mathrm{m}} = 4$ and $T_{\mathrm{m}} = 8$ is lower compared to the other movements, which is demonstrated by the dispersion in position trajectories during the green phases in the movements of $T_{\mathrm{m}} = 4$ and 8, as can be seen in Figure 5.3 (c), 5.4 (d), 5.5 (d) and (h), 5.6 (d) and (h). This lower efficiency in the movements of $T_{\mathrm{m}} = 4$ and 8 also affects the performance of the optimal signals, which will be detailed in the discussion of the traffic signal pattern.

Traffic signal pattern

In order to explore the signal pattern, the optimal signals under the balanced vehicle arrival rates of Case 1, 2, and 3 with the cycle lengths from 40 s to 60 s are listed, as in Table 5.4 ($T_{\mathrm{m}}^{\max} = 6$) and Table 5.5 ($T_{\mathrm{m}}^{\max} = 8$). Furthermore, the optimal signals under the cycle lengths of 40 s, 50 s, and 60 s are presented in Figure 5.7 for convenience of analysis, where the signal phase lengths are arranged in sequence. If P_j denotes the length of the jth signal phase, the green, grey, red and blue lines in Figure 5.7 represent the first phase length P_1 to the last phase length P_4 respectively.

Overall, the signals are optimized to release as many vehicles as possible by switching signal phases in time, owing to the travel delay cost term in the objective function of Equation (5.30). The benchmark values observed from the optimal signals are identified for analysis, that is, releasing all vehicles as soon as possible in P_1 under Case 1, 2 and 3 requires 14 s, 16 s and 20 s respectively, and the counterparts in P_2 are 8 s, 12 s and 17 s. Hereinafter, the oversaturated traffic flow represents the situation that some vehicles have to be left within the signal cycle. The undersaturated traffic flow refers to the condition that all vehicles can be released within the cycle, i.e., the signals are longer than or equal to the aforementioned benchmark signal values. The

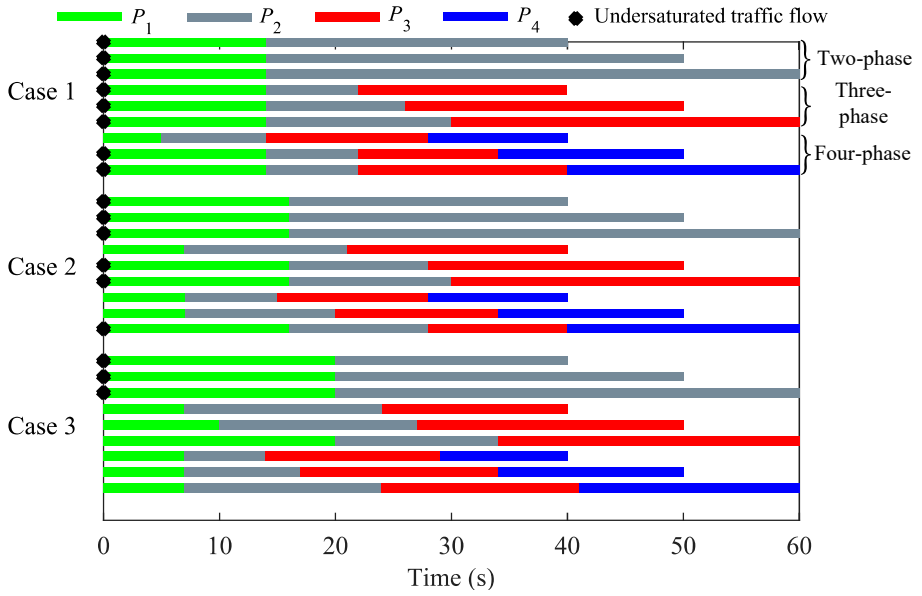

Figure 5.7: Optimal signals under the balanced vehicle arrival rates

optimal signals under the undersaturated traffic flow are demonstrated as the diamond markers in Figure 5.7 and also in the bold numbers of Table 5.4 and 5.5.

First, the optimal signal pattern in the undersaturated traffic flow with the balanced arrival rates is explored. The optimal signals tend to fix P_1 as the benchmark value, and then distribute more green time to the latter signal phases in the undersaturated traffic flow. As the bold numbers in Table 5.4 and 5.5, P_1 is always optimized to obey the benchmark signals when $T_{\mathrm{m}}^{\max} = 6$ and $T_{\mathrm{m}}^{\max} = 8$, while P_2 and P_3 are partially deviated from the benchmark values. This observation also holds for $T_{\mathrm{m}}^{\max} = 4$ ($J = 2$). The traffic flow is undersaturated with the cycle lengths from 40 s to 60 s when $J = 2$, so P_1 under $T_{\mathrm{m}}^{\max} = 4$ is always optimized to switch as the benchmark signals, as can be seen in Figure 5.7. It can be concluded that P_1 is independent of the signal cycle lengths and the signal phase numbers under the undersaturated traffic flow.

However, the optimal signal performance in the oversaturated traffic flow with the balanced vehicle arrival rates is different, as shown in the phase lengths without markers in Figure 5.7 and the normal numbers in Table 5.4 and 5.5. The joint controller tends to allocate more green time to the signal phases in middle (e.g., P_2 or P_3). On one hand, the approaching vehicles

in the movement of $T_m = 1$ have to utilize the green time to catch up with the queuing vehicles. This however is not a problem for the approaching vehicles of movements $T_m = 2,3,4$ during P_2, P_3 and P_4, because they are able to utilize the preceding red phase (at least P_1) to reach the stop bar. Thus, terminating P_1 earlier results in releasing more vehicles in the later green phases in the oversaturated traffic flow. As can be seen in Scenario 2, P_1 is switched even without releasing the last queuing vehicle in Figure 5.4 (a), and in this way all vehicles of movements $T_m = 2,3,4$ are dissipated, as in Figure 5.4 (b) to (d). On the other hand, the arrival speeds of the approaching vehicles in the last signal phase (e.g., P_3 or P_4) is lower compared to the counterparts in other signal phases, as discussed in the vehicle trajectory pattern. In other words, the signal phases in middle (P_2 or P_3) require less green time to release one more vehicle. The last signal phase is thereby less efficient (with respect to throughput and travel delay) under the oversaturated traffic flow.

The optimal signals under the unbalanced vehicle arrival rates from different arms basically obey the abovementioned patterns, and the signals are optimized to be responsive to the unbalanced vehicle actuations, as shown in Figure 5.5 of Scenario 3 and Figure 5.6 of Scenario 4. The optimal signal phase lengths of P_1 to P_4 are 15 s, 6 s, 13 s and 16 s under Scenario 4, and 3 s, 12 s, 13 s and 12 s under Scenario 4. Although the optimal signals under the unbalanced vehicle arrival rates do not obviously allocate more green time to the signal phases in middle as under the balanced vehicle arrival rates, the optimal signals can react to the actuation of the controlled vehicles based on the information of speed and position. It can be concluded that the traffic signals are optimized to release the most vehicles within the cycle under the unbalanced vehicle arrival rates, so the green time is rarely wasted without discharging any vehicle.

With an increase in the signal cycle length, the total number of passing vehicles within the cycle rises, but the objective function value decreases. Thus, the cycle length should be restricted as a constant or at least be bounded within a certain range; otherwise, the signal optimization will extend the current cycle as long as possible. In addition, the signal phase lengths in Table 5.4 and 5.5 show the tendency that the moments of switching signals are normally the same under similar signal cycle lengths.

Table 5.4: Optimal signals under the balanced vehicle arrival rates ($T_{\mathrm{m}}^{\max} = 6$)

Cycle length	**Case 1 (24 veh)**				**Case 2 (36 veh)**				**Case 3 (48 veh)**			
C (s)	P_1	P_2	P_3	Released vehicles	P_1	P_2	P_3	Released vehicles	P_1	P_2	P_3	Released vehicles
C=40	**14**	**8**	**18**	**24** veh	7	14	19	30 veh	7	17	16	38 veh
C=41	**14**	**8**	**19**	**24** veh	7	14	20	30 veh	7	17	17	38 veh
C=42	**14**	**8**	**20**	**24** veh	7	15	20	30 veh	7	17	18	38 veh
C=43	**14**	**8**	**21**	**24** veh	7	15	21	30 veh	7	17	19	38 veh
C=44	**14**	**9**	**21**	**24** veh	**16**	**12**	**16**	**36** veh	7	17	20	38 veh
C=45	**14**	**9**	**22**	**24** veh	**16**	**12**	**17**	**36** veh	7	17	21	38 veh
C=46	**14**	**10**	**22**	**24** veh	**16**	**12**	**18**	**36** veh	7	17	22	38 veh
C=47	**14**	**10**	**23**	**24** veh	**16**	**12**	**19**	**36** veh	7	17	23	38 veh
C=48	**14**	**11**	**23**	**24** veh	**16**	**12**	**20**	**36** veh	7	18	23	38 veh
C=49	**14**	**11**	**24**	**24** veh	**16**	**12**	**21**	**36** veh	7	18	24	38 veh
C=50	**14**	**12**	**24**	**24** veh	**16**	**12**	**22**	**36** veh	10	17	23	40 veh
C=51	**14**	**12**	**25**	**24** veh	**16**	**12**	**23**	**36** veh	10	17	24	40 veh
C=52	**14**	**13**	**25**	**24** veh	**16**	**12**	**24**	**36** veh	10	17	25	40 veh
C=53	**14**	**13**	**26**	**24** veh	**16**	**12**	**25**	**36** veh	10	17	26	40 veh
C=54	**14**	**14**	**26**	**24** veh	**16**	**12**	**26**	**36** veh	15	17	22	44 veh
C=55	**14**	**14**	**27**	**24** veh	**16**	**12**	**27**	**36** veh	20	14	21	46 veh
C=56	**14**	**15**	**27**	**24** veh	**16**	**13**	**27**	**36** veh	20	14	22	46 veh
C=57	**14**	**15**	**28**	**24** veh	**16**	**13**	**28**	**36** veh	20	14	23	46 veh
C=58	**14**	**16**	**28**	**24** veh	**16**	**14**	**28**	**36** veh	20	14	24	46 veh
C=59	**14**	**16**	**29**	**24** veh	**16**	**14**	**29**	**36** veh	20	14	25	46 veh
C=60	**14**	**16**	**30**	**24** veh	**16**	**14**	**30**	**36** veh	20	14	26	46 veh

Table 5.5: Optimal signals under the balanced vehicle arrival rates ($T_{\mathrm{m}}^{\max} = 8$)

Cycle length	**Case 1 (32 veh)**					**Case 2 (48 veh)**					**Case 3 (64 veh)**				
C (s)	P_1	P_2	P_3	P_4	Released vehicles	P_1	P_2	P_3	P_4	Released vehicles	P_1	P_2	P_3	P_4	Released vehicles
C=40	5	9	14	12	28 veh	7	8	13	12	38 veh	7	7	15	11	38 veh
C=41	5	9	14	13	28 veh	7	8	13	13	38 veh	7	7	17	10	40 veh
C=42	5	9	14	14	28 veh	7	10	12	13	40 veh	7	7	17	11	40 veh
C=43	5	10	15	13	28 veh	7	13	12	11	42 veh	5	10	17	11	40 veh
C=44	5	10	15	14	28 veh	7	13	12	12	42 veh	5	10	17	12	42 veh
C=45	5	10	15	15	28 veh	7	13	12	13	42 veh	5	10	17	13	42 veh
C=46	**14**	**8**	**10**	**14**	**32** veh	7	13	12	14	42 veh	7	12	14	13	44 veh
C=47	**14**	**8**	**10**	**15**	**32** veh	7	13	12	15	42 veh	7	12	14	14	46 veh
C=48	**14**	**8**	**10**	**16**	**32** veh	7	13	12	16	42 veh	7	12	14	15	46 veh
C=49	**14**	**8**	**12**	**15**	**32** veh	7	13	14	15	42 veh	7	10	17	15	46 veh
C=50	**14**	**8**	**12**	**16**	**32** veh	7	13	14	16	42 veh	7	10	17	16	48 veh
C=51	**14**	**8**	**12**	**17**	**32** veh	7	13	14	17	42 veh	7	10	17	17	48 veh
C=52	**14**	**8**	**14**	**16**	**32** veh	7	13	16	16	42 veh	7	17	14	14	50 veh
C=53	**14**	**8**	**14**	**17**	**32** veh	7	13	16	17	42 veh	7	17	14	15	50 veh
C=54	**14**	**8**	**14**	**18**	**32** veh	7	13	16	18	42 veh	7	17	14	16	52 veh
C=55	**14**	**8**	**16**	**17**	**32** veh	**16**	**12**	**12**	**15**	**48** veh	7	17	14	17	52 veh
C=56	**14**	**8**	**16**	**18**	**32** veh	**16**	**12**	**12**	**16**	**48** veh	7	17	14	18	52 veh
C=57	**14**	**8**	**16**	**19**	**32** veh	**16**	**12**	**12**	**17**	**48** veh	7	17	14	19	52 veh
C=58	**14**	**8**	**18**	**18**	**32** veh	**16**	**12**	**12**	**18**	**48** veh	7	17	17	17	54 veh
C=59	**14**	**8**	**18**	**19**	**32** veh	**16**	**12**	**12**	**19**	**48** veh	7	17	17	18	54 veh
C=60	**14**	**8**	**18**	**20**	**32** veh	**16**	**12**	**12**	**20**	**48** veh	7	17	17	19	54 veh

From the discussion above, the joint controller is capable of incorporating different traffic demand levels and signal designs, determining signals for the optimal performance of all vehicles from multiple movements in the control zone. The optimal signal pattern can provide design insights into engineering implementations. For instance, the first signal phase length P_1 can be pre-determined using the empirical data in the undersaturated traffic flow with balanced vehicle arrival rates, which can relieve the computational time to some extent.

5.4.3 Computational performance analysis

In this subsection, the computational performance of the proposed joint controller is analyzed, considering the dimension of control variables and the average running time under different traffic demand levels, the released traffic movement numbers and signal cycle lengths. The mean computational time is calculated by averaging ten runtimes on the desktop of Intel(R) Core(TM) i7-9700K CPU with 16 GB memory.

The average computational time under the balanced arrival rates is detailed in Figure 5.8. In the horizontal plane of Figure 5.8, the southwestern coordinate presents Case 1 to Case 3, and the southeastern coordinate implies the cycle lengths of 40 s, 50 s and 60 s under the maximal released traffic movement number $T_{\mathrm{m}}^{\max} = 4, 6, 8$. The vertical coordinate shows the average runtime in color, as demonstrated in the colorbar. The blue, green and orange bars represent the runtime sections of 0 to 2 s, 2 s to 10 s, and 10 s to 30 s, respectively, the total of which account for the majority of all runtimes. The longest mean running time, 153,21 s, occurs under Case 3 when $C = 60$ s and $T_{\mathrm{m}}^{\max} = 8$. It is obvious that the increases in the released movements T_{m}, signal cycle lengths C and vehicle numbers N result in longer runtime.

The relationship between the computational time and the control variable dimension is revealed in Figure 5.9. The vertical axis is presented compactly by way of the exponential scale. The horizontal axis shows the dimension of control variables, which ascends with the increases in the released movement numbers (see line colors), cycle lengths (see line markers), and Case 1 to Case 3 (see the grey dashed arrows). The cycle lengths with same markers on a certain line are distinguished by the case number, as the grey arrows from the left bottom to the top right. As can be seen, the average runtime normally undergoes the exponential growth when the control dimension increases.

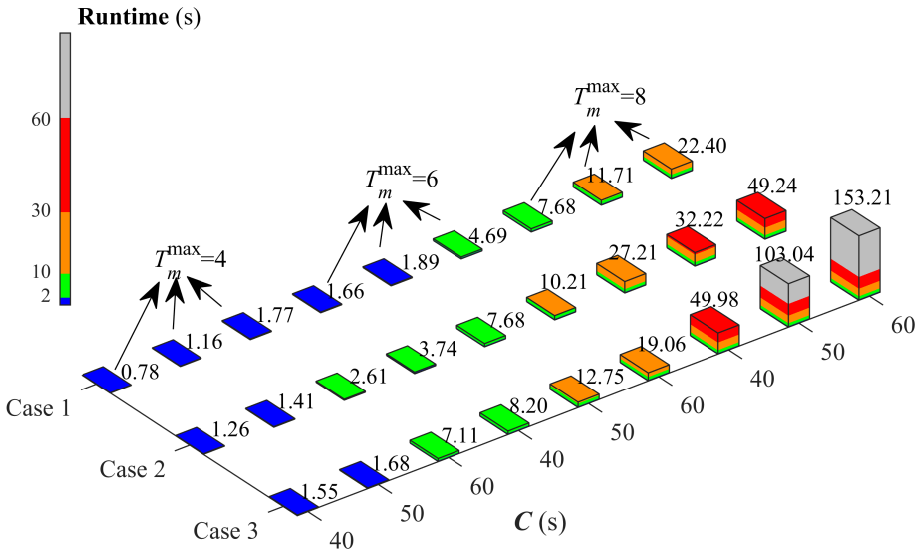

Figure 5.8: Average computational time under the balanced arrival rates

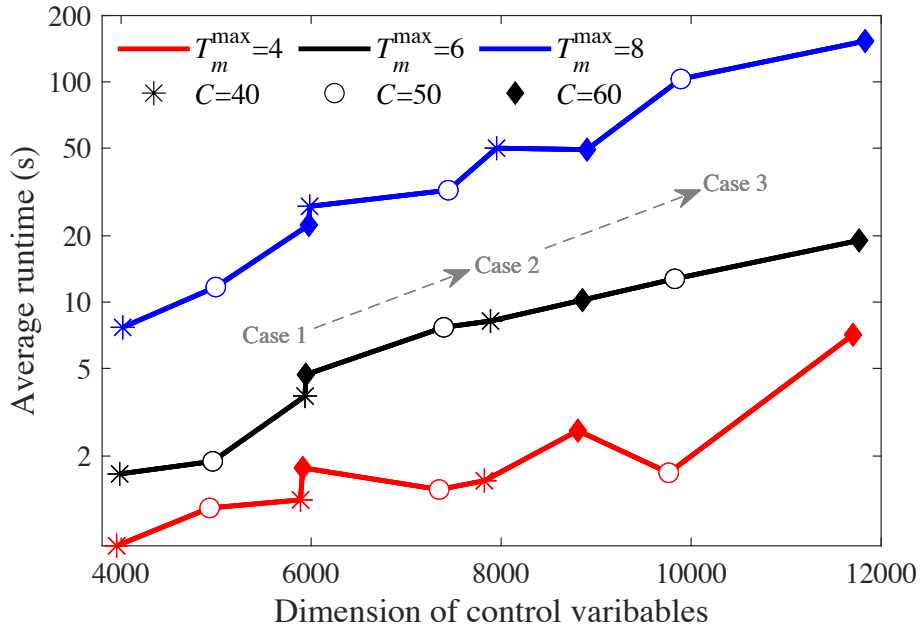

Figure 5.9: The relationship between the computational time and the control variable dimension

5.4.4 Comparison analysis

In order to demonstrate the advantages of the joint controller, the comparison is made between the proposed approach and five other approaches, i.e., the Intelligent Driver Model (IDM) (Treiber et al., 2000), the Webster model (Webster, 1958), the capacity factor maximization model (Cantarella & Improta, 1988), the delay minimization model (Improta & Cantarella, 1984), and the state of the art in Xu et al. (2018). The comparison scenario is designed similarly as Scenario 4. The left-turn movement is released afterwards with various turning proportions under the unbalanced vehicle arrival rates. The controlled vehicle numbers per movement are generated in the same way as in Scenario 4. The only differences are the cycle length of $C = 60$ s and the controlled vehicle number of $N = 64$. The same parameter values and settings are applied in all comparison cases.

The comparison cases are the indicators are listed in Table 5.6. In comparison cases I to IV, the signal parameters are calculated in the upper layer using the Webster model, the capacity factor maximization model, and the delay minimization model respectively. In the lower layer which treats the signal parameters generated from the upper layer as inputs, vehicle trajectories in the comparison case I are determined using IDM, while trajectories are optimized in comparison cases II to IV using Eq. (5.1) to (5.5), (5.11), (5.13) to (5.16), (5.26) to (5.30) to diminish the differences resulted from the trajectory optimization. The comparison case V jointly optimizes vehicle trajectories and traffic signals using the state-of-the-art approach (Xu et al., 2018), which excludes the stopping vehicles in the control design so they are removed in implementation. Finally, the comparison case VI aims at verifying the benefits of the proposed joint control approach. The performance of comparison cases II, V, and VI is illustrated in Figure 5.10 to Figure 5.12. The comparison cases III and IV are not presented owing to the similar performance as case II, resulted from their similar signal parameter values and the same trajectory optimization model.

The indicator of travel delay is calculated by vehicle arrival time minus the minimal traveling time from the initial position to the stop-bar (e.g., traveling with the limit speed $v_{\max}$). Throughput is the number of vehicles that can pass the intersection within the current signal cycle. The VT-Micro model of Rakha et al. (2004) is adopted to calculate the HC emission. The

instantaneous fuel consumption model in Kamal et al. (2011) and the traveling distance are applied to calculate the fuel consumption in ml/m. The fuel consumption rate (ml/s) can be estimated by

$$f_v = \begin{cases} b_0 + b_1 v_{ij} + b_2 v_{ij}^2 + b_3 v_{ij}^3 + a_{ij}\left(c_0 + c_1 v_{ij} + c_2 v_{ij}^2\right) & a_{ij} > 0 \\ b_0 + b_1 v_{ij} + b_2 v_{ij}^2 + b_3 v_{ij}^3 & a_{ij} \leq 0 \end{cases} \tag{5.31}$$

The indicator values of throughput, delay, fuel consumption, and emission are detailed in Table 5.6 (stopping vehicles in the state-of-the-art approach are excluded). The proposed control approach outperforms the other strategies of cases I to V in throughput and delay, and the proposed approach performs well on fuel consumption and emission, which proves the superiority of the proposed controller. The advantages of the proposed control approach over the signal-only optimization are revealed by comparing case I with case VI. The benefits of the joint optimization between trajectories and signals over the trajectory-only optimization can be demonstrated by the differences of indicator values between cases II to IV and cases V to VI. The advantages of the trajectory optimization model in this control approach are explored by the comparison between case I and case II. The benefits of the proposed approach over the state-of-the-art approach, which excludes all stopping vehicles, are verified by comparing case V with case VI.

Furthermore, the signal parameters generated from different signal control methods (comparison cases I to IV) are almost the same, because these signal optimization models generally reflect the traffic flow ratios. As a result, there are only minor differences in the values of all indicators among comparison cases II to IV. On the contrary, the proposed control approach can not only consider vehicle arrival rates but also take vehicle speeds and positions into account to release more vehicles during the green phases, which have been discussed in subsections 5.4.2.

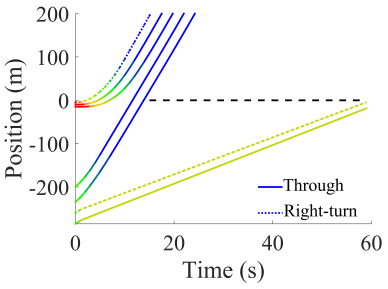

(a) trajectories of movement $T_{\mathrm{m}} = 1$ $(j = 1)$

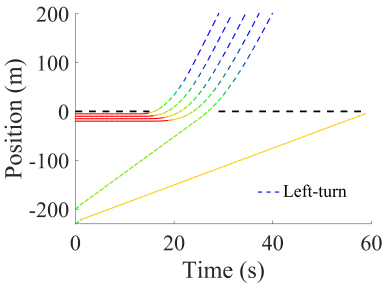

(b) trajectories of movement $T_{\mathrm{m}} = 2$ $(j = 2)$

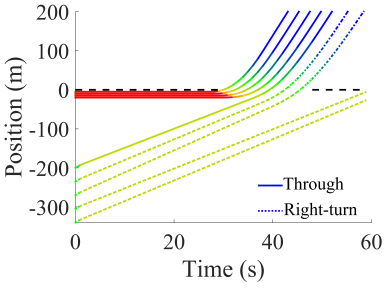

(c) trajectories of movement $T_{\mathrm{m}} = 3$ $(j = 3)$

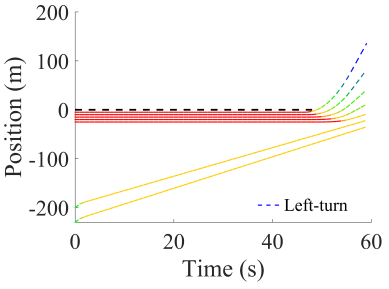

(d) trajectories of movement $T_{\mathrm{m}} = 4$ $(j = 4)$

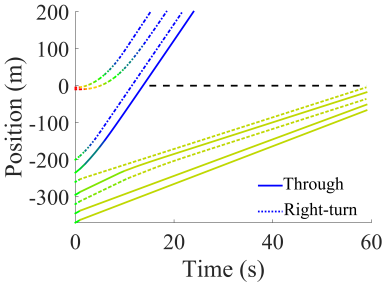

(e) trajectories of movement $T_{\mathrm{m}} = 5$ $(j = 1)$

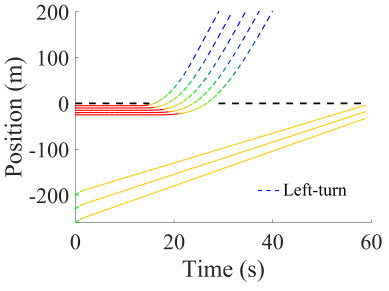

(f) trajectories of movement $T_{\mathrm{m}} = 6$ $(j = 2)$

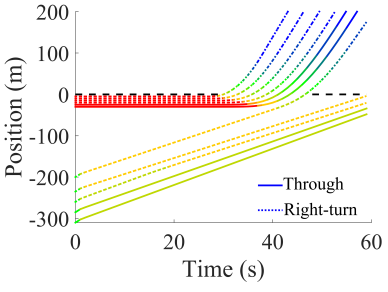

(g) trajectories of movement $T_{\mathrm{m}} = 7$ $(j = 3)$

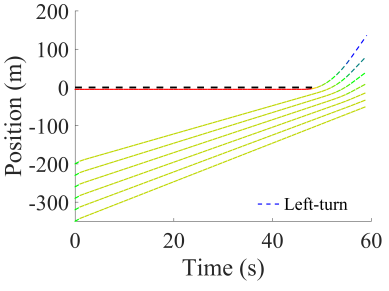

(h) trajectories of movement $T_{\mathrm{m}} = 8$ $(j = 4)$

Figure 5.10: The performance of Case II

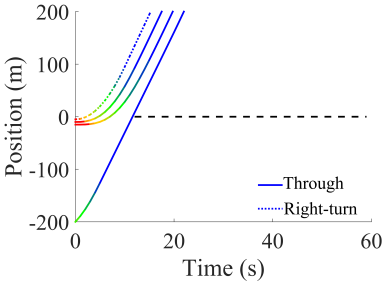

(a) trajectories of movement $T_{\mathrm{m}} = 1$ $(j = 1)$

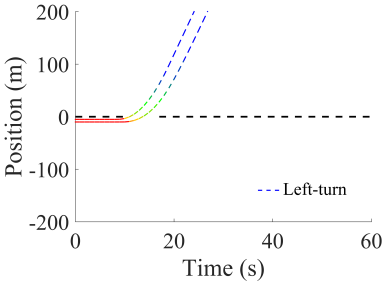

(b) trajectories of movement $T_{\mathrm{m}} = 2$ $(j = 2)$

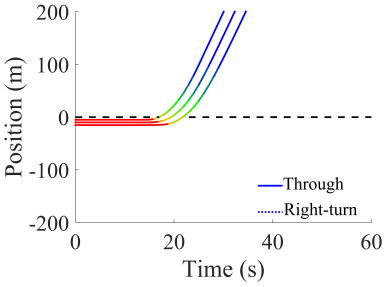

(c) trajectories of movement $T_{\mathrm{m}} = 3$ $(j = 3)$

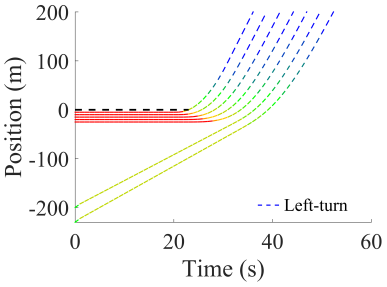

(d) trajectories of movement $T_{\mathrm{m}} = 4$ $(j = 4)$

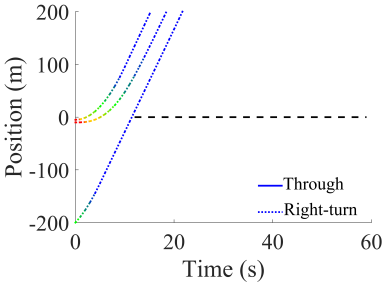

(e) trajectories of movement $T_{\mathrm{m}} = 5$ $(j = 1)$

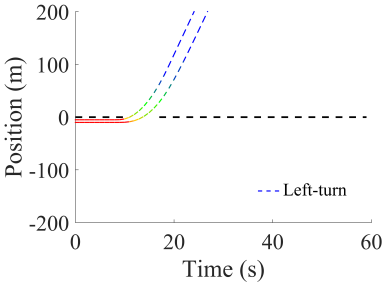

(f) trajectories of movement $T_{\mathrm{m}} = 6$ $(j = 2)$

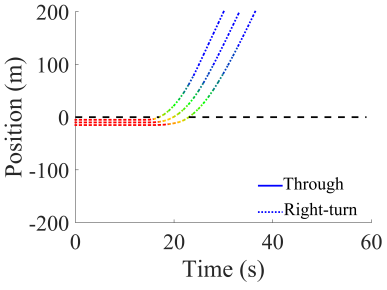

(g) trajectories of movement $T_{\mathrm{m}} = 7$ $(j = 3)$

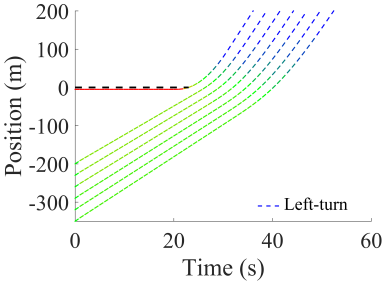

(h) trajectories of movement $T_{\mathrm{m}} = 8$ $(j = 4)$

Figure 5.11: The performance of Case V

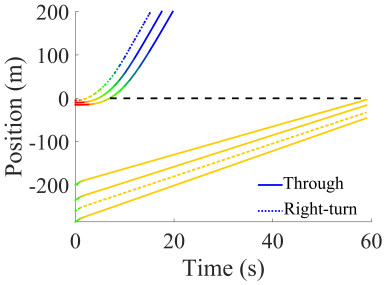

(a) trajectories of movement $T_{\mathrm{m}} = 1$ $(j = 1)$

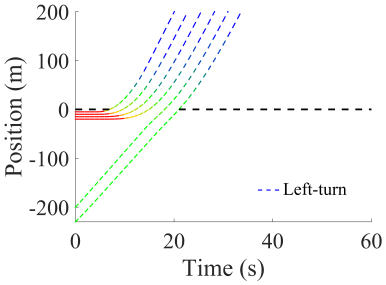

(b) trajectories of movement $T_{\mathrm{m}} = 2$ $(j = 2)$

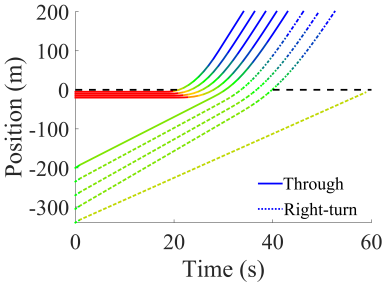

(c) trajectories of movement $T_{\mathrm{m}} = 3$ $(j = 3)$

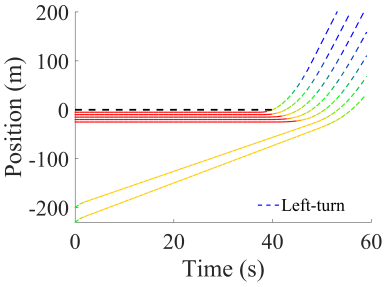

(d) trajectories of movement $T_{\mathrm{m}} = 4$ $(j = 4)$

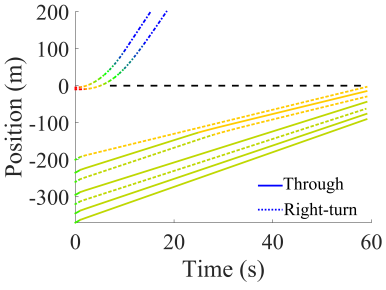

(e) trajectories of movement $T_{\mathrm{m}} = 5$ $(j = 1)$

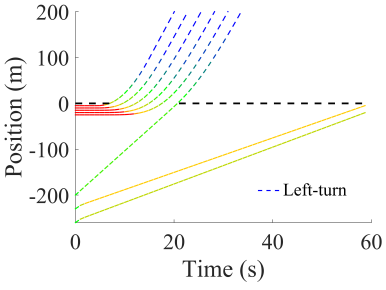

(f) trajectories of movement $T_{\mathrm{m}} = 6$ $(j = 2)$

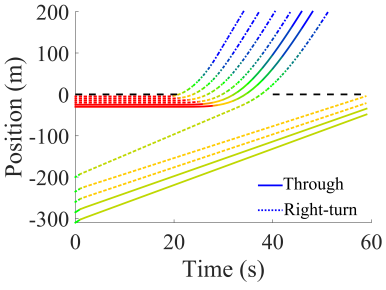

(g) trajectories of movement $T_{\mathrm{m}} = 7$ $(j = 3)$

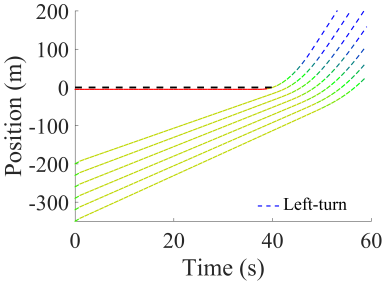

(h) trajectories of movement $T_{\mathrm{m}} = 8$ $(j = 4)$

Figure 5.12: The performance of Case VI

Table 5.6: Indicators of the comparison cases

	Signal control	**Trajectory**	**Phase lengths (s) (P_1 to P_4)**	**Throughput (veh)**	**Delay (s/veh)**	**Fuel consumption (ml/m)**	**Emission (HC: g/km)**
Case I	Webster model	IDM	15.69, 13.94, 19.17, 11.20	32	38.76	0.0814	0.0118
Case II	Webster model	Optimization	15.69, 13.94, 19.17, 11.20	41	34.62	0.0742	0.0106
Case III	Capacity factor maximization model	Optimization	15.43, 13.71, 18.86, 12.00	45	33.05	0.0739	0.0109
Case IV	Delay minimization model	Optimization	15.07, 15.49, 13.94, 15.50	45	33.18	0.0743	0.0108
Case V	Joint optimization of state-of-the-art (only passing vehicles)		12, 6, 6, 36	31	34.87	0.0692	0.0123
Case VI	Joint optimization of the proposed approach		7, 14, 19, 20	46	31.04	0.0739	0.0108

5.4.5 Discussion

The proposed controller jointly optimizes cooperative vehicle trajectories and traffic signal parameters at a standard four-arm signalized intersection with a pre-defined phase sequence, providing perfect V2V and I2V communication. It is observed from simulation results that the control objectives are fulfiled and all constraints are satisfied under different traffic demand levels with the balanced or unbalanced arrival rates from different arms, and the proposed controller has the flexibility in incorporating various cycle lengths, signal phase sequences, and turning proportions. Furthermore, the optimal trajectory and signal patterns are discovered based on the optimal performance of the joint controller. Multiple runs of different experiments show the generalizability of the proposed controller.

The dimensionality of the control problem will dramatically rise with an increase in vehicle numbers, resulting in long runtime. This is the main limitation of the proposed controller. A high performance computer is able to reduce the computational time and possibly solve this problem in real time. Decentralized computation approach can also contribute to expediting the solution time, which will be studied in the future to implement the joint control approach in real time.

5.5 Conclusions and future Work

In this chapter, we propose a joint control approach that simultaneously optimizes traffic signals and vehicle trajectories at isolated intersections in a cooperative vehicle environment. The objective of the proposed approach is to release as many vehicles as possible with ride comfort during the signal cycle (i.e., maximize comfort and minimize travel delay of the controlled platoons) by determining vehicle accelerations and signal phase lengths. The physical speeds, admissible accelerations, the safe gap requirement are imposed as linear constraints. The red phase logic constraint is recast into linear position constraints, which enables determining signal changes as vehicle-level variables without the need of the pre-specified terminal conditions on speed and position at the cycle tail. Our approach formulates the joint signal and trajectory control problem into a single-layer mixed linear integer framework, which bypasses the process of simulating vehicle trajectories when evaluating feasible signal plans and can be solved by standard solvers.

The flexibility of the joint control approach is revealed when integrating

multiple traffic movements under different traffic demand levels. Simulation under various scenarios is conducted at a standard four-arm intersection to validate the performance of the joint control approach considering the balanced/unbalanced vehicle arrival rates and different signal phase sequences. The simulation results demonstrate the characteristics of the optimal signals and the platoon performance of splitting, merging, accelerating and decelerating. Typical vehicle trajectories and the optimal signal performance can be extracted from the optimal trajectory and signal patterns respectively, and then be applied in similar control problems. Furthermore, the comparison is made with the two-layer approaches using the car following model, the signal optimization models, and the state-of-the-art approach, which demonstrate the benefits of the proposed approach in throughput, travel delay, fuel consumption, and emission.

Further research is directed to reducing the computational time of the optimization model for real-time control, and handling detection errors and uncertainties. The applicability under the sophisticated phasing plans (e.g., optimization of phase sequence) and intersection configuration designs will be verified in the next research step. Refining the design framework in the mixed traffic with human-driven vehicles and the extension to a corridor or a network level are also relevant topics for future research.

Chapter 6

Conclusions

In the final chapter, we summarize the research findings and the main contributions of this thesis in Section 6.1. Section 6.2 and Section 6.3 elaborate the recommendations for practice and for future research respectively.

6.1 Findings and conclusions

We established four research objectives in Section 1.3 of Chapter 1. Hereinafter, we will discuss the main findings and conclusions of this thesis aiming at reflecting the extent to which the objectives are accomplished.

Research objective 1: *To design a controller that optimizes the CAV platoon trajectories along a corridor with pre-timing signal controllers, taking throughput, ride comfort, travel delay of passing vehicles, and fuel consumption of stopping vehicles into account. The controller should respect vehicle position constraints when facing the red light and does not need to prescribe vehicle arrival time and terminal conditions of speed and position.*

To address this objective, Chapter 2 proposes a CAV trajectory control approach along a corridor with multiple pre-timing signalized intersections. Multiple measures of efficiencies are optimized via the objective function by determining vehicle accelerations of the CAV platoon subject to safe and physical constraints. In the multi-criteria objective function, the travel delay term stimulates vehicles to pass the stop-line as soon as possible; the fuel consumption term motivates the vehicles that cannot pass to decelerate and approach the stop-line slowly; the ride comfort term generates considerably smooth accelerations; and the throughput term aims to dissipate vehicle queues quickly during the green phases. The red phase representation is designed as constraining vehicle positions to stay behind the stop-line facing red phases. The safe driving requirement is guaranteed using the safe time gap constraint. The optimal control problem is solved using nonlinear programming (NLP) techniques after discretizing the control variables. The performance of the proposed control approach is verified by simulation on an intersection approach with/without vehicle queue and along an arterial of two intersections with queues. The results demonstrate the controlled vehicle behaviors of queue discharge, platoon split and merge due to signal changes at signalized intersections. Additionally, the comparison with the Intelligent Driver Model (IDM) reveals the benefits of the proposed control approach in throughput and fuel savings.

Research objective 2: *To design a controller that optimizes CAV platoon trajectories at actuated signalized intersections. The platoon controller should be able to anticipate signal plans and react to actuated signal changes by re-*

planning trajectories. Multi-criteria of safety, efficiency, sustainability, and comfort should be considered in the design.

To achieve this objective, we present a CAV trajectory control approach under actuated signals using the model predictive control framework which can adjust the trajectory planning according to dynamic signals. Throughput, ride comfort, travel delay, and fuel consumption are optimized by determining the accelerations of the controlled CAV platoon on an urban corridor with signalized intersections. The safe gap term in the running cost stimulates vehicles to track the vehicles in front with the desired and safe time gaps. The red phase is designed as switching cost terms in the objective function when the traffic signal changes, i.e., adding a virtually preceding vehicle for the first stopping vehicle facing the red phase and removing it during the green phase, so the shorter gaps between the virtually preceding vehicle and the first stopping vehicle are penalized. The red phase representation can be applied under both pre-timing and actuated signals, because the applied model predictive control framework allows for system feedback such as signal changes in the closed-loop. Therefore, traffic signals can be anticipated by the platoon controller on condition of implementing the red phase cost term since the beginning of the signal cycle, and be updated in the closed-loop by switching the cost weights in response to the actuated signals if the platoon controller receives signal changes.

To demonstrate the controller performance, simulation is conducted under different pre-timing and actuated signal plans. The actuated signal plans adjusts signal parameters by increasing/decreasing phase lengths according to the vehicle actuation to accommodate changes in the traffic flow after the optimization starts. The simulation results show that the proposed control approach can not only optimize vehicle trajectories under pre-timing signals with anticipation prior to the realistic phase starts/ends, but re-determine trajectories according to the actuated signal changes. The safe driving requirement, bounded accelerations, vehicle stops, queue discharge behaviors, and platoon merge/split performance are embodied in all scenarios. Spacing gaps of four scenarios are distinguished into four categories, i.e., the splitting gaps, the stopping gaps, the following gaps, and the merging/catching gaps, under which the safe requirement, signal changes, and platoon split/merge performance are reflected. In addition, the comparison with the baseline scenario which removes signal anticipation uncovers the benefits of signal anticipation in fuel economy, vehicle stops and smooth

accelerations/decelerations.

Research objective 3: *To design a bi-level controller that optimizes traffic signal timing at the upper layer and platoon trajectories at the lower layer at standard signalized intersections.*

To reach this objective, we hierarchically optimize vehicle trajectories and traffic signals at urban intersections in Chapter 4. The optimal signal parameters are determined in the upper layer by searching the minimal objective function value among all feasible signal plans. In the lower layer, CAV platoon accelerations are optimized under each feasible signal plan considering ride comfort and travel delay subject to motion constraints and safe driving requirement. The red phase design is enforced as the logic constraint to enable vehicles to respond to signal changes. The proposed control approach in Chapter 4 is adaptive to traffic demand levels, and is flexible in incorporating different traffic movements during multiple signal phases. The optimal performance of platoon split, merge/approach, acceleration/deceleration is verified by simulation of three scenarios.

Furthermore, the benefits of the integrated optimization of trajectories and signals are verified in comparison to signal-only optimization (Baseline Scenario 1) and trajectory-only optimization (Baseline Scenario 2). The comparison between the integrated control approach and the Intelligent Driver Model (IDM) under Baseline Scenario 1 demonstrates the advantages of trajectory optimization in fuel consumption (26.31%), travel delay (7.73%), and the number of stops (66.67%). Additionally, extra work on calibration of parameters is necessary when using the IDM model, or otherwise the simulated trajectories may be less efficient or unsmooth. The comparison between the integrated control approach and the pre-determined signal plan under Baseline Scenario 2 proves the advantages of signal optimization in travel delay (16.92%), and throughput (11.76%).

Research objective 4: *To design a computationally scalable single-level controller that simultaneously optimizes traffic signals and vehicle trajectories of a full intersection. The signal timing variables should be formulated as the vehicle-level control variables and no terminal conditions on speed and position at the cycle tail need to be pre-specified.*

To fulfil this objective, a single-layer approach for joint optimization of traffic signals and cooperative vehicle trajectories is presented in Chapter 5. The

controlled platoons are optimized by determining vehicle accelerations and signal phase starts/ends for releasing as many vehicles as possible with ride comfort, subject to constraints on admissible accelerations, physical speeds, and safe gaps. For simplification, the red phase design is recast into a set of linear position constraints to integrate signal variables with vehicle-level state space variables in a single layer, and therefore the process of simulating vehicle trajectories when evaluating feasible signal plans is bypassed. The reformulated problem can be solved using standard mixed-integer linear programming techniques. The proposed joint control approach is scalable to multiple traffic demand levels and is flexible in incorporating turning movements with balanced/unbalanced vehicle arrival rates under different signal phase sequences, which are demonstrated by a list of simulation experiments. The benefits of the proposed approach over the two-layer approaches using the car following model, the signal optimization models, and the state-of-the-art model are around 43.75%, 12.20%, and 48.39% in throughput and 19.91%, 10.34%, and 10.98% in travel delay.

The optimal platoon performance and the optimal signal features are derived based on the simulation results in Chapter 5. The optimal trajectory pattern is identified as follows: 1) vehicles try to avoid stops and exit the intersection with higher speeds; 2) the queuing vehicles accelerate dramatically when the green time starts to leave the intersection as soon as possible; 3) the platoon leader may experience decelerations to keep the safe gap when merging with the preceding platoon; and 4) the following vehicles show smaller acceleration fluctuations for platoon stability.

Systematic simulation experiments also reveal the optimal signal pattern as follows: 1) the optimal signals generally perform to release as many vehicles as possible by switching signal phases in time owing to the travel delay cost term; 2) the earliest signal phase length is constant under the under-saturated traffic flow with balanced arrival rates, regardless of cycle lengths and phase numbers; 3) the intermediate signal phase lengths are longer than the first and the last signal phase lengths under the oversaturated traffic flow with balanced arrival rates; 4) the optimal green time is reactive to the vehicle actuation under unbalanced arrival rates; 5) the optimal green time is rarely wasted without discharging any vehicle in the over-saturated traffic flow; and 6) the optimal signals show minor differences under similar cycle lengths.

In sum, we conclude that the proposed control methods can be successfully deployed to optimize trajectories of all vehicle platoons in the vicinity of intersections, taking into account different signal control approaches and thereby making it possible to jointly optimize vehicle trajectories and traffic signals in a unified framework. The control objectives aiming for efficiency, safety, and fuel economy are formulated as either constraints or a weighted combination of multiple criteria using tuned cost weights to make a trade-off between these objectives in this thesis. Platoon split and merge can be incorporated, and stochastic traffic flows (e.g., incoming vehicle numbers and turning proportions) and unbalanced vehicle arrivals can be handled. In terms of controller performance, the improvements in travel delay, throughput, and fuel savings are verified, but the computational time is excessive. For large scale applications, the network control problem can be decomposed into multiple sub-problems of interconnected individual intersections, which is further discussed in the topic for future research (see Section 6.3).

6.2 Recommendations for practice

The practical suggestions and implications of this thesis listed below may interest road traffic management authorities, AV and signal controller industries.

The joint optimization of vehicle trajectories and traffic signals can be deployed to optimally utilize the vehicle and infrastructure information. We conclude that this joint optimization outperforms the trajectory-only optimization (by 11.76% in throughput and 16.92% in travel delay) and the signal-only optimization using IDM (by 26.31% in fuel consumption, 7.73% in travel delay, and 66.67% in vehicle stops), and therefore is worthwhile to be applied in practice.

Such deployment of CAV platooning necessitates high-speed and low-latency network communications and high-performance computing power for real-time control. Therefore, road traffic management authorities are suggested to pave the way to future CAV platooning by establishing requisite facilities such as communication equipments, backhaul systems, traffic management centers, and roadside infrastructures (e.g., intelligent traffic signal controllers).

We believe that the joint optimization with pure CAV environment will not be practically feasible in the recent decades. The framework in this thesis

also determines the optimal vehicle platoon trajectories on urban roads under traditional signal control approaches. The generated outputs of the framework can supply speed guidance to cooperative vehicles on current urban roads, which facilitates the OEMs or AV industry in designing cooperative vehicle controllers.

The optimal signal pattern and the optimal trajectory pattern derived from the joint controller performance provide insights into signal design and speed guidance for the traffic control authority and the signal controller industry. For instance, the queuing vehicles can be guided to accelerate to the maximal speed with the maximal acceleration when the green time starts, and most of the optimal traffic signals can remain unchanged if the cycle lengths vary slightly.

The control framework in this thesis operates vehicles in platooning at urban intersections, taking multiple measures of efficiencies (comfort, safety, fuel economy, and travel delay) into account. These efficiency factors may be attractive to vehicle users and drivers, and thereby the user acceptability of CAV systems can be enhanced.

6.3 Recommendations for future research

The control framework of CAV trajectory optimization at urban intersections fills the theoretical gap in the field of integrating platoon controller design with traffic signal control. In this section, we propose a list of recommendations for future research in order to relax assumptions, address the shortcoming of online and offline optimization, and finally realize practical applications.

1. *Incorporate lateral lane-changing decision making.* (related to Chapter 2, Chapter 3, and Chapter 5)
   The control framework in this thesis focuses on longitudinal acceleration optimization assuming that lane changes are not allowed in the control zone. To relax this assumption, the mandatory lane changing behaviors can be integrated with the longitudinal platoon trajectories by defining and searching critical safe gaps for merging.

2. *Extend to a network level.* (related to Chapter 2, Chapter 3, and Chapter 5)

The performance of the proposed controllers are validated by simulation along an arterial in Chapter 2 and 3, and at an individual intersection in Chapter 4 and 5.The urban network control problem can be spatiotemporally decentralized into sub-problems of interconnected individual intersections to improve computation efficiency. The extension of the control zone to the urban network level should be elaborately treated, because the divisions between adjacent intersections for specifying the temporal and spatial boundaries of each sub-problem remain challenging. The temporal and spatial divisions decompose the network problem using the prediction horizon length (e.g., signal cycle length) and the lane section length, noticing the terminal conditions should be equal to the initial conditions of the next signal cycle and the adjacent downstream intersections.

3. *Refine the design framework in the mixed traffic with human-driven vehicles.* (related to Chapter 2, Chapter 3, and Chapter 5)
   In the mixed traffic of human-driven vehicles and cooperative vehicles, the cooperative vehicle trajectories can be optimized based on the perception of the preceding vehicles and the current/prospective signal plans. The uncertain human-driven vehicles can be regarded as model disturbances, so the difficulty is how to obtain the exact car-following behaviors of human-driven vehicles in the mixed traffic environment. The stochastic and robust control approaches should be able to handle uncertainties in the state estimation and prediction for human-driven vehicles. An alternative is to capitalize the recent advances of machine learning algorithms such as Long Short-Term Memory to predict human-driven vehicle trajectories. This may provide more accurate prediction if vehicle position and speed measurements are available in real time.

4. *Reduce the computational time to reach the real-time control.* (related to Chapter 5)
   Despite the advantages of the linear feature in the single-layer control approach which jointly optimizes traffic signals and vehicle trajectories, the scalability of centralized approach can be constrained by the computation load. To improve the computational efficiency, the centralized optimization problem can be decomposed using primal-dual methods, which enables the decentralized computation. In addition, trajectory planning using the reinforcement learning method can also

expedite the computation.

5. *Incorporate the sophisticated phasing plans and intersection configuration designs.* (related to Chapter 5)
   In the single-layer joint formulation, the intricate signal plans can be realized by introducing the corresponding signal control variables (i.e., signal switch of each phase) and the signal constraints (i.e., signal switch numbers). The intersection configurations can be reflected by separating and/or combining the traffic movements on each arm according to the intersection design.

Appendix

Iterative solution algorithm based on Pontryagin Maximum Principle

Based on the Pontryagin Maximum Principle, the Hamiltonian is defined as

$$H(\mathbf{x},\mathbf{u},\lambda) = L(\mathbf{x},\mathbf{u}) + \lambda^{\mathrm{T}}\mathbf{f}(\mathbf{x},\mathbf{u})$$

where λ is the co-state of the state $\mathbf{x}$. The necessary condition for optimal control $\mathbf{u}^*$ is derived using

$$\mathbf{u}^* = \min H(\mathbf{x},\mathbf{u},\lambda), \text{s.t. } \mathbf{u} \in U, \mathbf{x} \in X$$

subject to the admissible range U and the bounded set X. The co-state is required to satisfy the dynamic equation as

$$-\frac{\mathrm{d}}{\mathrm{d}t}\lambda = \frac{\partial H}{\partial \mathbf{x}} = \frac{\partial L}{\partial \mathbf{x}} + \lambda\frac{\partial \mathbf{f}}{\partial \mathbf{x}}$$

subject to the terminal conditions at the end of the prediction horizon $t = T_P$:

$$\lambda(T_P) = \frac{\partial G}{\partial \mathbf{x}}(\mathbf{x}(T_P))$$

The iterative solution based on Pontryagin Maximum Principle (iPMP) iteratively solves the state dynamics equation *forward* in time and subsequently the co-state equation *backward* in time (Hoogendoorn et al., 2012; Wang et al., 2014b). The essence of iPMP algorithm is the choice of α for fast convergence. The algorithm is summarized by the following procedure.

Algorithm Iterative solution algorithm based on Pontryagin Maximum Principle

1: Select values for the error threshold $\varepsilon_{\max}$ and the weight factor α ($0 < \alpha < 1$) to smoothly update the co-state.
2: Set the iteration number $n = 1$.
3: Set the initial co-state to be identity matrices $\Upsilon^{(0)}(t) = 0$ ($0 \leqslant t \leqslant T_P$).
4: Solve the state dynamics equation $\frac{\mathrm{d}}{\mathrm{d}t}\mathbf{x}^{(n)} = \mathbf{f}(\mathbf{x}^{(n)}, \mathbf{u}^*(\mathbf{x}^{(n)}, \Upsilon^{(n-1)}))$ forward in time subject to the initial conditions of state variables $\mathbf{x}^{(n)}(0) = \mathbf{x}_0$.
5: Solve the co-state dynamics equation backward in time $-\frac{\mathrm{d}}{\mathrm{d}t}\lambda^{(n)} = \frac{\partial H}{\partial \mathbf{x}}(\mathbf{x}^{(n)}, \mathbf{u}^*(\mathbf{x}^{(n)}, \Upsilon^{(n-1)}))$ subject to the terminal conditions of co-state at the end of the prediction horizon $\lambda^{(n)}(T_P) = \frac{\partial G}{\partial \mathbf{x}}(\mathbf{x}^{(n)}(T_P))$.
6: Update the co-state $\Upsilon^{(n)}$ using the weight factor α: $\Upsilon^{(n)} = (1 - \alpha)\Upsilon^{(n-1)} + \alpha\Upsilon^{(n)}$.
7: The algorithm stops if the error between the state and the co-state is less than the threshold value, i.e., $\varepsilon = ||\Upsilon^{(n)} - \lambda^{(n)}||^2 < \varepsilon_{\max}$, and otherwise goes to the next iteration, $n := n + 1$ (step 4).

Bibliography

Ahmane, M., A. Abbas-Turki, F. Perronnet, J. Wu, A. El Moudni, J. Buisson, R. Zeo (2013) Modeling and controlling an isolated urban intersection based on cooperative vehicles, *Transportation Research Part C: Emerging Technologies*, 28, pp. 44–62.

Ahn, K., H. Rakha, A. Trani, M. Van Aerde (2002) Estimating vehicle fuel consumption and emissions based on instantaneous speed and acceleration levels, *Journal of transportation engineering*, 128(2), pp. 182–190.

Akcelik, R. (1989) Efficiency and drag in the power-based model of fuel consumption, *Transportation Research Part B: Methodological*, 23(5), pp. 376–385.

Al Islam, S. B., A. Hajbabaie (2017) Distributed coordinated signal timing optimization in connected transportation networks, *Transportation Research Part C: Emerging Technologies*, 80, pp. 272–285.

Altan, O. D., G. Wu, M. J. Barth, K. Boriboonsomsin, J. A. Stark (2017) Glidepath: Eco-friendly automated approach and departure at signalized intersections, *IEEE Transactions on Intelligent Vehicles*, 2(4), pp. 266–277.

Asadi, B., A. Vahidi (2010) Predictive cruise control: Utilizing upcoming traffic signal information for improving fuel economy and reducing trip time, *IEEE transactions on control systems technology*, 19(3), pp. 707–714.

Åström, K. J., R. M. Murray (2010) *Feedback systems*, Princeton university press.

Beak, B., K. L. Head, Y. Feng (2017) Adaptive coordination based on connected vehicle technology, *Transportation Research Record*, 2619(1), pp. 1–12.

Bodenheimer, R., A. Brauer, D. Eckhoff, R. German (2014) Enabling glosa for adaptive traffic lights, in: *2014 IEEE Vehicular Networking Conference (VNC)*, IEEE, pp. 167–174.

Cantarella, G. E., G. Improta (1988) Capacity factor or cycle time optimization for signalized junctions: a graph theory approach, *Transportation Research Part B: Methodological*, 22(1), pp. 1–23.

Chen, S., D. J. Sun (2016) An improved adaptive signal control method for isolated signalized intersection based on dynamic programming, *IEEE Intelligent Transportation Systems Magazine*, 8(4), pp. 4–14.

Feng, Y., K. L. Head, S. Khoshmagham, M. Zamanipour (2015) A real-time adaptive signal control in a connected vehicle environment, *Transportation Research Part C: Emerging Technologies*, 55, pp. 460–473.

Feng, Y., C. Yu, H. X. Liu (2018) Spatiotemporal intersection control in a connected and automated vehicle environment, *Transportation Research Part C: Emerging Technologies*, 89, pp. 364–383.

Fountoulakis, M., N. Bekiaris-Liberis, C. Roncoli, I. Papamichail, M. Papageorgiou (2017) Highway traffic state estimation with mixed connected and conventional vehicles: Microscopic simulation-based testing, *Transportation Research Part C: Emerging Technologies*, 78, pp. 13–33.

Guanetti, J., Y. Kim, F. Borrelli (2018) Control of connected and automated vehicles: State of the art and future challenges, *Annual reviews in control*, 45, pp. 18–40.

Guler, S. I., M. Menendez, L. Meier (2014) Using connected vehicle technology to improve the efficiency of intersections, *Transportation Research Part C: Emerging Technologies*, 46, pp. 121–131.

Guo, Q., L. Li, X. J. Ban (2019a) Urban traffic signal control with connected and automated vehicles: A survey, *Transportation research part C: emerging technologies*, 101, pp. 313–334.

Guo, Y., J. Ma, C. Xiong, X. Li, F. Zhou, W. Hao (2019b) Joint optimization of vehicle trajectories and intersection controllers with connected automated vehicles: Combined dynamic programming and shooting heuristic approach, *Transportation research part C: emerging technologies*, 98, pp. 54–72.

Gutesa, S., J. Lee, D. Besenski (2021) Development and evaluation of cooperative intersection management algorithm under connected and automated vehicles environment, *Transportation Research Record*, p. 0361198121994580.

Han, Y., D. Chen, S. Ahn (2017) Variable speed limit control at fixed freeway bottlenecks using connected vehicles, *Transportation Research Part B: Methodological*, 98, pp. 113–134.

Hao, P., G. Wu, K. Boriboonsomsin, M. J. Barth (2018) Eco-approach and departure (ead) application for actuated signals in real-world traffic, *IEEE Transactions on Intelligent Transportation Systems*, 20(1), pp. 30–40.

He, X., H. X. Liu, X. Liu (2015) Optimal vehicle speed trajectory on a signalized arterial with consideration of queue, *Transportation Research Part C: Emerging Technologies*, 61, pp. 106–120.

HomChaudhuri, B., A. Vahidi, P. Pisu (2016) Fast model predictive control-based fuel efficient control strategy for a group of connected vehicles in urban road conditions, *IEEE Transactions on Control Systems Technology*, 25(2), pp. 760–767.

Hoogendoorn, S., R. Hoogendoorn, M. Wang, W. Daamen (2012) Modeling driver, driver support, and cooperative systems with dynamic optimal control, *Transportation research record*, 2316(1), pp. 20–30.

Hu, J., Y. Shao, Z. Sun, M. Wang, J. Bared, P. Huang (2016) Integrated optimal eco-driving on rolling terrain for hybrid electric vehicle with vehicle-infrastructure communication, *Transportation Research Part C: Emerging Technologies*, 68, pp. 228–244.

Improta, G., G. Cantarella (1984) Control system design for an individual signalized junction, *Transportation Research Part B: Methodological*, 18(2), pp. 147–167.

Jiang, H., J. Hu, S. An, M. Wang, B. B. Park (2017) Eco approaching at an isolated signalized intersection under partially connected and automated vehicles environment, *Transportation Research Part C: Emerging Technologies*, 79, pp. 290–307.

Kamal, M. A. S., M. Mukai, J. Murata, T. Kawabe (2011) Ecological vehicle control on roads with up-down slopes, *IEEE Transactions on Intelligent Transportation Systems*, 12(3), pp. 783–794.

Kamal, M. A. S., M. Mukai, J. Murata, T. Kawabe (2012) Model predictive control of vehicles on urban roads for improved fuel economy, *IEEE Transactions on control systems technology*, 21(3), pp. 831–841.

Kamalanathsharma, R. K., H. A. Rakha (2013) Multi-stage dynamic programming algorithm for eco-speed control at traffic signalized intersections, in: *16th International IEEE Conference on Intelligent Transportation Systems (ITSC 2013)*, IEEE, pp. 2094–2099.

Kamalanathsharma, R. K., H. A. Rakha, H. Yang (2015) Networkwide impacts of vehicle ecospeed control in the vicinity of traffic signalized intersections, *Transportation Research Record*, 2503(1), pp. 91–99.

Katsaros, K., R. Kernchen, M. Dianati, D. Rieck (2011a) Performance study of a green light optimized speed advisory (glosa) application using an integrated cooperative its simulation platform, in: *2011 7th International Wireless Communications and Mobile Computing Conference*, IEEE, pp. 918–923.

Katsaros, K., R. Kernchen, M. Dianati, D. Rieck, C. Zinoviou (2011b) Application of vehicular communications for improving the efficiency of traffic in urban areas, *Wireless Communications and Mobile Computing*, 11(12), pp. 1657–1667.

Krajewski, R., P. Themann, L. Eckstein (2016) Decoupled cooperative trajectory optimization for connected highly automated vehicles at urban intersections, in: *2016 IEEE Intelligent Vehicles Symposium (IV)*, IEEE, pp. 741–746.

Le, T., P. Kovács, N. Walton, H. L. Vu, L. L. Andrew, S. S. Hoogendoorn (2015) Decentralized signal control for urban road networks, *Transportation Research Part C: Emerging Technologies*, 58, pp. 431–450.

Lee, J., B. Park (2012) Development and evaluation of a cooperative vehicle intersection control algorithm under the connected vehicles environment, *IEEE Transactions on Intelligent Transportation Systems*, 13(1), pp. 81–90.

Lee, J., B. Park, I. Yun (2013a) Cumulative travel-time responsive real-time intersection control algorithm in the connected vehicle environment, *Journal of Transportation Engineering*, 139(10), pp. 1020–1029.

Lee, J., B. B. Park, K. Malakorn, J. J. So (2013b) Sustainability assessments of cooperative vehicle intersection control at an urban corridor, *Transportation Research Part C: Emerging Technologies*, 32, pp. 193–206.

Li, J., M. Dridi, A. El-Moudni (2014a) Multi-vehicles green light optimal speed advisory based on the augmented lagrangian genetic algorithm, in: *17th International IEEE Conference on Intelligent Transportation Systems (ITSC)*, IEEE, pp. 2434–2439.

Li, J.-Q., G. Wu, N. Zou (2011) Investigation of the impacts of signal timing on vehicle emissions at an isolated intersection, *Transportation Research Part D: Transport and Environment*, 16(5), pp. 409–414.

Li, W., X. Ban (2018) Connected vehicles based traffic signal timing optimization, *IEEE Transactions on Intelligent Transportation Systems*, 20(12), pp. 4354–4366.

Li, X., A. Ghiasi, Z. Xu, X. Qu (2018) A piecewise trajectory optimization model for connected automated vehicles: Exact optimization algorithm and queue propagation analysis, *Transportation Research Part B: Methodological*, 118, pp. 429–456.

Li, Z., L. Elefteriadou, S. Ranka (2014b) Signal control optimization for automated vehicles at isolated signalized intersections, *Transportation Research Part C: Emerging Technologies*, 49, pp. 1–18.

Liu, M., S. Hoogendoorn, M. Wang (2020) Receding horizon cooperative platoon trajectory planning on corridors with dynamic traffic signal, *Transportation Research Record*, p. 0361198120954869.

Liu, M., M. Wang, S. Hoogendoorn (2019) Optimal platoon trajectory planning approach at arterials, *Transportation Research Record*, 2673(9), pp. 214–226.

Liu, M., J. Zhao, S. Hoogendoorn, M. Wang (2021) An optimal control approach of integrating traffic signals and cooperative vehicle trajectories at intersections, *Transportmetrica B: Transport Dynamics (under review)*.

Lu, M. (2016) *Evaluation of Intelligent Road Transport Systems: Methods and Results*.

Mandava, S., K. Boriboonsomsin, M. Barth (2009) Arterial velocity planning based on traffic signal information under light traffic conditions, in: *2009 12th International IEEE Conference on Intelligent Transportation Systems*, IEEE, pp. 1–6.

Niroumand, R., M. Tajalli, L. Hajibabai, A. Hajbabaie (2020) Joint optimization of vehicle-group trajectory and signal timing: Introducing the white phase for mixed-autonomy traffic stream, *Transportation Research Part C: Emerging Technologies*, 116, p. 102659.

Rakha, H., K. Ahn, A. Trani (2004) Development of vt-micro model for estimating hot stabilized light duty vehicle and truck emissions, *Transportation Research Part D: Transport and Environment*, 9(1), pp. 49–74.

Rakha, H., R. K. Kamalanathsharma (2011) Eco-driving at signalized intersections using v2i communication, in: *2011 14th international IEEE conference on intelligent transportation systems (ITSC)*, IEEE, pp. 341–346.

Rao, A. V. (2009) A survey of numerical methods for optimal control, *Advances in the Astronautical Sciences*, 135(1), pp. 497–528.

SAE. (2018) Taxonomy and definitions for terms related to on-road motor vehicles, Tech. Rep. J3016, SAE International On-Road Automated Driving (ORAD) committee, United States.

Sciarretta, A., A. Vahidi (2020) *Energy-Efficient Driving of Road Vehicles*, Springer.

Seredynski, M., B. Dorronsoro, D. Khadraoui (2013) Comparison of green light optimal speed advisory approaches, in: *16th International IEEE Conference on Intelligent Transportation Systems (ITSC 2013)*, IEEE, pp. 2187–2192.

Shladover, S. E. (2018) Connected and automated vehicle systems: Introduction and overview, *Journal of Intelligent Transportation Systems*, 22(3), pp. 190–200.

Sivak, M., B. Schoettle (2015) Road safety with self-driving vehicles: General limitations and road sharing with conventional vehicles, Tech. rep., University of Michigan, Ann Arbor, Transportation Research Institute.

Stebbins, S., M. Hickman, J. Kim, H. L. Vu (2017) Characterising green light optimal speed advisory trajectories for platoon-based optimisation, *Transportation Research Part C: Emerging Technologies*, 82, pp. 43–62.

Stevanovic, A., J. Stevanovic, C. Kergaye (2013) Green light optimized speed advisory systems: Impact of signal phasing information accuracy, *Transportation research record*, 2390(1), pp. 53–59.

Treiber, M., A. Hennecke, D. Helbing (2000) Congested traffic states in empirical observations and microscopic simulations, *Physical review E*, 62(2), p. 1805.

Typaldos, P., I. Papamichail, M. Papageorgiou (2020) Minimization of fuel consumption for vehicle trajectories, *IEEE Transactions on Intelligent Transportation Systems*, 21(4), pp. 1716–1727.

Ubiergo, G. A., W.-L. Jin (2016) Mobility and environment improvement of signalized networks through vehicle-to-infrastructure (v2i) communications, *Transportation Research Part C: Emerging Technologies*, 68, pp. 70–82.

Wan, N., A. Vahidi, A. Luckow (2016) Optimal speed advisory for connected vehicles in arterial roads and the impact on mixed traffic, *Transportation Research Part C: Emerging Technologies*, 69, pp. 548–563.

Wang, M., W. Daamen, S. Hoogendoorn, B. Van Arem (2014a) Potential impacts of ecological adaptive cruise control systems on traffic and environment, *IET Intelligent Transport Systems*, 8(2), pp. 77–86.

Wang, M., W. Daamen, S. P. Hoogendoorn, B. van Arem (2012) Driver assistance systems modeling by model predictive control, in: *2012 15th International IEEE Conference on Intelligent Transportation Systems*, IEEE, pp. 1543–1548.

Wang, M., W. Daamen, S. P. Hoogendoorn, B. van Arem (2014b) Rolling horizon control framework for driver assistance systems. part i: Mathematical formulation and non-cooperative systems, *Transportation research part C: emerging technologies*, 40, pp. 271–289.

Wang, M., W. Daamen, S. P. Hoogendoorn, B. van Arem (2014c) Rolling horizon control framework for driver assistance systems. part ii: Cooperative sensing and cooperative control, *Transportation research part C: emerging technologies*, 40, pp. 290–311.

Wang, M., W. Daamen, S. P. Hoogendoorn, B. van Arem (2016) Connected variable speed limits control and car-following control with vehicle-infrastructure communication to resolve stop-and-go waves, *Journal of Intelligent Transportation Systems*, 20(6), pp. 559–572.

Wang, M., S. P. Hoogendoorn, W. Daamen, B. van Arem, R. Happee (2015) Game theoretic approach for predictive lane-changing and car-following control, *Transportation Research Part C: Emerging Technologies*, 58, pp. 73–92.

Wang, Z., G. Wu, M. J. Barth (2018) A review on cooperative adaptive cruise control (cacc) systems: Architectures, controls, and applications, in: *2018 21st International Conference on Intelligent Transportation Systems (ITSC)*, IEEE, pp. 2884–2891.

Wang, Z., G. Wu, M. J. Barth (2019) Cooperative eco-driving at signalized intersections in a partially connected and automated vehicle environment, *IEEE Transactions on Intelligent Transportation Systems*, 21(5), pp. 2029–2038.

Webster, F. V. (1958) Traffic signal settings, Tech. rep.

Xia, H., K. Boriboonsomsin, M. Barth (2013) Dynamic eco-driving for signalized arterial corridors and its indirect network-wide energy/emissions benefits, *Journal of Intelligent Transportation Systems*, 17(1), pp. 31–41.

Xiao, L., F. Gao (2010) A comprehensive review of the development of adaptive cruise control systems, *Vehicle system dynamics*, 48(10), pp. 1167–1192.

Xu, B., X. J. Ban, Y. Bian, W. Li, J. Wang, S. E. Li, K. Li (2018) Cooperative method of traffic signal optimization and speed control of connected vehicles at isolated intersections, *IEEE Transactions on Intelligent Transportation Systems*, 20(4), pp. 1390–1403.

Yang, H., H. Rakha, M. V. Ala (2016a) Eco-cooperative adaptive cruise control at signalized intersections considering queue effects, *IEEE Transactions on Intelligent Transportation Systems*, 18(6), pp. 1575–1585.

Yang, K., S. I. Guler, M. Menendez (2016b) Isolated intersection control for various levels of vehicle technology: Conventional, connected, and automated vehicles, *Transportation Research Part C: Emerging Technologies*, 72, pp. 109–129.

Yu, C., Y. Feng, H. X. Liu, W. Ma, X. Yang (2018) Integrated optimization of traffic signals and vehicle trajectories at isolated urban intersections, *Transportation Research Part B: Methodological*, 112, pp. 89–112.

Yu, C., W. Sun, H. X. Liu, X. Yang (2019) Managing connected and automated vehicles at isolated intersections: From reservation-to optimization-based methods, *Transportation research part B: methodological*, 122, pp. 416–435.

Zhao, J., V. L. Knoop, M. Wang (2020) Two-dimensional vehicular movement modelling at intersections based on optimal control, *Transportation Research Part B: Methodological*, 138, pp. 1–22.

Zhao, W., D. Ngoduy, S. Shepherd, R. Liu, M. Papageorgiou (2018) A platoon based cooperative eco-driving model for mixed automated and human-driven vehicles at a signalised intersection, *Transportation Research Part C: Emerging Technologies*, 95, pp. 802–821.

Zohdy, I. H., H. A. Rakha (2016) Intersection management via vehicle connectivity: The intersection cooperative adaptive cruise control system concept, *Journal of Intelligent Transportation Systems*, 20(1), pp. 17–32.

Summary

Growth in the number of vehicles causes excessive traffic congestion and travel delay on urban roads, especially at signalized intersections. The recent advances in connected and automated vehicle (CAV) technology and the upgrade of Vehicle-to-Vehicle (V2V), Vehicle-to-Infrastructure (V2I), and Infrastructure-to-Vehicle (I2V) communications have been proposed as potential solutions to efficient and effective urban transportation. CAVs enable the capability to share data, communicate with neighboring vehicles and roadside infrastructures, and connect to traffic control systems, and therefore offer the benefits to reduce congestion and pollution levels and improve comfort and road safety. CAV platoons can coordinate member vehicles for a common goal in platooning. In this way, vehicles can be cooperative to accelerate/decelerate facing the traffic signal controllers on urban roads. The challenge is posed by the diversity of signal control approaches, such as fixed-timing, actuated, and adaptive signals. However, the benefits and effectiveness of CAV platoon trajectory optimization for all those various systems in the vicinity of signalized intersections remain unclear in research and also practice.

To gain insights generated from the integration between CAVs and signal controllers, this thesis focuses on not only CAV trajectory optimization under traditional signals but also simultaneous optimization of traffic signals and vehicle trajectories in a unified framework. To this end, a novel control framework of CAV platoon trajectory optimization is proposed for urban roads for multiple signal control approaches. This thesis aims at applying the optimal control theory to address the research problems. Optimal control is a mathematical approach for purpose of optimizing the objective function by searching the paths of the controls for a dynamical system.

Firstly, we develop a control approach to optimize CAV platoon trajectories

under pre-timing signals considering efficiency, comfort, energy economy, safe gaps, and vehicle deceleration during red phases. This optimal control problem is solved by nonlinear programming techniques. We conclude from the simulation results that the proposed controller works under pre-timing signals and contributes to higher throughput and more fuel savings compared with the Intelligent Driver Model, which is a longitudinal car-following model for the simulation of traffic flow.

Secondly, we propose a receding horizon control approach using the model predictive control (MPC) framework to optimize CAV platoon trajectories under actuated signals. The proposed controller acquires signal parameters since the cycle begins and incorporates changes of signal parameters as system feedback in the MPC framework. Simulation results verify the workings of re-planed trajectories under actuated signals and the benefits in fuel consumption, comfort, and the number of stops.

Thirdly, we focus on hierarchical optimization of traffic signals and CAV trajectories at isolated signalized intersections. Signals and trajectories are determined respectively in the upper layer and the lower layer. In this formulation, the signal control parameters are adapted (within certain constraints) in such a way to enable CAVs to react to the red indication. Based on simulation results, we conclude that the proposed approach can control various traffic movements during signal phases, and outperform the individual trajectory optimization and the individual signal optimization of the proposed approach in throughput (by 11.76%), fuel consumption (by 26.31%), travel delay (by 12.33%), and vehicle stops (by 66.67%).

Fourthly, we integrate the traffic signal optimization and CAV trajectory optimization in a single-layer by recasting the red phase constraint into a set of linear position constraints for the convenience of identifying CAV position conditions when the adaptive traffic signals change. This formulation overcomes the limitations of the state of the art which requires the simulated or approximated trajectories when evaluating feasible signal parameters and pre-specifying terminal conditions on speed and position. The proposed joint controller is solved using mixed-integer linear programming techniques. The optimal trajectory and signal patterns are derived based on the simulation results. The joint controller performs better than Webster and the state-of-the-art methods in throughput (12.20% and 48.39%), fuel consumption (5.62% and 3.45%), and travel delay (10.34% and 10.98%).

In summary, this thesis provides a CAV trajectory control framework under a list of signal control approaches, aiming at optimizing multiple measures of efficiencies (comfort, safety, fuel economy, and travel delay). The improvements of the control framework in efficiency, comfort, and energy consumption are verified, but at the cost of high computational load. This thesis can provide insights into signal designs and speed guidance for better traffic management. Future research will be extended to the urban network level after reducing the computational time.

Samenvatting

De groeiende verkeersvraag veroorzaakt aanzienlijke congestie op (stedelijke) wegen, met name bij geregelde kruisingen. De recente technologische ontwikkelingen op het gebied van communicerende en geautomatiseerde voertuigen (CAV), voertuig-naar-voertuig (V2V) en voertuig-naar-infrastructuur (V2I)-communicatie, leveren mogelijke oplossingen voor efficiënter en effectiever transport. CAVs maken het mogelijk om gegevens te delen, te communiceren met voertuigen in hun omgeving en met de wegkant, en verbinding te maken met verkeersregelsystemen (VRI), en bieden daarom de voordelen om congestie en vervuiling te verminderen en het comfort en de verkeersveiligheid te verbeteren. CAV-pelotons kunnen voertuigen coördineren voor een gemeenschappelijk doel. Op deze manier kunnen voertuigen samenwerken om te versnellen/vertragen ten opzichte van verkeersregelingsinstallaties op wegen binnen de bebouwde kom. De uitdaging om CAV systemen te gebruiken zitin de diversiteit van verkeersregelsystemen, zoals starre regelingen, voertuigafhankelijke regelingen of verkeersafhankelijke regelingen. Het blijft echter onduidelijk hoe groot de effectiviteit en voordelen zijn van de toepassing van trajectoptimalisatie van CAV-pelotons bij geregelde kruispunten.

Om inzicht te verwerven aangaande de integratie van CAVs in de verkeersregelsystemen, richt dit proefschrift zich niet enkel op CAV-trajectoptimalisatie onder traditionele regelsystemen, maar op een totaalsyteem: een gezamenlijke optimalisatie van zowel het verkeersregelsysteem als de voertuigtrajecten. Hiertoe wordt een nieuw regelsysteem voor trajectoptimalisatie voor CAV-pelotons voorgesteld voor stedelijke wegen met verschillende regelsysteem-benaderingen. In dit proefschrift wordt de “optimal control theory” toegepast, dit is een wiskundige optimalisatiebenadering die de doelfunctie te optimaliseert voor een dynamisch systeem door de regelvariabelen te bepalen binnen een bepaald gegeven domein.

Ten eerste ontwikkelen we een optimalisatie van de trajecten van het CAV-peloton binnen een starre regelingen, daarbij rekening houdend met efficiëntie, comfort, brandstofverbruik, veilige afstanden tussen voertuigen, en voertuigvertraging gedurende de roodtijd. Voor dit optimalisatieprobleem worden niet-lineaire programmeertechnieken toegepast. We concluderen uit de simulatieresultaten dat de voorgestelde starre regeling werkt, en bijdraagt aan een hogere doorvoer en meer brandstofbesparing vergeleken met het "Intelligent Driver Model".

Ten tweede stellen we een regeling voor met een "receding horizon-approach" binnen een "Model Predictive Control" (MPC)-kader om CAV pelotontrajecten te optimaliseren voor voertuigafhankelijke regelingen. De voorgestelde regeling bepaalt de parameters vanaf de start van de cyclus en neemt veranderingen van de parameters mee in de terugkoppeling naar het MPC-kader. Simulatieresultaten tonen de opnieuw geplande trajecten bij de voertuigafhankelijke regelingen, en de voordelen in brandstofverbruik, comfort en het aantal stoppende voertuigen.

Ten derde richten we ons op het hiërarchisch optimaliseren van verkeerslichten en CAV-trajecten op geïsoleerde geregelde kruispunten. In de bovenlaag en de onderlaag worden respectievelijk de regeling en trajecten bepaald. In deze formulering worden de regelparameters van de voertuigafhankelijke regeling binnen zekere grenzen aangepast om CAV's in staat te stellen te reageren op rood. Op basis van simulatieresultaten concluderen we dat de voorgestelde regeling verschillende combinaties van richtingen tegelijk kan regelen, en beter presteert op gebied van doorvoer (met 11,76%), brandstofverbruik (met 26,31%), verliestijd (met 12,33% en het gemiddeld aantal stops (met 66,67%) als vergeleken wordt met optimalisatie van de trajecten.

Ten vierde integreren we de verkeersregeling-optimalisatie en CAV-traject-optimalisatie in een enkele laag door de begrenzingen van de roodtijd te definiëren als een reeks lineaire positiebeperkingen van de CAVs. Met voorgestelde formulering kan de beperking van de huidige stand van techniek ondervangen worden, deze vereist nu dat evaluatie van de parameters plaatsvindt door de trajecten van de voertuigen vooraf te simuleren of te benaderen, met gespecificeerde voorwaarden voor uiteindelijke snelheid en locatie. De voorgestelde gezamenlijke regeling wordt bepaald met behulp van lineaire programmeertechnieken met "mixed integers". De optimale trajecten, regelstructuren en signaalgroepafwikkeling worden afgeleid op basis van de

simulatieresultaten. Bovendien presteert deze voorgestelde regeling beter dan Webster en de state-of-the-art methoden, namelijk 12,20% en 48,39% in doorvoer, 5,62% en 3,45% in brandstofverbruik, 10,34% en 10,98% in verliestijd.

Samenvattend biedt dit proefschrift een kader voor een CAV-trajectregeling met een reeks verkeersregelsysteem-benaderingen, gericht op het optimaliseren van verschillende efficiëntiemetingen (comfort, veiligheid, brandstofverbruik en verliestijd). Deze verbeteringen, die de efficiëntie, comfort en energieverbruik verifiëren, resulteren wel in een hoge rekenbelasting. Dit proefschrift kan inzicht verschaffen in optimale regelstructuren en signaalgroepafwikkeling, en bijbehorend snelheidsadvies, voor een beter verkeersmanagement en betere verkeersregelsystemen. Voorstellen voor toekomstig onderzoek zijn ten eerste het verminderen van de rekentijd, vervolgens het uitbreiden tot een stedelijk netwerkniveau.

About the author

Meiqi Liu was born in Liaoning, China on September 23, 1992. She obtained her B.Sc degree from Dalian Maritime University in 2014 with specialization in Shipping Management. Afterwards, she received her M.Sc degree from the Department of Transport Planning and Management, Zhejiang University in 2017.

In September 2017, she started her PhD project "Cooperative urban driving strategies at signalized intersections" at the Department of Transport & Planning, Delft University of Technology in Delft, the Netherlands, funded by China Scholarship Council (CSC). Her research interests include trajectory planning for cooperative vehicles and traffic signal optimization.

Publications

Journal papers

1. **Liu, M.**, Zhao, J., Hoogendoorn, S. and Wang, M., 2022. A single-layer approach for joint optimization of traffic signals and cooperative vehicle trajectories at isolated intersections. Transportation Research Part C: Emerging Technologies. https://doi.org/10.1016/j.trc.2021.103459

2. **Liu, M.**, Zhao, J., Hoogendoorn, S. and Wang, M., 2021. An optimal control approach of integrating traffic signals and cooperative vehicle trajectories at intersections. Transportmetrica B. https://doi.org/10.1080/21680566.2021.1991505

3. **Liu, M.**, Hoogendoorn, S. and Wang, M., 2020. Receding horizon cooperative platoon trajectory planning on corridors with dynamic traffic signal. Transportation Research Record, 2674(12), pp.324-338. https://doi.org/10.1177/0361198120954869

4. **Liu, M.**, Wang, M. and Hoogendoorn, S., 2019. Optimal platoon trajectory planning approach at arterials. Transportation Research Record, 2673(9), pp.214-226. https://doi.org/10.1177/0361198119847474

5. **Liu, M.**, Xu, L., Shen, L. and Jin, S., 2019. Modeling capacity at signalized intersections with a left-turn storage bay considering signal timing plan. Journal of Transportation Engineering, Part A: Systems, 145(2).

6. Xu, L., **Liu, M.**, Song, X. and Jin, S., 2018. Analytical model of passing events for one-way heterogeneous bicycle traffic flows. Transportation Research Record, 2672(36), pp.125-135.

7. **Liu, M.**, Shen, L. and Jin, S., 2017. Modeling capacity of shared right-turn lanes considering right turn on red and lag green time of right-turn. Journal of ZheJiang University (Engineering Science), 51(7), pp.1347-1354. (Chinese)

8. Jin, S., Shen, L., **Liu, M.** and Ma, D., 2017. Modeling speed-flow relationships for bicycle traffic flow. Proceedings of the Institution of Civil Engineers-Transport, 170(4), pp.194-204.

9. Qi, H., **Liu, M.**, Wang, D. and Chen, M., 2016. Spatial-temporal congestion identification based on time series similarity considering missing data. Plos One, 11(9).

10. Qi, H., **Liu, M.**, Zhang, L. and Wang, D., 2016. Tracing road network bottleneck by data driven approach. PloS One, 11(5).

11. Hao, R., **Liu, M.**, Ma, W., van Arem, B. and Wang, M. A flock-like two-dimensional cooperative vehicle formation model based on potential functions. Transportmetrica B. (under review)

Conference papers

1. **Liu, M.**, Zhao, J., Hoogendoorn, S. and Wang, M. Integrated optimization of traffic signal plans and cooperative vehicle trajectories at urban isolated intersections. The 100th Annual Meeting of the Transportation Research Board, Washington, D.C., 2021.

2. **Liu, M.**, Hoogendoorn, S. and Wang, M. Receding horizon cooperative platoon trajectory planning on corridors with dynamic traffic signal. The 99th Annual Meeting of the Transportation Research Board, Washington, D.C., 2020.

3. **Liu, M.**, Hoogendoorn, S. and Wang, M. Optimal platoon trajectory planning approach at arterials. The 98th Annual Meeting of the Transportation Research Board, Washington, D.C., 2019.

4. **Liu, M.**, Wang, M. and Hoogendoorn, S. Trajectory planning of cooperative vehicles on urban roads using model predictive control. The COTA International Symposium on Emerging Trends in Transportation (ISETT), Rome, 2019.

5. Alagbe, J., **Liu, M.** and Jin, S. Drivers' phone use at red traffic signals: a comparison of two studies to investigate factors influencing the individual behavior. The 97th Annual Meeting of the Transportation Research Board, Washington, D.C., 2018.

6. Xu, L., **Liu, M.** and Jin, S. Analytical model of passing events in the heterogeneous bicycle traffic flow. The 97th Annual Meeting of the Transportation Research Board, Washington, D.C., 2018.

7. **Liu, M.**, Shen, L. and Jin, S. Probabilistic model of capacity at signalized intersections with a left-turn short lane. The 96th Annual Meeting of the Transportation Research Board, Washington, D.C., 2017.

8. **Liu, M.**, Shen, L. and Jin, S. Modeling capacity of shared right-turn lanes at signalized intersections considering lag green time of right-turn. The 16th COTA International Conference of Transportation Professionals (CICTP), Shanghai, 2016.

TRAIL Thesis Series

The following list contains the most recent dissertations in the TRAIL Thesis Series. For a complete overview of more than 275 titles see the TRAIL website: www.rsTRAIL.nl.

The TRAIL Thesis Series is a series of the Netherlands TRAIL Research School on transport, infrastructure and logistics.

Liu, M., *Cooperative Urban Driving Strategies at Signalized Intersections*, T2022/3, January 2022, TRAIL Thesis Series, the Netherlands

Feng, Y., *Pedestrian, Wayfinding and VR*, T2022/2, T2022/1, January 2022, TRAIL Thesis Series, the Netherlands

Scheepmaker, G.M., *Energy-efficient Train Timetabling*, T2022/1, January 2022, TRAIL Thesis Series, the Netherlands

Chen, N., *Coordination Strategies of Connected and Automated Vehicles near On-ramp Bottlenecks on Motorways*, T2021/29, December 2021, TRAIL Thesis Series, the Netherlands

Onstein, A.T.C., *Factors influencing Physical Distribution Structure Design*, T2021/28, December 2021, TRAIL Thesis Series, the Netherlands

Olde Kalter, M.-J. T., *Dynamics in Mode Choice Behaviour*, T2021/27, November 2021, TRAIL Thesis Series, the Netherlands

Los, J., *Solving Large-Scale Dynamic Collaborative Vehicle Routing Problems: an Auction-Based Multi-Agent Approach*, T2021/26, November 2021, TRAIL Thesis Series, the Netherlands

Khakdaman, M., *On the Demand for Flexible and Responsive Freight Transportation Services*, T2021/25, September 2021, TRAIL Thesis Series, the

Netherlands

Wierbos, M.J., *Macroscopic Characteristics of Bicycle Traffic Flow: a bird's-eye view of cycling*, T2021/24, September 2021, TRAIL Thesis Series, the Netherlands

Qu, W., *Synchronization Control of Perturbed Passenger and Freight Operations*, T2021/23, July 2021, TRAIL Thesis Series, the Netherlands

Nguyen, T.T., *Highway Traffic Congestion Patterns: Feature Extraction and Pattern Retrieval*, T2021/22, July 2021, TRAIL Thesis Series, the Netherlands

Pudāne, B., *Time Use and Travel Behaviour with Automated Vehicles*, T2021/21, July 2021, TRAIL Thesis Series, the Netherlands

Gent, P. van, *Your Car Knows Best*, T2021/20, July 2021, TRAIL Thesis Series, the Netherlands

Wang, Y., *Modeling Human Spatial Behavior through Big Mobility Data*, T2021/19, June 2021, TRAIL Thesis Series, the Netherlands

Coevering, P. van de, *The Interplay between Land Use, Travel Behaviour and Attitudes: a quest for causality*, T2021/18, June 2021, TRAIL Thesis Series, the Netherlands

Landman, R., *Operational Control Solutions for Traffic Management on a Network Level*, T2021/17, June 2021, TRAIL Thesis Series, the Netherlands

Zomer, L.-B., *Unravelling Urban Wayfinding: Studies on the development of spatial knowledge, activity patterns, and route dynamics of cyclists*, T2021/16, May 2021, TRAIL Thesis Series, the Netherlands

Núñez Velasco, J.P., *Should I Stop or Should I Cross? Interactions between vulnerable road users and automated vehicles*, T2021/15, May 2021, TRAIL Thesis Series, the Netherlands

Duivenvoorden, K., *Speed Up to Safe Interactions: The effects of intersection design and road users' behaviour on the interaction between cyclists and car drivers*, T2021/14, April 2021, TRAIL Thesis Series, the Netherlands

Nagalur Subraveti, H.H.S., *Lane-Specific Traffic Flow Control*, T2021/13,

March 2021, TRAIL Thesis Series, the Netherlands

Beirigo, B.A., *Dynamic Fleet Management for Autonomous Vehicles: Learning- and optimization-based strategies*, T2021/12, March 2021, TRAIL Thesis Series, the Netherlands

Zhang, B., *Taking Back the Wheel: Transition of control from automated cars and trucks to manual driving*, T2021/11, February 2021, TRAIL Thesis Series, the Netherlands

Boelhouwer, A., *Exploring, Developing and Evaluating In-Car HMI to Support Appropriate use of Automated Cars*, T2021/10, January 2021, TRAIL Thesis Series, the Netherlands

Li, X., *Development of an Integrity Analytical Model to Predict the Wet Collapse Pressure of Flexible Risers*, T2021/9, February 2021, TRAIL Thesis Series, the Netherlands

Li, Z., *Surface Crack Growth in Metallic Pipes Reinforced with Composite Repair System*, T2021/8, January 2021, TRAIL Thesis Series, the Netherlands

Gavriilidou, A., *Cyclists in Motion: From data collection to behavioural models*, T2021/7, February 2021, TRAIL Thesis Series, the Netherlands

Methorst, R., *Exploring the Pedestrians Realm: An overview of insights needed for developing a generative system approach to walkability*, T2021/6, February 2021, TRAIL Thesis Series, the Netherlands

Walker, F., *To Trust or Not to Trust? Assessment and calibration of driver trust in automated vehicles*, T2021/5, February 2021, TRAIL Thesis Series, the Netherlands

Schneider, F., *Spatial Activity-travel Patterns of Cyclists*, T2021/4, February 2021, TRAIL Thesis Series, the Netherlands